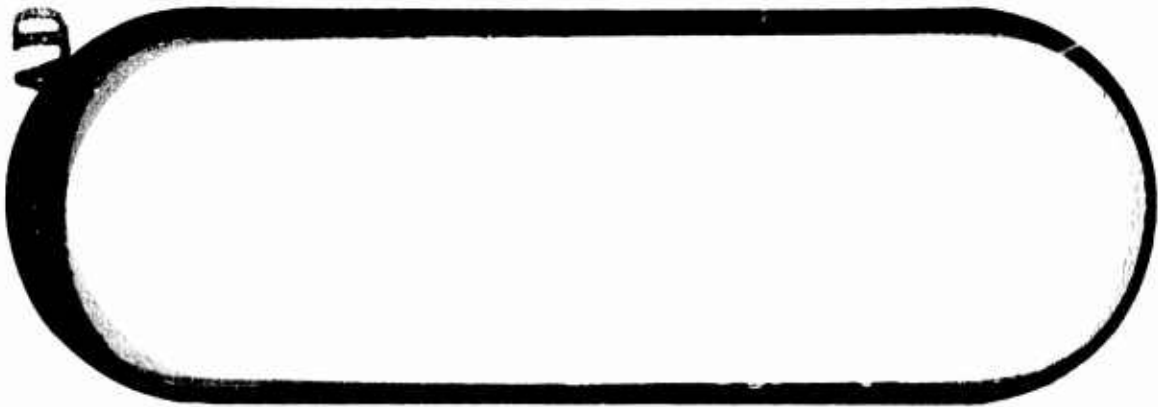


AD 712645



This document has been approved
for public release and sale; its
distribution is unlimited.

DDC
RECEIVED
OCT 19 1970
C

BOEING

VERTOL DIVISION

108

**Best
Available
Copy**

THE ~~DEFENSE~~ COMPANY
VERTOL DIVISION • PHILADELPHIA, PENNSYLVANIA

CODE IDENT. NO. 77272

NUMBER D8-207C

TITLE EVALUATION OF GEARED FLAP CONTROL SYSTEM
FOR TILTWING V/STOL AIRCRAFT

ORIGINAL RELEASE DATE 1/69. FOR THE RELEASE DATE OF
SUBSEQUENT REVISIONS, SEE THE REVISION SHEET. FOR LIMITATIONS
IMPOSED ON THE DISTRIBUTION AND USE OF INFORMATION CONTAINED
IN THIS DOCUMENT, SEE THE LIMITATIONS SHEET.

MODEL _____ CONTRACT _____

ISSUE NO. _____ ISSUED TO: _____

This document is approved
for public release and its
distribution is unlimited

001
RESERVED
C

PREPARED BY

G. B. CHURCHILL

DATE 8/11/70

APPROVED BY

F. BOVEN

DATE 8/11/70

APPROVED BY

R. B. GILLMORE

DATE 8/11/70

APPROVED BY

W. B. POCK

DATE 8/11/70

LIMITATIONS

DDC AVAILABILITY NOTICE:

Distribution of this document is unlimited.

This document is controlled by V/STOL Aerodynamics - 7481

All revisions to this document shall be approved by the
above noted organization prior to release.

ABSTRACT

The Geared Flap control system* provides a means for controlling a tiltwing V/STOL aircraft in hover and transition flight without the use of auxiliary systems such as cyclic propeller pitch or tail jets/rotors. The system is based on using the flap as an aerodynamic servo to position the wing relative to the fuselage. Although the system is mechanically simple, the control characteristics are difficult to visualize because of the coupled body dynamics involved. Therefore, a comprehensive analytical and model testing program has been performed to evaluate the system.

KEY WORDS

Geared Flap

Coupled Body Dynamics

Transition Corridor

Aerodynamic Servo

V/STOL Control System

Cyclic Propellers

*U.S. Patent 3,029,043, "Free Floating Wing Structure and Control System for Convertible Aircraft." Issued to G.B. Churchill, 10 April 1962 (Reference 4).

TABLE OF CONTENTS

	<u>Page</u>
ABSTRACT/KEY WORDS	iii
LIST OF ILLUSTRATIONS	vi
INTRODUCTION	1
DESCRIPTION OF GEARED FLAP CONCEPT	3
NOMENCLATURE	11
TECHNICAL ANALYSIS	15
General	15
Transition Corridor Definition	16
Control Analysis	21
Hover Trim Capability	29
DYNAMIC MODEL TESTS	31
General	31
Model and Test Setup	31
Model Tests	33
CONCLUSIONS	37
APPENDIX A - Basic Data Required for Analysis of Geared Flap Transition	65
APPENDIX B - Longitudinal Equations of Motion for Tiltwing Aircraft	95
REFERENCES	103

LIST OF ILLUSTRATIONS

<u>Figure</u>		<u>Page</u>
1	Schematic Drawing of Geared Flap System	4
2	Schematic of Constant Force Actuator	7
3	Dynamic Model Used for Flight Evaluations (T-Tail Configuration)	8
4	Dynamic Model Used for Flight Evaluations (Low-Tail Configuration)	9
5	Basic Aerodynamic Data (3 Sheets)	42,43,44
6	Wing Inertia Effects on (3 Sheets) Hinge Moment	45,46,47
7	Total Aircraft Moments about Pivot- Tail Off, $\theta_f = 0^\circ$ (3 Sheets)	48,49,50
8	Variation of Total Moment at Constant CT_S (3 Sheets)	51,52,53
9	Variation of Total Moment with Fuselage Angle of Attack (3 Sheets)	54,55,56
10	Geared Flap Control Trimmed Polars	57
11	Geared Flap Transition Corridor	58
12	Fuselage Response to Wing Incidence Change	59
13	Geared Flap Hovering Control Response	60
14	Fuselage Response to Propeller Blade Pitch Changes	61
15	Geared Flap Transition Horizontal Tail Effective- ness Low Horizontal Tail @ $CL_T = 1.0$	62
16	Aerodynamic Characteristics in Hover ($CT_S = 1.0$)	63
17	Hover Trim with Geared Flap	64

Appendix A

1	Three View and Principal Model Dimensions	66
2	Pivot Point Positions	67
3	Slat Arrangement	68
4	Spoiler-Deflector and Flap Arrangement	69

<u>Figure</u>		<u>Page</u>
5	Lift Coefficient vs. Thrust Coefficient $\delta_f = 0^\circ \quad \alpha_f = 0^\circ \quad \beta = 12^\circ \quad$	70
6	Lift Coefficient vs. Thrust Coefficient $\delta_f = 20^\circ \quad \alpha_f = 0^\circ \quad \beta = 12^\circ \quad$	71
7	Lift Coefficient vs. Thrust Coefficient $\delta_f = 40^\circ \quad \alpha_f = 0^\circ \quad \beta = 12^\circ \quad$	72
8	Longitudinal Force Coefficient vs. Thrust Coefficient $\delta_f = 0^\circ \quad \alpha_f = 0^\circ \quad \beta = 12^\circ \quad$	73
9	Longitudinal Force Coefficient vs. Thrust Coefficient $\delta_f = 20^\circ \quad \alpha_f = 0^\circ \quad \beta = 12^\circ \quad$	74
10	Longitudinal Force Coefficient vs. Thrust Coefficient $\delta_f = 40^\circ \quad \alpha_f = 0^\circ \quad \beta = 12^\circ \quad$	75
11	Level Flight Acceleration Capability $\delta_f = 0^\circ \quad \alpha_f = 0^\circ \quad \beta = 12^\circ \quad$	76
12	Level Flight Acceleration Capability $\delta_f = 20^\circ \quad \alpha_f = 0^\circ \quad \beta = 12^\circ \quad$	77
13	Level Flight Acceleration Capability $\delta_f = 40^\circ \quad \alpha_f = 0^\circ \quad \beta = 12^\circ \quad$	78
14	Wing Hinge Moment $\delta_f = 0^\circ \quad \alpha_f = 0^\circ \quad \beta = 12^\circ \quad$	79
15	Wing Hinge Moment $\delta_f = 20^\circ \quad \alpha_f = 0^\circ \quad \beta = 12^\circ \quad$	80
16	Wing Hinge Moment $\delta_f = 40^\circ \quad \alpha_f = 0^\circ \quad \beta = 12^\circ \quad$	81
17	Effect of Flap on Downwash at Low Tail Position $\alpha_f = 0^\circ \quad \beta = 12^\circ \quad$	82
18	Effect of Flap on Downwash $i_w = 20^\circ \quad \beta = 12^\circ \quad C_{TS} = 0.3 \quad$	83
19	Effect of Flap on Downwash $i_w = 20^\circ \quad \beta = 12^\circ \quad C_{TS} = 0.5 \quad$	84
20	Effect of Flap on Downwash $i_w = 20^\circ \quad \beta = 12^\circ \quad C_{TS} = 0.7 \quad$	85
21	Effect of Flap on Downwash $i_w = 20^\circ \quad \beta = 12^\circ \quad C_{TS} = 0.9 \quad$	86

<u>Figure</u>		<u>Page</u>
22	Effect of Flap on Tail Efficiency of Low Tail $\alpha_f = 0^\circ \quad \beta = 12^\circ \quad C_{TS} = 0.3 \quad$	87
23	Effect of Flap on Tail Efficiency of Low Tail $\alpha_f = 0^\circ \quad \beta = 12^\circ \quad C_{TS} = 0.5 \quad$	88
24	Effect of Flap on Tail Efficiency of Low Tail $\alpha_f = 0^\circ \quad \beta = 12^\circ \quad C_{TS} = 0.7 \quad$	89
25	Effect of Flap on Tail Efficiency of Low Tail $\alpha_f = 0^\circ \quad \beta = 12^\circ \quad C_{TS} = 0.9 \quad$	90
26	Effect of Flap on Tail Efficiency of Low Tail $i_w = 20^\circ \quad \beta = 12^\circ \quad C_{TS} = 0.3 \quad$	91
27	Effect of Flap on Tail Efficiency of Low Tail $i_w = 20^\circ \quad \beta = 12^\circ \quad C_{TS} = 0.5 \quad$	92
28	Effect of Flap on Tail Efficiency of Low Tail $i_w = 20^\circ \quad \beta = 12^\circ \quad C_{TS} = 0.7 \quad$	93
29	Effect of Flap on Tail Efficiency of Low Tail $i_w = 20^\circ \quad \beta = 12^\circ \quad C_{TS} = 0.9 \quad$	94

Appendix B

1	Axis System	100
2	Schematic Definition of Parameters	101

INTRODUCTION

The tiltwing concept for a V/STOL aircraft has been in practical existence for approximately 15 years. During this time three aircraft configurations have been flown extensively, demonstrating the validity of the basic concept, as well as the operational feasibility of the systems. In spite of the research programs supporting these aircraft, the tiltwing concept has changed very little from the original Vertol-76 Army research aircraft. Both the XC-142, built by Ling-Temco-Vought, and the CL-84, built by Canadair, have retained the tail rotor for longitudinal control, although they have eliminated the yaw control rotor by using the ailerons for yaw control in hover. Employing the tail rotor for pitch control is the source of much of the complexity; however, it is currently being replaced on advanced concepts by reaction jets at the tail or by using cyclic propellers. Although these systems may eliminate the tail rotor, they do not affect the aircraft weights in either case, or complexity, in the case of using cyclic propellers. Although there is some data cyclic propellers (References 1, 2, and 3), a full scale cyclic propeller has yet to be built. Therefore, a complete picture of the relative complexity is not available.

The complexity of the tiltwing V/STOL concept generally is accepted as being necessary to provide the required control and response characteristics in hover and transition for the attainment of good handling qualities. Conventional treatment of the control problem in these flight regimes results in a pitch control being required to control fuselage attitude, which generates a linear acceleration through attitude perturbations, while a thrust control device is necessary to control linear accelerations along the axis approximately orthogonal to that controlled by pitch. However, the pilot's task is to fly a trajectory

which is dependent upon the linear accelerations, while maintaining some pitch stability. An examination of the inherent characteristics of the tiltwing V/STOL concept shows that the longitudinal linear accelerations normally generated by pitching the total aircraft can be generated by simply tilting the wing, and the resulting pitching acceleration is the same order of magnitude as that obtained using a conventional pitching control system. Therefore, by taking advantage of the system's inherent characteristics, with no auxiliary pitch control system, such as cyclic propellers or tail jets, a significant reduction in weight and complexity could be achieved.

The Geared Flap control system, described in References 4 and 5, was developed specifically to take advantage of the inherent characteristics of the tiltwing concept, and to eliminate the auxiliary pitch control system requirement. The basis of the Geared Flap concept consists of using the flap as a servo-tab to control the wing incidence during hover and transition flight, whereby the flap is linked directly to the longitudinal stick to give the pilot an indirect control of wing incidence. In hovering flight, pitching moments on the fuselage are generated by the horizontal component of force at the wing hinge line caused by wing incidence changes. The sensitivity of the flap to stick deflections is phased with wing incidence, and becomes zero for the cruise configuration. When used in this manner, the flap programming becomes dependent on flight condition, and the deflection is optimized automatically for various flight conditions. An advantage of the system is that it uses only known aircraft systems and analytical methods. The concept has been analyzed and dynamic model tests have demonstrated the system feasibility in hover, transition, and cruise flight. These initial studies are presented in Reference 5 and its film supplement.

The analyses presented in Reference 5 were limited to basic hover dynamics, and level flight in transition, and the results left two basic issues regarding practicality of the system unanswered:

1. Does there exist any condition in hover and transition where a dangerous control response characteristic could exist due to the basic system concept?
2. Do any adverse stability and control characteristics exist in ground effect during hover and STOL operations?

The present report provides answers to these two questions: by detailed analyses, using recent wind tunnel test data (Reference 6) for the first question, and by extensive dynamic model flight testing for the second question.

DESCRIPTION OF GEARED FLAP CONCEPT

The Geared Flap control system is based on utilizing the wing flap as an aerodynamic servomechanism (as a servo tab) to control the wing incidence relative to the fuselage, and is shown schematically in Figure 1. The system was developed for hover and transition flight as a means of utilizing the total longitudinal control capability of the tiltwing concept without employing auxiliary pitch control, thereby providing an integrated pitching and axial control system. Thus, it takes advantage of inherent characteristics, such as:

- . the effects of flap deflection on pitching and axial accelerations
- . the effects of wing incidence on pitching and axial accelerations
- . the effect of wing incidence on aircraft center of gravity location

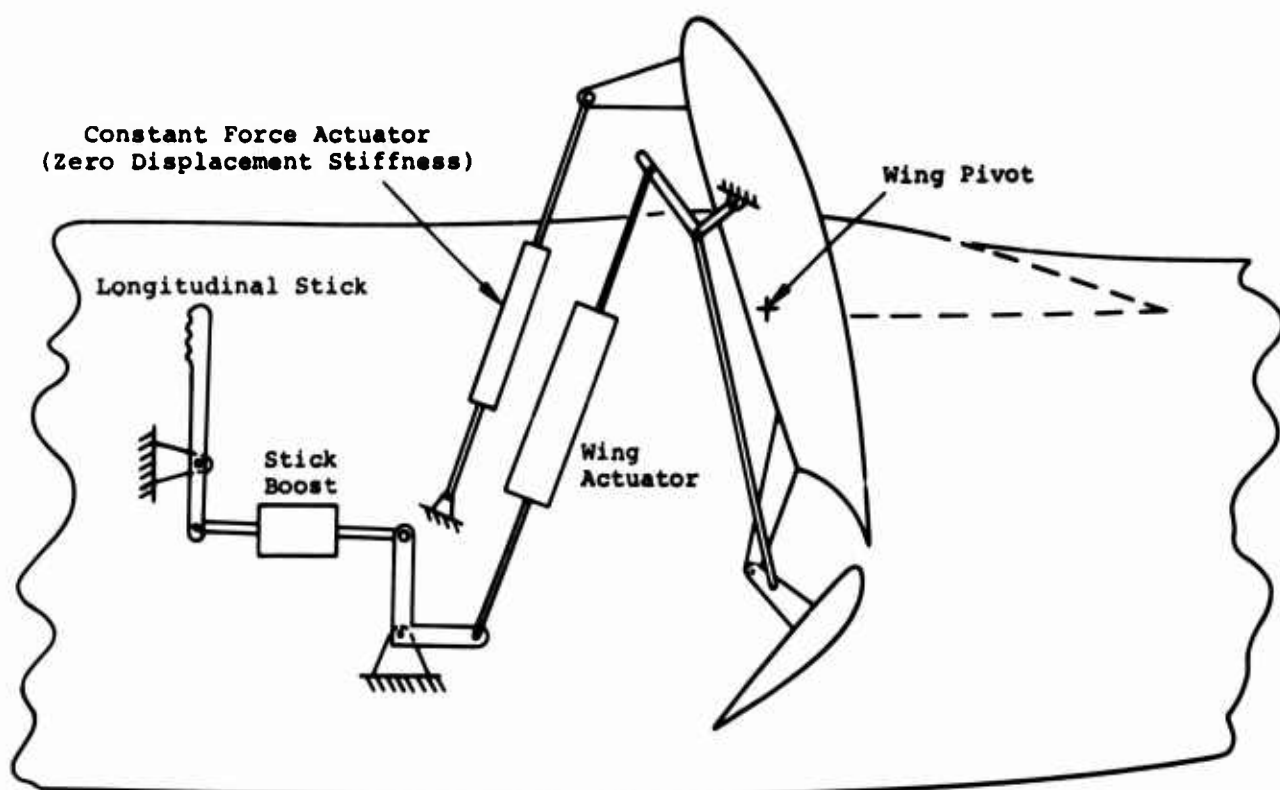


Figure 1. Schematic Drawing of Geared Flap System.

It should be noted that in using the Geared Flap system, a different control philosophy is observed at hover and low speed. A conventional control system in hover develops axial control by pitching the aircraft, whereas the Geared Flap system provides axial control directly, and pitch response follows. Therefore, it satisfies the pilot's basic control requirements directly; moreover, stabilization, rather than control, of the pitch mode is required. This is accomplished simply because the forces at the wing pivot are above the non-tilting system center of gravity, and the fuselage axis then tends to remain normal to the resultant vector acting at the pivot.

As shown in Figure 1, the wing hinge pivot is located above the thrust axis to favor a normal downward flap deflection at all times. A forward control input by the pilot causes an increase in flap deflection, which creates a diving moment about the wing pivot and initiates the wing motion. A moment unbalance exists until the wing displacement is sufficient to neutralize the moment caused by flap through the follow-up linkage; then the wing displacement results in both pitching and axial accelerations of the aircraft caused by shifting the total aircraft center of gravity forward and applying an axial force above the fuselage cg.

The system is analogous longitudinally, to a single-rotor helicopter in control concept: The entire tilting system (wing, propeller, engines, etc.) represents the rotor, which produces a resultant force. An input of control (flap deflection) is equivalent to a cyclic pitch input, and causes the resultant vector to rotate about the wing hinge (rotor-flapping response). Wing motion ceases when the steady-state equivalent flapping (wing incidence change) cancels the equivalent cyclic input (initial flap deflection).

In hovering flight the pilot's control inputs operate the flap, giving him a second order wing incidence response. Pitch trim in hover is accomplished by biasing the wing hinge moment using the constant force actuator to force an additional flap deflection. The moment created by the additional flap deflection is then transferred to the fuselage via the constant force actuator. A possible constant force actuator schematic is shown in Figure 2. The trim actuator sets the length of the spring, and any relative motion of the actuator ends causes the hydraulic actuator to maintain the spring length at the desired value.

In transition flight, the Geared Flap control system provides tight control of the aircraft linear accelerations, with the fuselage being relatively unaffected by the wing-propeller moment variations. These variations are cancelled by use of the flap linkage system, and the fuselage pitch stability is then primarily dependent upon the horizontal tail. In high speed transition flight, the Geared Flap system provides a time-constant for normal g response of about 0.3 second, which is about the same as a conventional pitching moment control system. Due to the manner of coupling the wing and flap, the flap programming for transition is adaptive, varying with the flight condition. The flap deflection increases in descent and in positive normal acceleration maneuvers, while it decreases with power application or climb. This provides automatic flap deflection optimization, and eliminates certain problems, such as pitch trim during waveoff and adverse ground effects, encountered by the XC-142.

The system has been thoroughly analyzed and tested by using the dynamic model shown in Figures 3 and 4 for all flight conditions in hover and transition. The model tests include flights in and out of ground effect, and steady-state and transient maneuver evaluations.

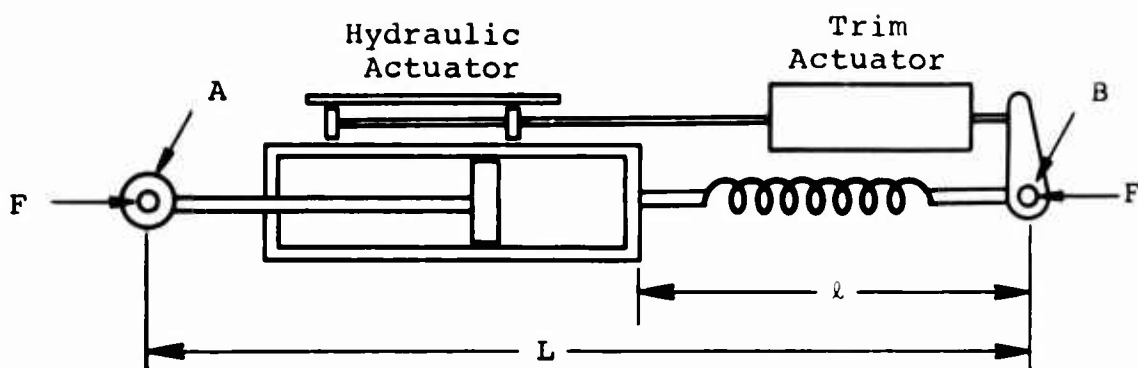


Figure 2. Schematic of Constant Force Actuator.

The distance ℓ is established by the length established by the trim actuator, and defines the length of the spring. Assuming point A is fixed, should point B move, the valve of the hydraulic actuator is displaced in such a manner as to maintain length ℓ constant, for any length L within the actuator stroke limits. If the free spring length is ℓ_0 , the force is;

$$F = -k (\ell_0 - \ell)$$

and the gradient will be,

$$dF/dL = 0$$

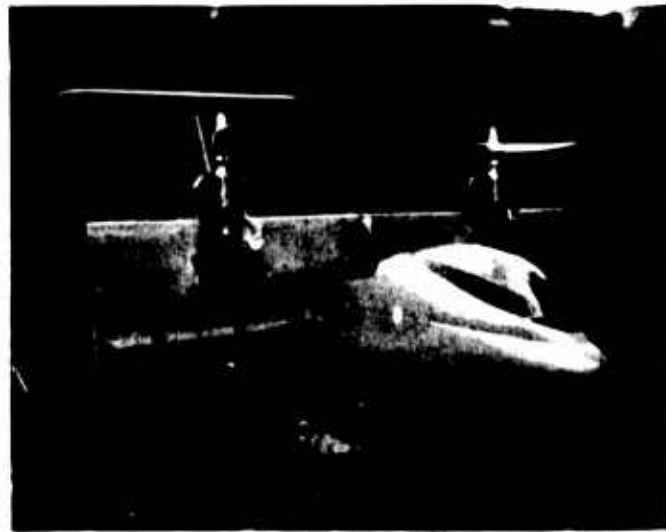
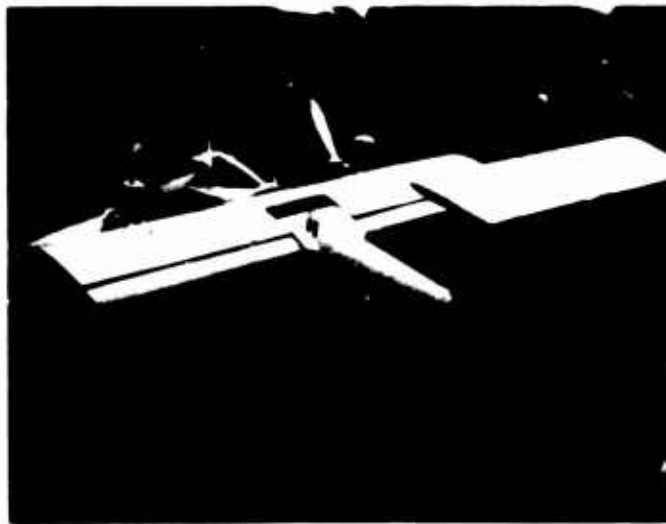
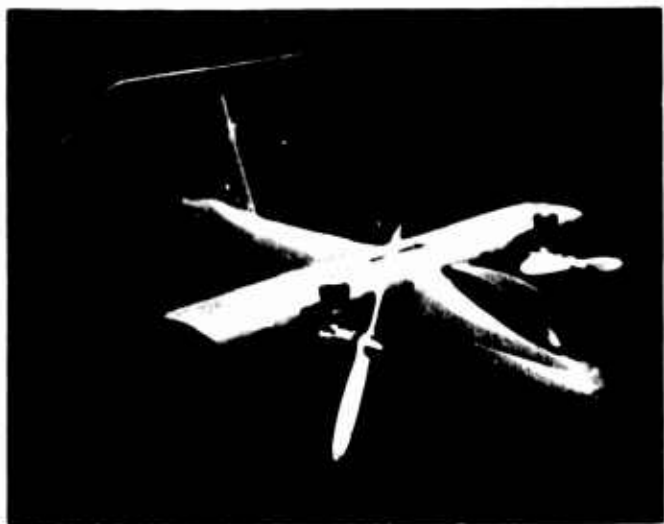


Figure 3. Dynamic Model Used for Flight Evaluations
(T-Tail Configuration).

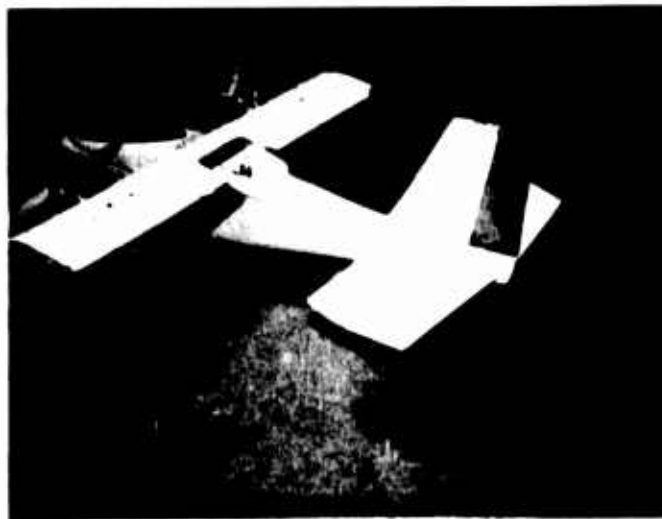
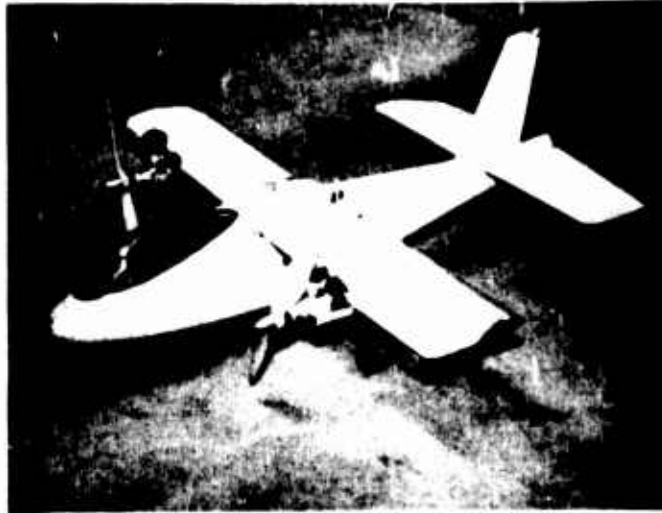


Figure 4. Dynamic Model Used for Flight Evaluations (Low-Tail Configuration).

NOMENCLATURE

A_p	Propeller rise area, ft^2
\bar{c}	Wing geometric chord length, ft.
C_{L_S}	Lift coefficient based on q_s , $L/q_s S$
$C_{M_{P_S}}$	Moment coefficient about the wing pivot point, $M_p/q_s S \bar{c}$
C_{R_S}	Resultant force coefficient based on q_s , $\sqrt{C_{X_S}^2 + C_{L_S}^2}$
C_{T_S}	Thrust coefficient based on q_s , $T/q_s A_p$
$C_{W_{H_S}}$	Wing hinge moment coefficient based on q_s , $H/q_s S \bar{c}$
C_{X_S}	Longitudinal force coefficient based on q_s , $(-D/q_s S)$
D	Propeller diameter, feet; Drag, lbs.
F	Force, lbs.
g	Acceleration due to gravity, 32.2 ft/sec^2
h	Waterline distance from wing pivot to fuselage CG, positive down, feet
h_w	Distance of tilting system CG below wing chord line, feet
n_x	Acceleration in X direction, g's
n_z	Acceleration in Z direction, g's
H	Wing hinge moment, lbs.
i_w	Wing incidence angle, degrees, measured between wing chord line and fuselage reference axis (x-axis)
I_y	Fuselage pitching moment of inertia about non-tilting CG
I_{y_w}	Tilting system pitching moment of inertia about tilting system CG
x	Distance of non-tilting CG forward of wing pivot, feet

L	Lift, lbs.
L_w	Distance from wing hinge to tilting system CG, feet = $(h_w^2 + \ell_w^2)$
ℓ_w	Distance of tilting system CG forward of wing pivot, feet, parallel to chordline
M	Pitching moment, foot-pounds, positive nose up
m	Total mass of the aircraft, slugs
m_f	Mass of non-tilting components, slugs
m_w	Mass of tilting components, slugs
η_t	Tail efficiency factor, q_t/q
q	Freestream dynamic pressure, lbs/ft ² , $- 1/2\rho U_0^2$
q_s	Slipstream, dynamic pressure, lbs/ft ² , $(q + T/S_p)$
S	Wing area, ft ²
T	Propeller thrust, lbs.
u	Velocity in the x direction, ft/sec
u_0	Resultant aircraft velocity, ft/sec, $= (u^2 + w^2)$
w	Velocity in the z direction, ft/sec
X	Force in x direction, lbs, positive forward
x_p	Distance of wing pivot aft of $\bar{c}/4$, ft, parallel to chordline
x_{cg}	Distance of CG from wing leading edge at $i_w = 0^\circ$
Z	Force in the Z direction, positive down
z_p	Distance of wing pivot below wing chord line, feet
α	Free stream angle of attack
α_{TL}	Thrust line angle of attack
β	Propeller blade angle at .75 radius to wing angle of attack

δ_f	Flap deflection, degrees
δ_s	Stick deflection, in.
α	Downwash at the horizontal tail, degrees
θ	Fuselage attitude relative to gravity, radians
λ	Angle between fuselage reference line and line between wing pivot and tilting system CG, $= \left(i_w - \tan^{-1} \frac{h_w}{l_w} \right)$
γ	$\tan^{-1} (C_{X_S}/C_{L_S})$; Flight path angle in steady-state flight only

Superscripts

- . First derivative with respect to time
- .. Second derivative with respect to time

Subscripts

f	Fuselage; non-tilting system
p	Wing pivot (see particular term)
t	Tail
tot	Total
TL	Thrust line
w	Wing; tilting system
y	About y axis
δ_f	Derivative with respect to flap deflection
δ_s	Derivative with respect to stick deflection

TECHNICAL ANALYSIS

GENERAL

Although the Geared Flap control system concept can be extremely simple mechanically, the analysis is complex. This is caused by the extra degree of freedom provided between the wing and fuselage, requiring that an additional equation of motion for trim or control be satisfied. Because of this complexity, the trim and control margins available in transition cannot be easily established, and a basic question developed.

"The system, based on the results of analyses and model flights presented in Reference (5), apparently works very well in normal flight conditions in transition. However, is it possible, at the limits of the transition corridor envelope, to encounter an adverse control or response characteristic which is inherent to the system?" The following analyses have shown that no control problems exist as a result of basic system characteristics.

In order to provide perspective to the analysis, the configuration of Reference 6 was scaled to a gross weight of 18,000 pounds at a hovering disc loading of 40-pounds per square foot. This aircraft has approximately the same weight and loadings as the Vertol Model 147, thus permitting direct application of Model 147 weights, inertia, and dimensional data to the analysis. The aircraft characteristics required for the analysis are presented in Table I.

The Advanced Geometry Tilt Wing (AGTW) model (Reference 6) differed from the Model 147 in flap geometry and thrust line location. The AGTW flap slot lip was located at $0.75\bar{c}$, and the Model 147 at approximately $0.65\bar{c}$. The AGTW thrust line is $0.12\bar{c}$ below the wing chord plane, while the Model 147 was $0.20\bar{c}$. The AGTW model description and test data used in the present analyses are

presented in Appendix A. In addition to the improved flap system, the AGTW tests verified the improvements in control power using a low, fuselage-mounted (rather than "T"), horizontal tail configuration. These advantages also were shown during the dynamic model flight tests. Therefore, the tail control powers shown are based on a low tail configuration, using the tail efficiency and downwash data presented in Appendix A.

TRANSITION CORRIDOR DEFINITION

The calculation of the transition performance characteristics of a conventional tiltwing system with cyclic propellers (rigid link between wing and fuselage) is rather uncomplicated, and requires satisfying only the linear acceleration criteria for the defined flight path. Trimming the aircraft with cyclic pitch does not change the basic forces, since application of cyclic pitch results in essentially a pure couple. However, the Geared Flap system provides a moment balance for both the tilting and nontilting portions of the system, and therefore, requires that two moment equations as well as the linear accelerations be satisfied to define the transition characteristics.

The derivation of the complete longitudinal equations of motion, based on body axes, for a tiltwing aircraft is presented in Appendix B. The static transition performance is obtained from the steady-state solution to these ($\dot{u}, \dot{w}, \ddot{\theta}, \dot{\theta} = 0$).

The steady-state equations are:

$$X_{\text{tot}} + mg \cos \lambda = 0 \quad (1)$$

$$Z_{\text{tot}} + W_{\text{a/c}} = 0 \quad (2)$$

$$M_w + M_p + \frac{m_w}{m} L_w (X_{\text{tot}} \sin \lambda + Z_{\text{tot}} \cos \lambda) = 0 \quad (3)$$

$$M_{ft} - M_p - \frac{m_f}{m} (X_{tot} h - Z_{tot} l) = 0 \quad (4)$$

A characteristic of the Geared Flap system is that the fuselage axis tends to remain normal to the resultant acceleration vector. Therefore, the analysis for hover and transition equilibrium flight conditions can be performed with the assumption of a level fuselage. This, in part, neglects the effects of fuselage and tail aerodynamics. However, the fuselage is in an essentially free stream "q" flow field, and the only requirement of the horizontal tail is to stabilize and trim the fuselage aerodynamic moments. Therefore, an analysis of transition assuming zero tail load and level fuselage appears to be justified.

The conversion of the force terms in equations (1) to (4) to wind axis forces and coefficients gives:

$$X_{tot} = q_s S [C_{X_S} \cos \alpha_f + C_{L_S} \sin \alpha_f] \quad (5)$$

$$Z_{tot} = q_s S [C_{L_S} \cos \alpha_f - C_{X_S} \sin \alpha_f] \quad (6)$$

$$M_w = q_s \bar{S} C_{W_{HS}} \quad (7)$$

$$M_{ft} = q_s \bar{S} C_{M_{S_{ft}}} \text{ (Assumed zero)} \quad (8)$$

$$M_p = q_s \bar{S} C_{M_{PS}} \quad (9)$$

For the assumption of a level fuselage, α_f is defined by:

$$\alpha_f = -\gamma = -\tan^{-1} \frac{C_{X_S}}{C_{L_S}} \quad (10)$$

(since $X_{tot} = 0$)

Then, defining

$$C_{RS} = \sqrt{C_{XS}^2 + C_{LS}^2} \quad (11)$$

gives

$$X_{tot} = q_s S C_{RS} \sin (\alpha_f + \gamma) \quad (12)$$

$$Z_{tot} = -q_s S C_{RS} \cos (\alpha_f + \gamma) = -W_{a/c} \quad (13)$$

For the Model 147 with the AGTW pivot location ($0.35\bar{c}$ chord, $0.07\bar{c}$ below chord plane), $\lambda_o = 0^\circ$ and, therefore

$$\lambda = i_w \quad (14)$$

Substituting equations (5) to (14) in (1) to (4), and dividing by $q_s S$, gives:

$$C_{RS} \sin (\alpha_f + \gamma) = 0 \quad (15)$$

$$\frac{W/S}{q_s} - C_{RS} \cos (\alpha_f + \gamma) = 0 \quad (16)$$

$$C_{WH_S} + C_{MP_S} - \frac{m_w}{m} \frac{L_w}{\bar{c}} C_{RS} \cos i_w = 0 \quad (17)$$

$$C_{MP_S} + \frac{m_f}{m} \frac{\ell}{\bar{c}} C_{RS} = 0 \quad (18)$$

The value of the required moment across the pivot is defined in equation (18) by the fore and aft location of the nontilting mass cg. Substituting equation (18) in equation (17), leaves

only two equations required to define the transition corridor (for level fuselage):

$$q_s = \frac{C_{RS}}{W/S} \quad (19)$$

$$C_{W_{HS}} - \frac{m_f}{m} \frac{\ell}{\bar{c}} C_{RS} - \frac{m_w}{m} \frac{L_w}{\bar{c}} C_{RS} \cos i_w = 0 \quad (20)$$

The wing incidence, i_w , is simply obtained for the level fuselage case from the following:

$$i_w = \alpha_{TL} - \alpha_f = \alpha_{TL} + \gamma \quad (21)$$

The distinction between the three terms in equation (20) is important in understanding the system: The first term, $(C_{W_{HS}})$, is the aerodynamic moment about the hinge, and is a function of thrust, angle of attack, and flap deflection; the second term, $(m_f/m \cdot \ell/\bar{c} \cdot C_{RS})$, represents the constant moment required for fuselage cg location compensation and is the fuselage inertia contribution to the moment about the pivot. This term is generated by the constant force actuation, and may be varied to compensate for cg location. The third term, $(m_w/m \cdot L_w/\bar{c} \cdot C_{RS} \cos i_w)$, is the moment created by the tilting system cg being forward of the pivot. This is the inertial relief moment due to the tilting system, and is of prime importance in making the system operative.

The aerodynamic data for the configuration analyzed is presented in Appendix A. These data were replotted at constant thrust coefficients and are presented in Figure 5. The data were plotted to the extreme angles of attack obtained during the test to define the shapes of the polars and moment curves at the limits of the operational envelope. Where the data extended

beyond stall, no adverse moment characteristics were obtained, and the moment curve breaks appeared to be stable.

The total contribution of the tilting system to the moments about the pivot consists of the sum of the inertial relief and aerodynamic moments. The wing inertia contribution to the tilting system moment is presented in Figure 6 as well as the total tilting system contribution to the pivot moment.

The fuselage inertia contribution to the moment is relatively small for the case analyzed (wing down cg at $0.25\bar{c}$), and is not presented. The values range from approximately -0.02 to -0.05.

The total aircraft (less fuselage and tail aerodynamics) moments about the wing hinge point as a function of longitudinal force coefficient, C_{X_S} , are presented in Figure 7 for constant flap deflections, and in Figure 8 for constant thrust coefficient (C_{T_S}).

The data presented in Figures 8 and 9 define the relationship of flap deflection, thrust line angle of attack, and flight path angle (or fuselage angle of attack for level fuselage) at constant C_{T_S} . These are defined at $C_{M_{Spiv}} = 0$, until the maximum flap deflection of 40 degrees is attained, where the $C_{M_{Sp}}$ value follows the 40-degree flap deflection line. This condition is shown for C_{T_S} values of 0.5 and greater. For the condition where the flap does not provide sufficient trim, the fuselage attitude may be increased, or the horizontal tail may be used. The increments in fuselage attitude required at the extreme conditions are shown in Figure 9 (b and c). The horizontal tail effectiveness is discussed in a later section.

With the relationship of flap deflection, thrust line angle of attack, and flight path angle defined in Figure 9, a set of trimmed lift-drag polars may be developed at constant C_{T_S} for

variable flap deflection, and are presented in Figure 10. These polars define the transition performance corridor for the geared flap system.

In order to provide visibility to the transition performance, the complete corridor has been calculated and is presented in Figure 11. The calculations are based on the AGTW configuration presented in Appendix A and Reference 6 with a 40-pound per square foot disc loading, and the estimated weights and inertias presented in Table I. The presentation is in terms of horizontal component of velocity and rate of climb, since true airspeed and flight path angle become discontinuous near zero velocity. The upper limit of the envelope will be the maximum power condition, which was arbitrarily selected as power required for $T/W = 1.15$ in hovering flight. The propeller data of Reference 7 were used to calculate thrust. The lower boundary of the corridor is established by buffet or stall limits in descending flight, and the approximate boundary is shown as a dashed line.

Figure 11 shows readily the variation of the flap deflection and wing incidence with flight condition, and the capability of the Geared Flap control system to operate throughout the flight envelope.

CONTROL ANALYSIS

Analysis of the Geared Flap system requires the definition of the aircraft response to wing incidence changes and propeller blade pitch changes. Also required is the time necessary to change wing incidence by driving with the flap, since this can present an appreciable control response lag to the pilot.

The equations of motion presented in Appendix B are unwieldy for manual solution. so an approximation has been used to define the control powers. The assumption was made that the effect of

wing pitching inertia had relatively little effect on the fuselage pitch response. This is justified by the fact that the tilting system moment of inertia about the wing hinge is approximately one-twelfth that of the nontilting system. This is similar to a single rotor helicopter, where a control analysis can be done considering the tilting of the thrust vector about the hub center, and a definition of the time lag in attaining a given deviation.

Fuselage Response to Δi_w

The analysis of the fuselage response to wing incidence change used the following assumptions:

1. The variation of aerodynamic moments due to the fuselage and tail (M_{ft}) is ignored. This is not justified since both ϵ and η_t will change with wing incidence (see Appendix A). However, the tail incidence will be a function of wing incidence, and this variation can be zero, or any value up to the maximum available from the horizontal tail.
2. The moment between the fuselage and wing (M_p) is constant.
3. The pitch acceleration of the wing is zero following the Δi_w perturbation. This is roughly equivalent to attitude stabilization of the system.

The fuselage pitch equation is:

$$\ddot{\theta}_f \left[I_f + m_w \frac{m_f}{m} (h^2 + l^2) \right] + \ddot{\theta}_w m_w \frac{m_f}{m} L_w (h \sin \lambda - l \cos \lambda) \\ = M_{ft} - M_p - \frac{m_f}{m} q_s S C_{RS} [h \sin(\gamma + \alpha_f) + l \cos(\gamma + \alpha_f)] \quad (22)$$

Differentiating within the above assumption gives:

$$\begin{aligned}
 \frac{d^2\theta_f}{di_w} [I_f + m_w \frac{m_f}{m} (h^2 + \ell^2)] = & \quad (23) \\
 - \frac{m_f}{m} q_s S \frac{dC_{RS}}{di_w} [h \sin(\gamma + \alpha_f) + \ell \cos(\gamma + \alpha_f)] \\
 - \frac{m_f}{m} q_s S C_{RS} \frac{d\gamma}{di_w} [h \cos(\gamma + \alpha_f) - \ell \sin(\gamma + \alpha_f)]
 \end{aligned}$$

The performance in the transition corridor has been defined for $(\alpha_f + \gamma) = 0$, which is the initial condition for the control deflection. Therefore, equation (23) becomes:

$$\begin{aligned}
 \frac{d^2\theta}{di_w} [I_f + m_w \frac{m_f}{m} (h^2 + \ell^2)] = & \\
 - \frac{m_f}{m} q_s Sh \left[\frac{\ell}{h} \frac{dC_{RS}}{di_w} + C_{RS} \frac{d\gamma}{di_w} \right] & \quad (24)
 \end{aligned}$$

Similar derivations for the axial and normal accelerations give:

$$\frac{d\dot{u}}{di_w} = g \frac{d\gamma}{di_w} \quad (25)$$

$$\frac{d\dot{w}}{di_w} = - \frac{g}{C_{RS}} \frac{dC_{RS}}{di_w} \quad (26)$$

It should be noted that the definition

$$\gamma = \tan^{-1} C_{X_S}/C_{L_S}$$

is valid for flight path angle only for unaccelerated flight, and that

$$di_w = d\alpha_{TL}$$

The control response due to wing incidence for the aircraft described in Table I and Appendix A are presented in Figure 12. The response at $CT_S = 1.0$ are shown along the $\gamma = 0$ axis, although γ is indeterminate at hover.

The control response in pitch due to wing incidence is of major importance only at low speeds (hover to about 50 knots). Beyond 50 knots the horizontal tail generates a sufficient moment to control the pitch mode. If the pilot is provided with sufficient wing incidence due to stick deflection to fly from hover to 60 knots without retrimming, he will have approximately 60 degrees of wing incidence for control (see Figure 11). This is more than adequate to meet any of the pitch acceleration control specifications for hover, and, in view of the axial and normal accelerations obtained, is probably too much to be used in a practical way. (The derivatives presented in Figure 12 are based on perturbations. $\ddot{\theta}$ and η_x are $\sin \Delta i_w$ functions, η_z is $\cos \Delta i_w$ for large angles, but only for high CT_S .)

Time Lag for Δi_w Response

The control responses shown in Figure 12 are those attained after a wing perturbation occurs. The lag in development of response is critical in establishing the handling qualities. In order to provide some visibility to the magnitude of the lag, a simplified wing response analysis has been performed. The analysis assumes the fuselage to be a stable platform during the wing movement, which, again is justified by the 12:1 ratio of nontilting/tilting systems inertias. For $\ddot{\theta}_f = 0$, the

simplified tilting system pitch equation is:

$$\ddot{\theta}_w \left[I_w + m_f \frac{m_w}{m} L_w^2 \right] = M_w + M_p \quad (27)$$

The X and Z terms have been dropped from equation (27) since their effect is relatively small and favorable. The equation relating wing incidence, stick position and flap deflection is:

$$i_w = i_{w_0} + i_{w_0 \delta_s} \delta_s + k \delta_f \quad (28)$$

Where i_{w_0} = wing incidence at zero stick
and flap deflection

$i_{w_0 \delta_s}$ = sensitivity of wing reference
position to stick deflection

k = flap linkage gain, $\frac{\Delta i_w}{\Delta \delta_f}$ for
 i_{w_0} constant

The term ($i_{w_0 \delta_s}$) represents the output of the wing actuator, and, in this analysis, is represented as a first order lag. The hovering flight condition was chosen since it is the most critical for control (and also where the lag may be greatest).

The hovering control responses are presented in Figure 13. The tilting system pitch damping ($M_{\theta_w}^{\cdot}$) was assumed to be 10 percent greater than the pitch damping of the propellers, as estimated by the methods of Reference (8).

The upper plot in Figure 13 presents the time history of wing displacement for a step flap deflection. For a 10-degree flap deflection, the wing incidence change will be 10 degrees at

0.72 seconds. Based on Figure 12, this will give a pitch acceleration on the fuselage of 0.23 rad/sec^2 , and an axial acceleration of 5.6 ft/sec^2 . The lower plot of Figure 13 presents the time histories of wing incidence for a step stick deflection, with a flap gain of 10-degree flap deflection per degree wing incidence change. For this gain, the damping ratio is 0.133, for no damper between the wing and fuselage; a damping ratio of 0.7 was assumed for the case with a damper between the wing and fuselage. Also shown in this plot is a time history for critical damping, and no lag for the control actuator. These time histories show that the 60 percent of the desired control response is achieved in approximately 0.25 seconds. It should be noted that this is only for small perturbations. For large deflections, it may be desirable to rate limit the actuator to prevent driving the flap to its stops, or to limit the flap deflection used for control to approximately 10 degrees.

Fuselage Response to Propeller Blade Pitch Changes

The fuselage response to a thrust change (blade pitch change) may be calculated neglecting the wing transients. At a flap gain of 10 degrees flap per degree wing incidence, the maximum wing incidence change, with flap deflection going from 0 to 40 degrees, is 4 degrees. Also, with attitude stabilization the wing rate and acceleration tend to be zero following the perturbation. The following analysis also neglects the horizontal tail contribution to the response, which is not justified in view of the changes in ϵ and η_t that will occur with a thrust change. At hover and low speed (C_{T_S} values .7 and lower), this tends to attenuate the pitch response, which is desirable.

Differentiating equation (22) within the above assumptions gives:

$$\begin{aligned} \frac{d\ddot{\theta}_f}{dT} [I_f + m_f \frac{m_w}{m} (h^2 + \ell^2)] = \\ - \frac{m_f}{m} S \left[\frac{\partial q_s}{\partial T} C_{RS} + \frac{\partial C_{RS}}{\partial T} q_s \right] [h \sin(\gamma + \alpha_f) + \ell \cos(\gamma + \alpha_f)] \\ - \frac{m_f}{m} S q_s C_{RS} \frac{\partial \gamma}{\partial T} [h \cos(\gamma + \alpha_f) - \ell \sin(\gamma + \alpha_f)] \end{aligned} \quad (29)$$

For all analyses thus far, $(\gamma_o + \alpha_{fo}) = 0$, or $\theta_{fo} = 0$ for un-accelerated flight conditions.

The derivatives required are:

$$\frac{\partial q_s}{\partial T} = \frac{1}{\pi R^2}$$

$$\frac{\partial C_{RS}}{\partial T} = \frac{\partial C_{RS}}{\partial C_{TS}} \frac{(1 - C_{TS})}{q_s \pi R^2}$$

$$\frac{\partial \gamma}{\partial T} = \frac{\partial \gamma}{\partial C_{TS}} \frac{(1 - C_{TS})}{q_s \pi R^2}$$

Substituting gives (for $\gamma_o = \alpha_{fo}$):

$$\begin{aligned} \frac{d\ddot{\theta}_f}{dT} [I_f + m_w \frac{m_f}{m} (h^2 + \ell^2)] = \\ - \frac{m_f}{m} \left(\frac{S}{\pi R^2} \right) h \left\{ \frac{\ell}{h} \left[C_{RS} + (1 - C_{TS}) \frac{\partial C_{RS}}{\partial C_{TS}} \right] + C_{RS} (1 - C_{TS}) \frac{\partial \gamma}{\partial C_{TS}} \right\} \end{aligned} \quad (30)$$

The linear acceleration responses, similarly obtained are:

$$\frac{d\dot{u}}{dT} = \frac{1}{m} \left(\frac{S}{R^2} \right) C_{RS} (1 - C_{TS}) \frac{\partial \gamma}{\partial C_{TS}} \quad (31)$$

$$\frac{d\dot{w}}{dT} = -\frac{1}{m} \left(\frac{S}{R^2} \right) \left[C_{RS} + (1 - C_{TS}) \frac{\partial C_{RS}}{\partial C_{TS}} \right] \quad (32)$$

The derivatives are obtained by reading slopes from plots of C_{RS} vs C_{TS} , and γ vs C_{TS} at $\alpha_{TL} = \text{constant}$.

The results of the analyses are presented in Figure 14, as a function of C_{TS} and initial flight path angle. Based on the results presented in Figure 12, the pitch response due to a propeller blade pitch change may be compensated for by 1 to 3 degrees of wing incidence change. If the horizontal tail were included in the analyses, the coupling would be less.

Horizontal Tail Control Effectiveness

In order to approach presenting a complete picture of the control characteristics in transition, the effectiveness of the horizontal tail is required. The tests presented in Reference 6 showed a low horizontal tail location to be most effective for a tiltwing aircraft, and this was also born out during the dynamic model tests. Therefore, an analysis of the low horizontal tail effectiveness was performed, and is presented in Figure 15 for flight path angles of 0 and ± 14 degrees. These data are presented for a tail volume coefficient, \bar{V} , of one and for a unity lift coefficient. No attempt has been made to define the tail lift coefficient required for fuselage trim, but at high C_{TS} values, this should be quite low. At low values of C_{TS} , the horizontal tail is sufficiently powerful to handle large values, if required.

The calculations are based on the downwash and tail efficiency data presented in Appendix A, assuming the tail drag coefficient is 0.2 of the tail lift coefficient.

HOVER TRIM CAPABILITY

The Geared Flap system is trimmed in hover using a combination of flap deflection, wing incidence, and fuselage attitude variations and is affected using variations of the constant force actuator between the wing and fuselage. The individual effects are as follows:

1. Flap deflection causes a diving aerodynamic moment about the hinge, and rotates the resultant motor, requiring a change in wing incidence to maintain zero horizontal acceleration.
2. Wing incidence change to compensate for turning moves to the total aircraft cg forward, reducing the Δcg to be trimmed.
3. The fuselage acts as a pendulum, with the nontilting mass cg tending to fall below the wing pivot for zero wing hinge moment. Allowing fuselage attitude to vary with cg, gives the same sort of variations with cg as in a single rotor helicopter.

The equilibrium pitch equation in hover is:

$$M_w - W_w L_w \cos \theta_w - W_f \left[h \sin \theta_f + l \cos \theta_f \right] = 0 \quad (33)$$

In coefficient form:

$$C_{H_{WS}} - \frac{m_w}{m} C_{RS} \left(\frac{L_w}{\bar{c}} \right) \cos \theta_w - \frac{m_f}{m} C_{RS} \left[\frac{h}{\bar{c}} \sin \theta_f + \frac{l}{\bar{c}} \cos \theta_f \right] = 0 \quad (34)$$

The required wing attitude, θ_w , is defined by the aerodynamic turning due to wing-propeller-flap system. The flap deflection determines the wing hinge moment, C_{HWS} . The resultant force coefficient, C_{RS} , is in general slightly dependent upon flap deflection because of the turning efficiency but may be assumed to be constant.

The turning effectiveness and wing hinge moment data obtained during hover tests prior to the tests reported in Reference (6) are presented in Figure 16. Figure 17 presents the hover trim capability carpet plot as a function of the "wing down" cg location.

Assuming that ± 10 degrees of flap deflection is required for control, and fuselage attitude may vary from 0 to 10 degrees in hover, a cg range of $0.11\bar{c}$ can be trimmed. The plot shows this to be well aft of the desired cg range; however, this range can be shifted by designing the aircraft with a pivot location closer to the wing chord line. This shifts the thrust line forward in hover, and the plot moves downward, and also changes the requirements of the constant force actuator. For the assumed configuration, placing the hinge line $0.007\bar{c}$ below the chord will shift the plot by $0.045\bar{c}$. Thus, the $0.25\bar{c}$ cg would trim at 15 degrees of flap deflection for the fuselage level.

DYNAMIC MODEL TESTS

GENERAL

The control system characteristics during transition at the limits of the flight envelope were possible to define analytically because sufficient data were available. This is not the case for the investigation of the stability and control characteristics during hover and STOL operations. In order to provide qualitative information in this area, a dynamic model flight test program was carried out.

MODEL AND TEST SETUP

The model used for the tests is basically similar to that described in Reference (5), with many modifications. Photographs of the model are shown in Figures 3 and 4, with two horizontal tail configurations. The low tail was used in the final evaluations, which will be discussed later. Table II presents a summary of the model geometric characteristics, and Table III, the weights, inertias, and center-of-gravity locations. The model is approximately a 1/19 scale of the configuration used for analysis and presented in Table I and Appendix B. Table IV presents a comparison of the full-scale and model parameters.

Tests were conducted indoors in a room approximately 50 feet square. The model was mounted to a boom 12 feet long and was flown in a circular path. The model pilot held a handle mounted to the inner end of the boom, and the actual radius of the circle flown was approximately 14 feet. A linkage from the boom to the control actuator in the model provided an attitude reference for stabilization, with the pilot's control (rotation of the boom) providing a bias signal. Throttle control was provided by a trigger on the control handle, linked to the

engines by a piano wire. The electrical tilt actuator received signals through two additional wires from a battery box and control switch carried by the pilot. Both the control and flap actuators were pneumatic, with the compressed air being supplied through the boom via an air hose connected to the boom handle.

The control system in the model is similar to that shown in Figure 1, except for the addition of powered actuators for the flaps, and substitution of a viscous damper for the constant force actuator. The pitch displacement of the boom actuated the pilot's stick. The stick boost was connected directly to the horizontal tail, as well as to the bellcrank shown.

The boom was made from 5/16-inch aluminum tubing with a wall thickness of 0.030 inch, and was mounted slightly above the nontilting system center of gravity. The mass and stiffness appeared to be negligible in their effect on the aircraft dynamics. Whipping the boom would cause only rolling or yawing motion, but no apparent linear or pitching accelerations. At marginal thrust/weight ratios, where the model would hover in ground effect, it was not possible to change the altitude by lifting on the boom. The boom was mounted to the fuselage through line-reamed brass bushings, and, therefore provided no pitch restraint. There was no discernible friction in the valve connected to the boom, and the air line in the fuselage contained a large loop to eliminate any pitch constraint due to tubing stiffness.

Check flights were made with only the pilot in the center of the circle; then, flights were made with a cameraman and helper using a sun-gun light standing in the center with the pilot. (Occasionally giving comically disastrous results, with three people tangled in an air hose, and the model still flying.) Filming of the model flights was done at 50 frames per second (maximum available) to provide approximate full-scale time when projected at 16 frames per second.

MODEL TESTS

The initial flights of the model were rather erratic, due to improper relative control system gain settings and low pilot proficiency. On the model, there are two gains to be set: the attitude stabilization into wing incidence, and into tail incidence. In addition, the total control throw must provide sufficient wing and tail incidence changes to cover the flight condition variations possible with a given wing trim position. The trim is defined by the electrical actuator position with the control actuator neutral. The gain settings used for the horizontal tail were not measured, but the wing incidence control gain was approximately unity (in effect this means simply maintaining wing attitude independent of fuselage perturbations). The final total control throw provided approximately 60 degrees of wing and tail incidence variation. Once the final gains and control throws were set, the flights progressed rather smoothly.

The model flights were performed to demonstrate the following points:

1. The aircraft with the Gear Flap control system is capable of flying continuous, reversible transitions, to and from hover, in and out of ground effect.
2. Self-induced turbulence in STOL operations presents no adverse effects on aircraft dynamics or control capability.

The flights demonstrating these points included rearward flight, and high rate accelerating and decelerating maneuvers as well.

In order to help define the tail incidence variations required, several flights were made with the horizontal tail linkage

disconnected. The tail center of gravity was close to the tail pivot, and the mass was quite low. This caused the tail to align (because of a forward pivot) closely to the local flow, even at very low speeds, and permitted observation of downwash changes in and out of ground effect as well as variations with angle of attack at various airspeeds in transition. Films of these flights were obtained, but are limited because of an inadvertent entry into a high speed flight condition where tail control power would have been important. The landing was semi-disastrous, but reparable.

Flow Visualization Technique

The demonstration of having flown through the self-induced turbulence condition was accomplished using a flow visualization technique. After considerable practice flying continuous accelerating transitions in ground effect in one revolution of the flight circle, the path was sprinkled liberally with balsa dust. The flow patterns generated were rather spectacular, and showed the recirculation to be most severe at about a 45-degree wing incidence. The films obtained were limited in the field of view and show only the flow in the immediate vicinity of the model. The conditions defined by the balsa dust tests were later investigated more thoroughly by additional flights at high and low speeds with no apparent problems.

Results

The demonstration of the capability to fly continuous transitions was performed first, since it also required development of pilot capability to provide proper balance between tail and wing incidence controls to establish trim (this would not be required if sufficient data were available to define and build into the model the required tail incidence variation as a function of wing incidence and stick deflection). Following the development of

pilot proficiency, the flights were conducted demonstrating the system capability in STOL operations and in self-induced turbulence. The results of these flights can only be evaluated qualitatively by opinions expressed either by the pilot or observers, or by viewing the flight films. (These are available in the film file at the Vertol Division of Boeing.) The consensus of both the pilot and those who observed the final flights is that the two basic issues were firmly resolved, and there exist no apparent problems.

CONCLUSIONS

As a result of a detailed analysis and evaluation of the Geared Flap control system, the following conclusions are drawn:

- . The system has the capability for controlling a tiltwing aircraft throughout its transition corridor with no auxiliary controls such as tail jets/rotors or cyclic propeller pitch.
- . There are no inherent system characteristics which generate adverse control responses throughout the transition corridor, including operation in ground proximity.

TABLE I

AIRCRAFT CONFIGURATION PARAMETERS REQUIRED FOR ANALYSIS
(HOVER DISC LOADING = 40 LB/FT²)

Weights:

Gross Weight, lbs	18,000
Non-tilting System Weight (Fuselage), lbs	13,360
Tilting System Weight (Wing, Prop., etc.), lbs	6,640

Inertias and cg Dimensions (In form required for analysis)

Fuselage Inertia Term, $[I_f + m \frac{m_f}{m} (h + l^2)]$, slug-ft ²	39,568
Wing Inertia Term, $[I_w + m \frac{m_f}{m} L_w^2]$, slug-ft ²	3,165
L_w , Distance from wing pivot to tilting cg, ft	1.74
α , Angle between wing chord and line between wing pivot and tilting cg, deg.	0
h , Vertical distance between wing pivot and fuselage cg., ft	4.71
l , Horizontal distance between wing pivot and fuselage cg., ft	.34

Aircraft Dimensions and Areas

Wing:

Area, ft ²	310
Span, ft	36.4
Mean chord, ft	8.54

Propellers:

Disc Area, ft ²	225
Diameter, ft	17.95
Solidity	.25
Tip Speed (assumed), ft/sec	900

TABLE II

MODEL GEOMETRIC CHARACTERISTICS

<u>Fuselage Length, in.</u>	26.7
<u>Propeller Diameter, in</u>	9.0
(Standard model propellers were used, with pitch selection dependent of hover performance)	
<u>Wing: (Rectangular planform)</u>	
Area, in ²	120.0
Span, in	24.0
Chord, in	5.0
Aspect Ratio	4.8
Airfoil Section	NACA 4415
Flap chord, in	2.0
Flap Geometry -- See Appendix A, Figure 4	
Wing hinge location (from leading edge), in	2.0
<u>Vertical Tail (including fixed rudder)</u>	
Area (from mounting), in ²	26.6
Span (from mounting), in	6.00
Root chord, in	6.0
Tip chord, in	3.50
Sweepback (leading edge), deg	27.
<u>Horizontal Tail (all movable):</u>	
Area, in ²	53.6
Span, in	15.0
Aspect Ratio	4.20
Root Chord, in	5.25
Tip Chord, in	4.50
Hinge line, percent tail mcg,	.25
Sweepback, leading edge, deg	0
Tail Volume Coefficient	1.05
<u>Miscellaneous:</u>	
Horizontal distance from wing pivot to horizontal tail, in	11.75
Vertical distance from wing pivot to horizontal tail, in	0
Location of wing pivot relative to mcg, percent	40
Distance of propellers from wing leading edge, in	2.50
Distance of thrust axis below pivot, in	.35
Distance of thrust axis below chord line, in	.60
Distance between propellers, in	13.50
<u>Engines:</u> Thimble-Drome Olympic's equipped with Thimble-Drome Sportsman carburetor bodies and Roto-Valve throttle Assemblies.	
Manufacturer: L. M. Cox Mfg. Co., Inc., Santa Anna, Calif.	

TABLE III

WEIGHTS AND INERTIAS

Item	W, lbs	$I_{y_{cg}}$, Slug-ft ²
Total Aircraft (No Fuel)	3.470	0.02050
Total Aircraft (With Fuel)	3.689	.02211
Fuselage (No Fuel)	1.813	.01429
Fuselage (With Fuel)	2.032	.01500
Wing	1.657	.001422

CENTER-OF-GRAVITY LOCATIONS
(PERCENT MGC)

Item	Longitudinal (mgc)	Vertical (from wing pivot)
Total Aircraft (No Fuel)	24.4	18.3
Total Aircraft (With Fuel)	28.8	18.2
Fuselage (No Fuel)	35.6	35.0
Fuselage (With Fuel)	42.5	33.0
Wing	12.0	0

TABLE IV
COMPARISON OF MODEL AND FULL SCALE
AIRCRAFT CHARACTERISTICS

	Full scale	1/19 Scale	Model
Weight, lb	18,000	2.62	— —
	24,000	3.50	3.47
Wing Area, ft ²	310	.858	.833
Wing Span, ft	36.4	1.915	2.00
Chord, ft	8.54	.449	.417
Prop. Diam., ft	17.95	.945	.750
Pitch Inertia, slug-ft ²	43,300	.0175	.02050

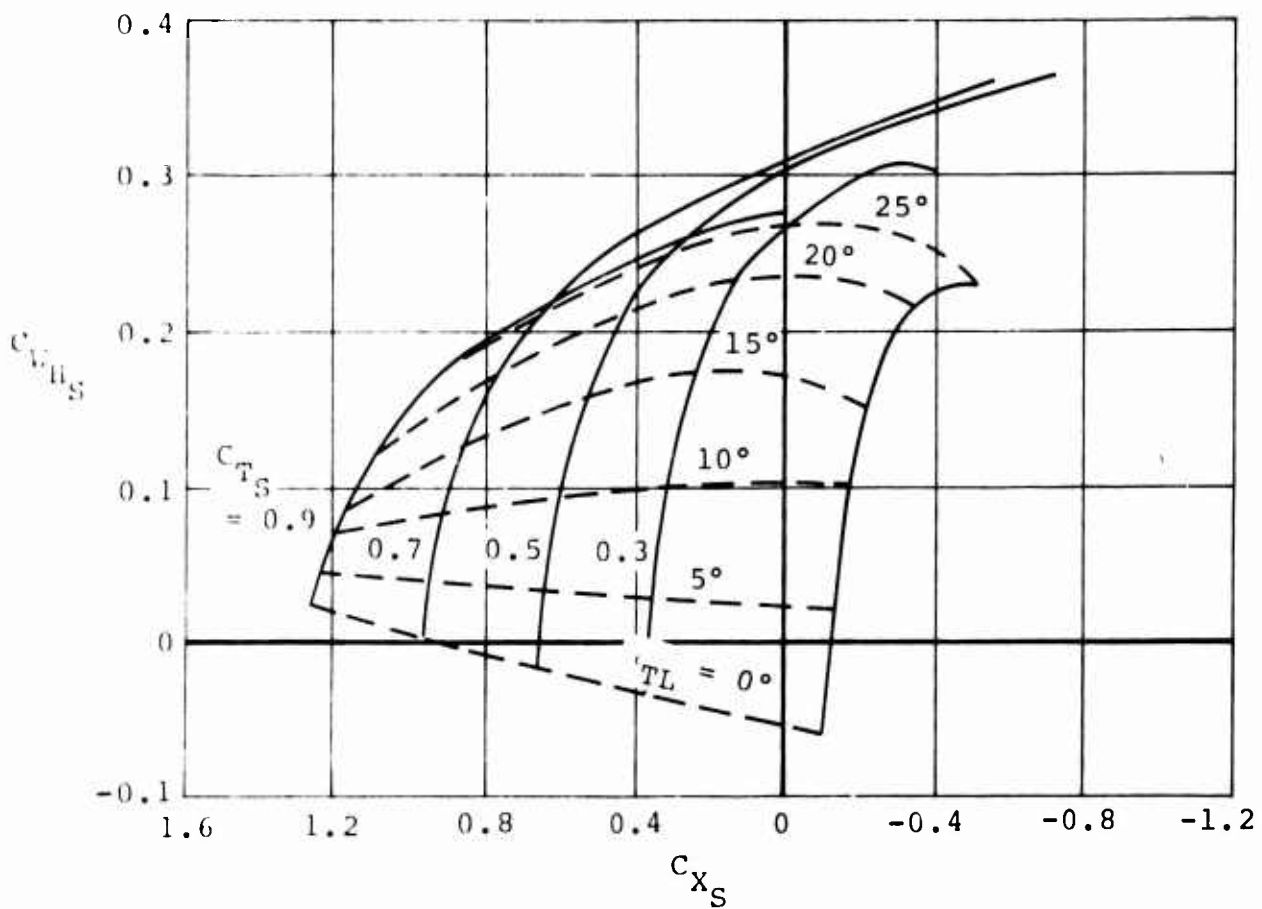
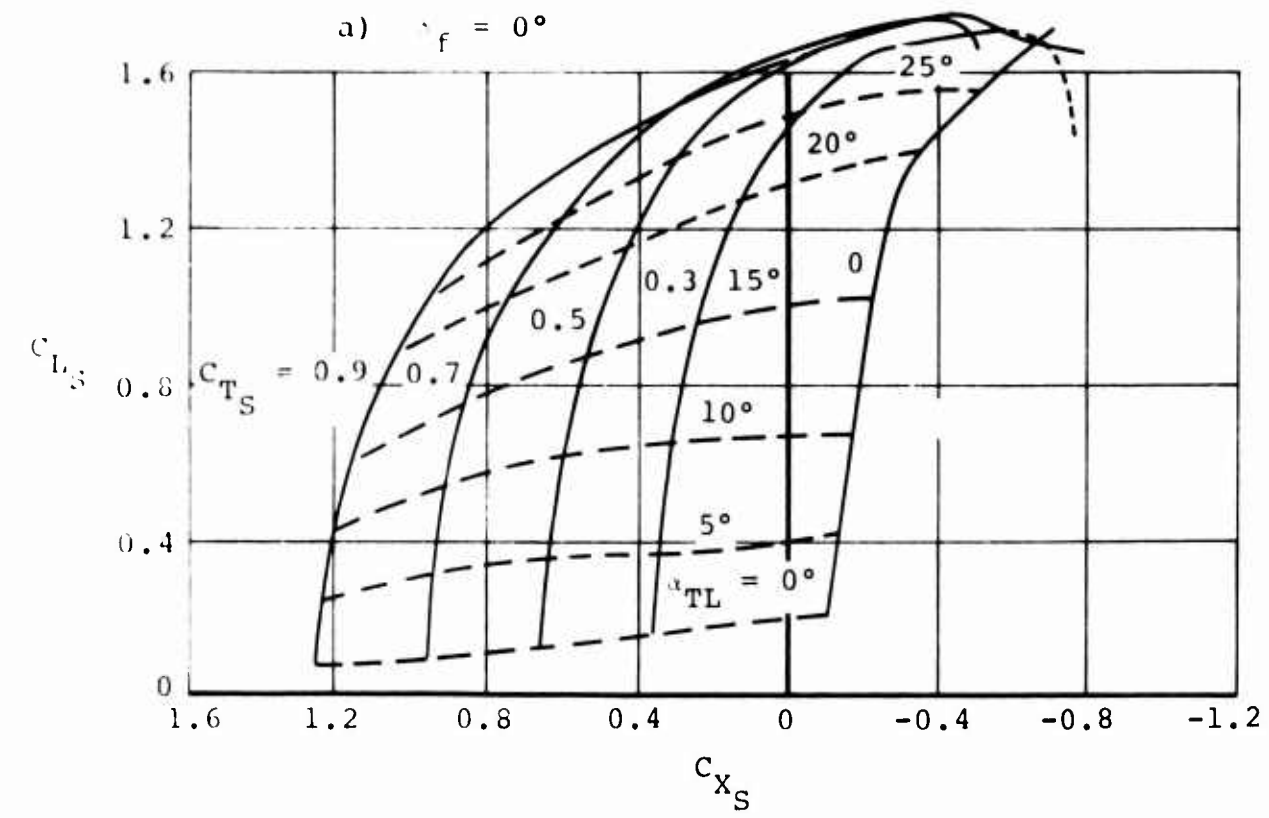


Figure 5. Basic Aerodynamic Data. (1 of 3)

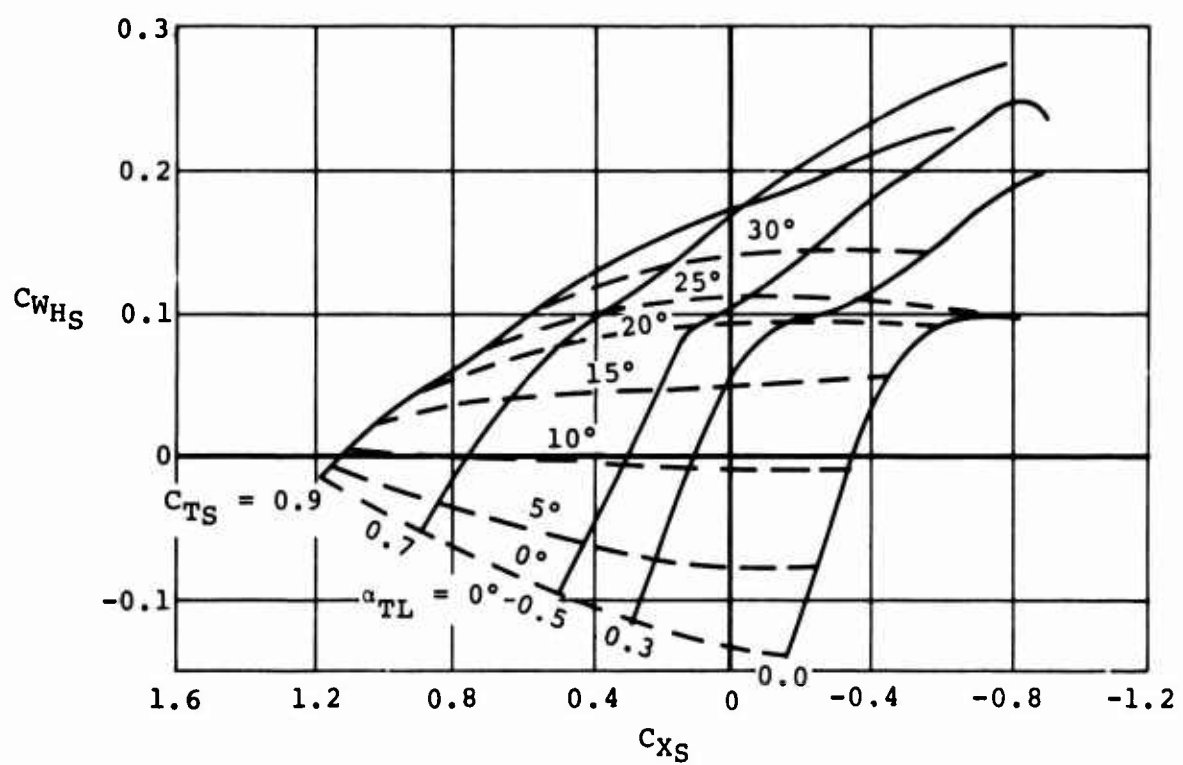
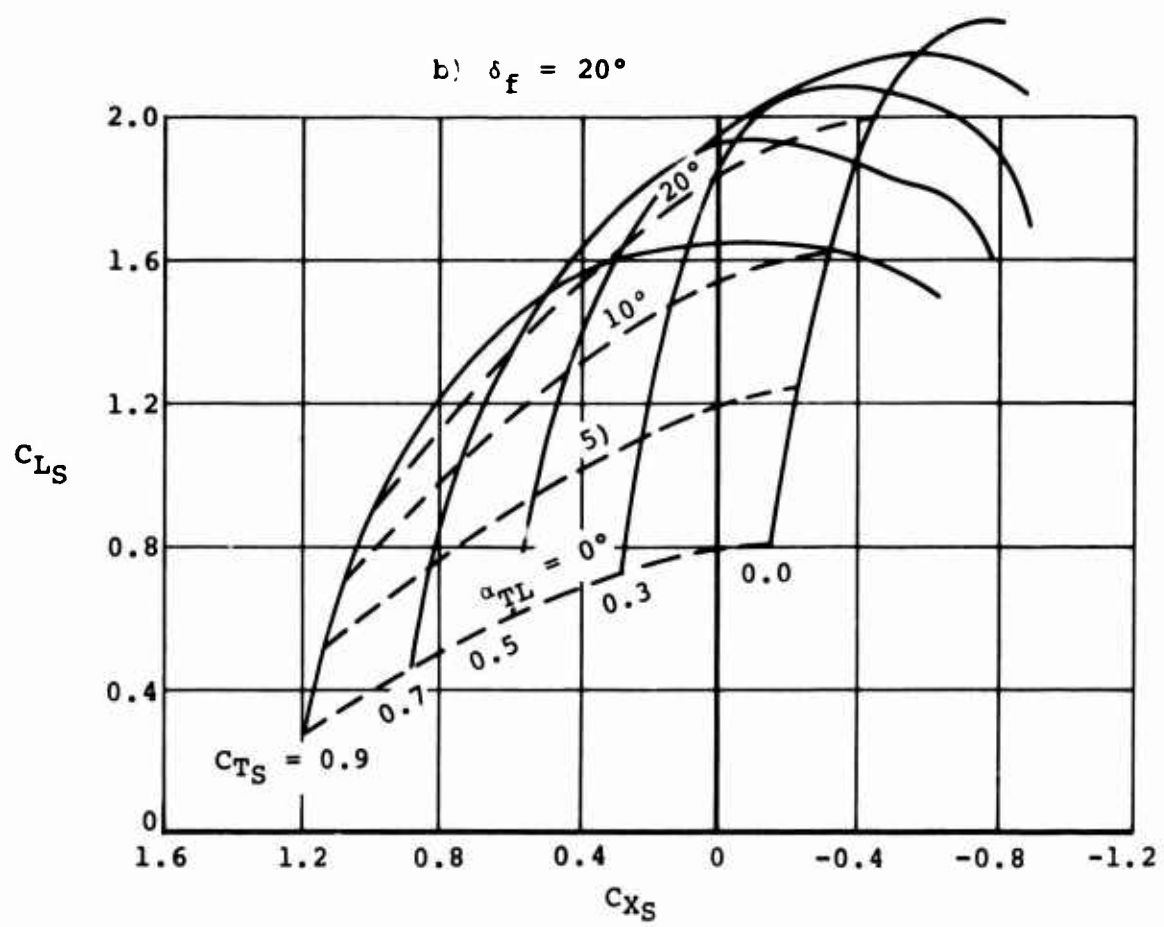


Figure 5. Basic Aerodynamic Data. (2 of 3)

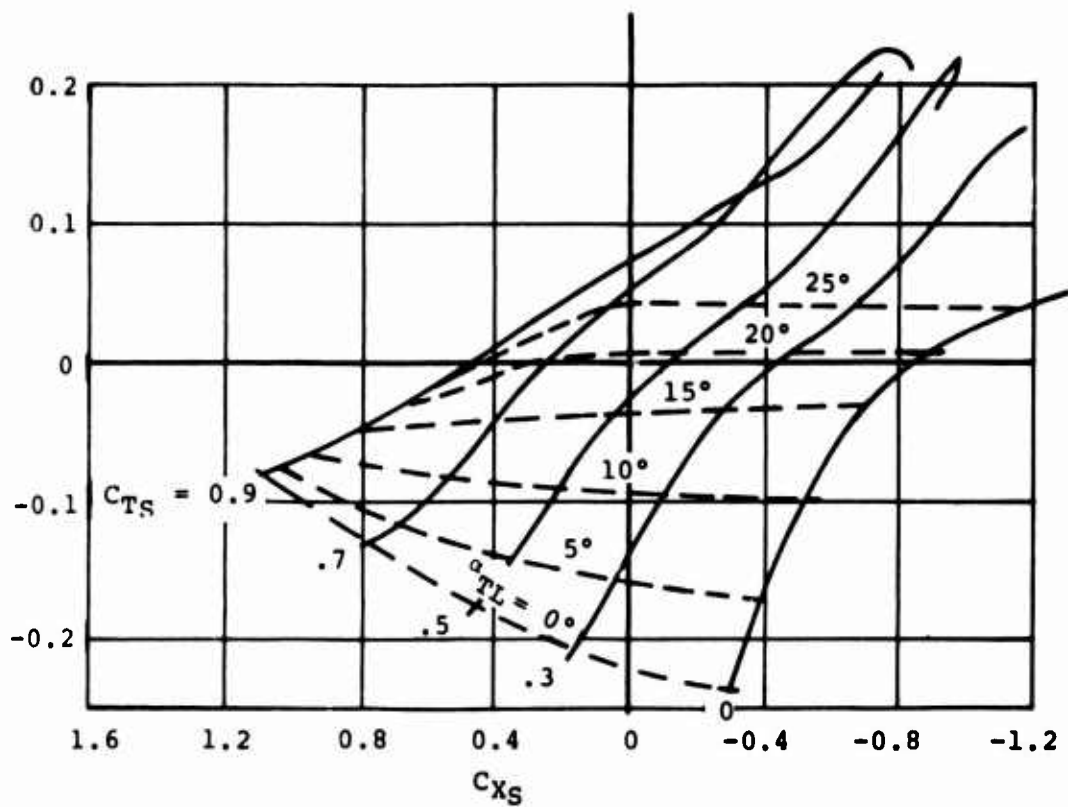
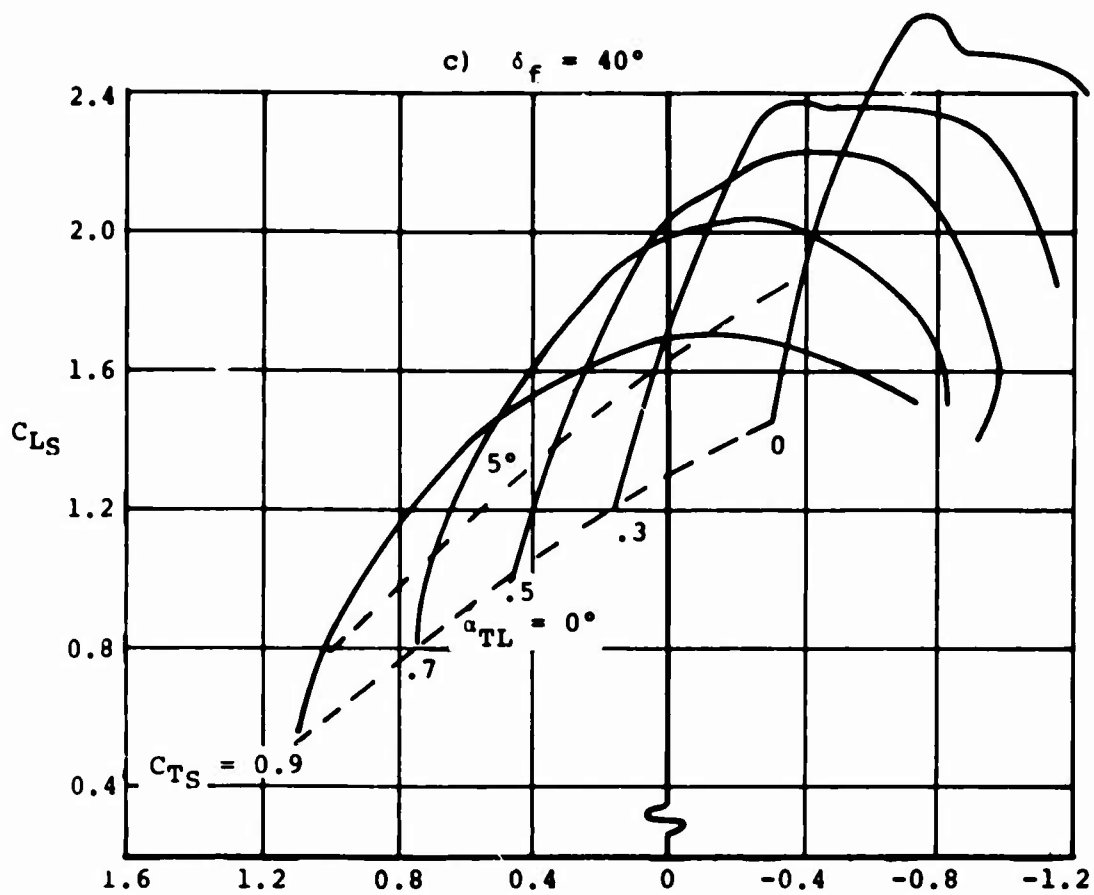


Figure 5. Basic Aerodynamic Data. (3 of 3)

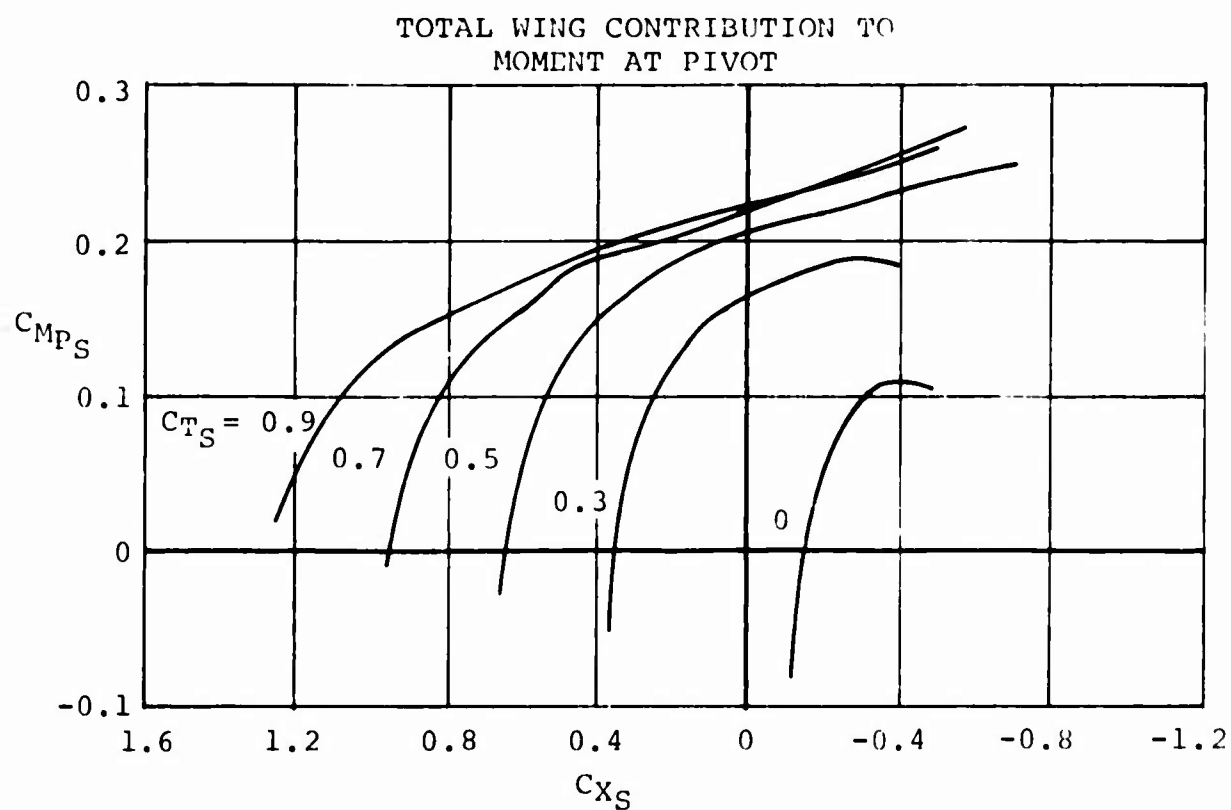
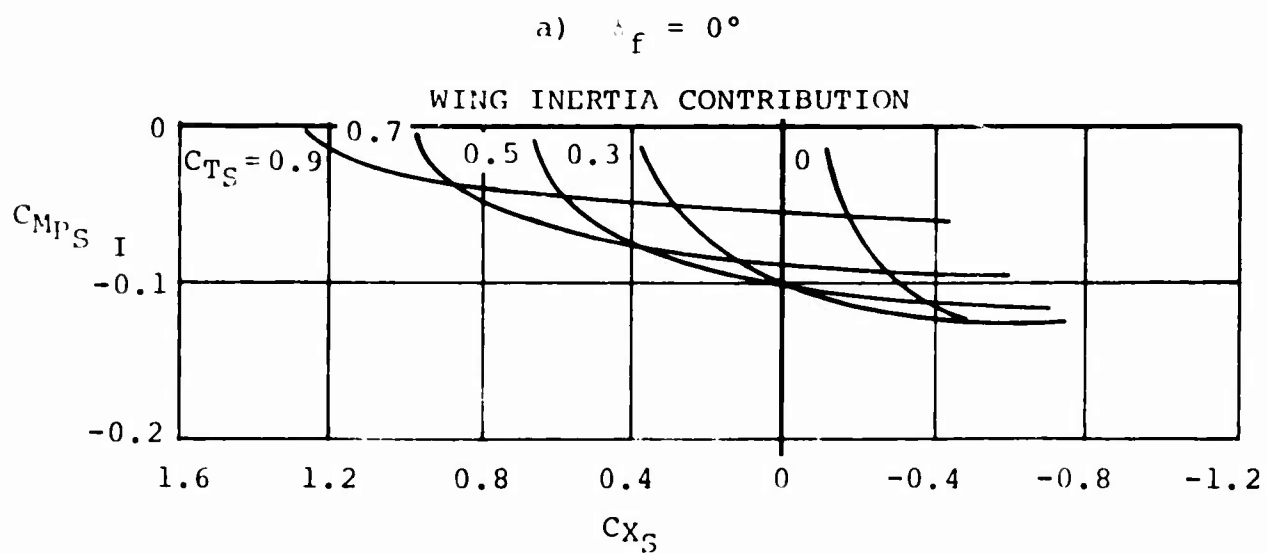


Figure 6. Wing Inertia Effects on Hinge Moment. (1 of 3)

b) $\alpha = 20^\circ$

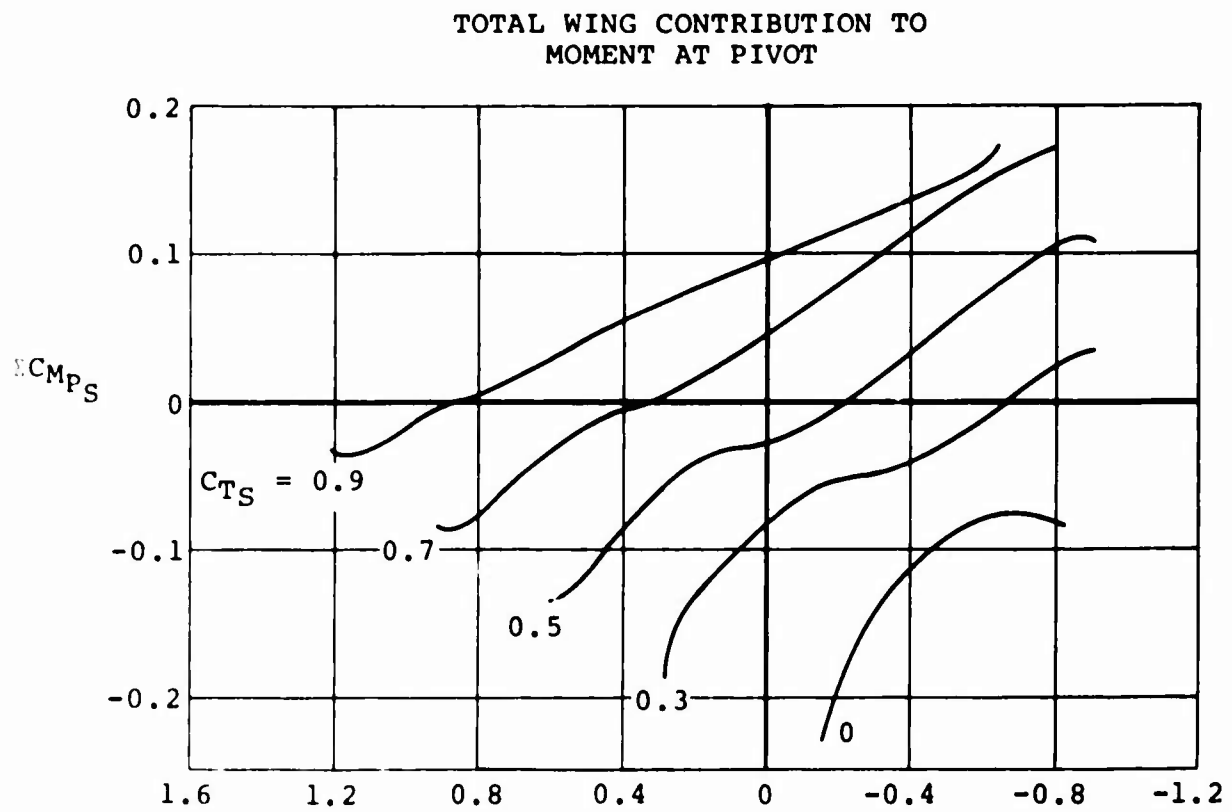
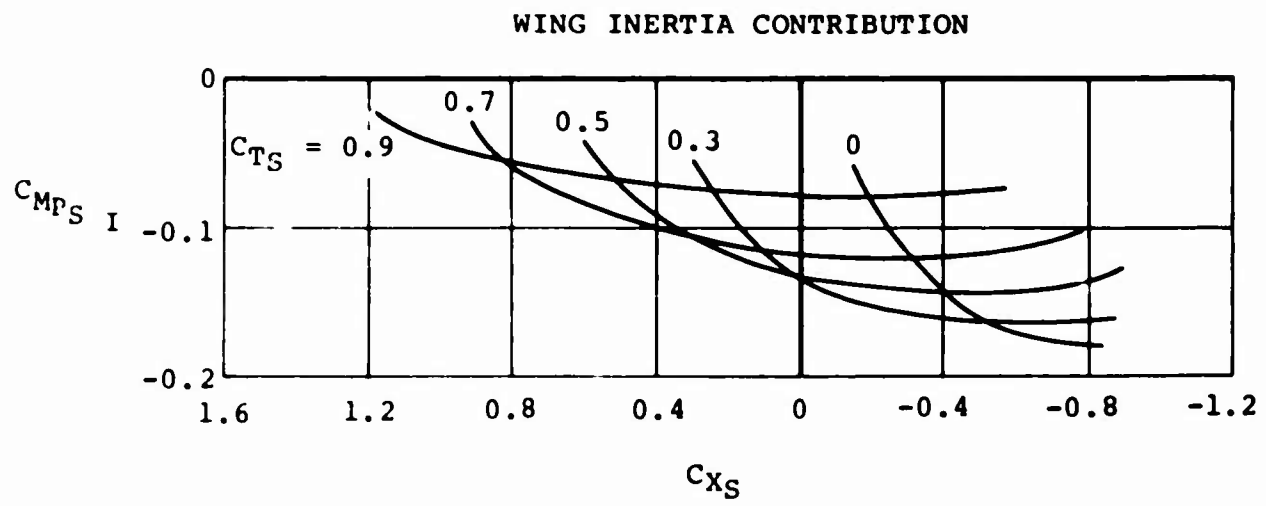


Figure 6. Wing Inertia Effects on Hinge Moment. (2 of 3)

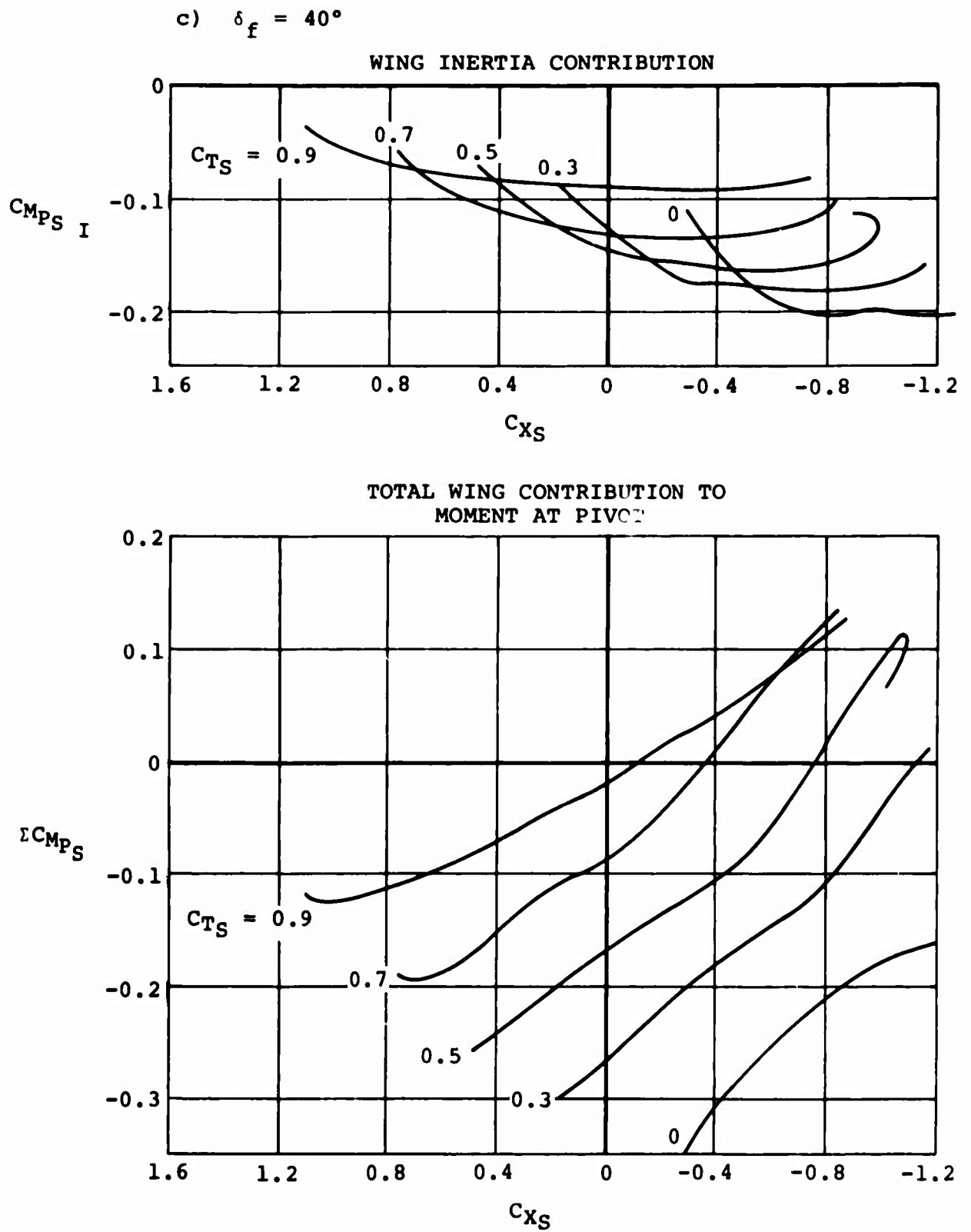


Figure 6. Wing Inertia Effects on Hinge Moment. (3 of 3)

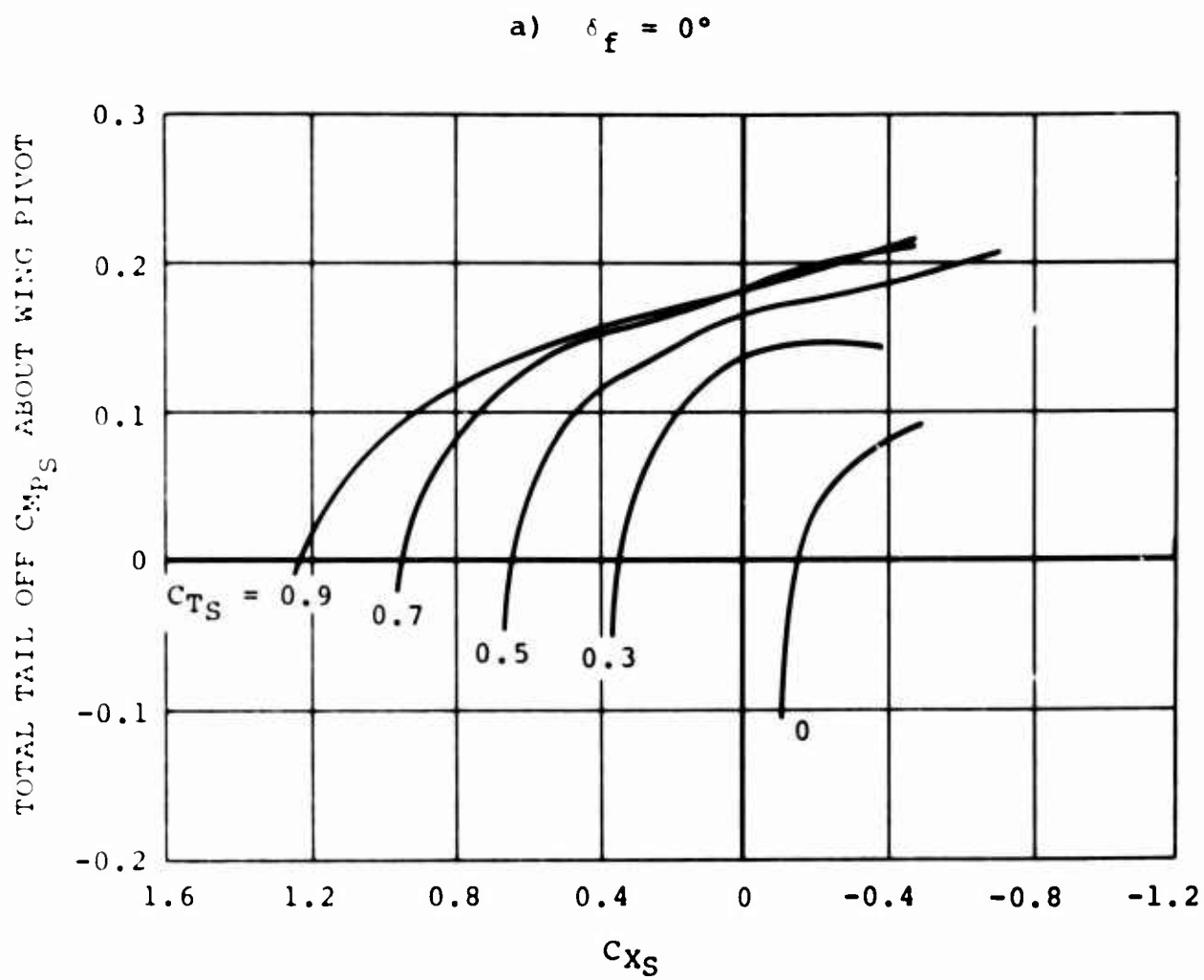


Figure 7. Total Aircraft Moments About Pivot - Tail Off,
 $\delta_f = 0^\circ$. (1 of 3)

b) $\alpha_f = 20^\circ$

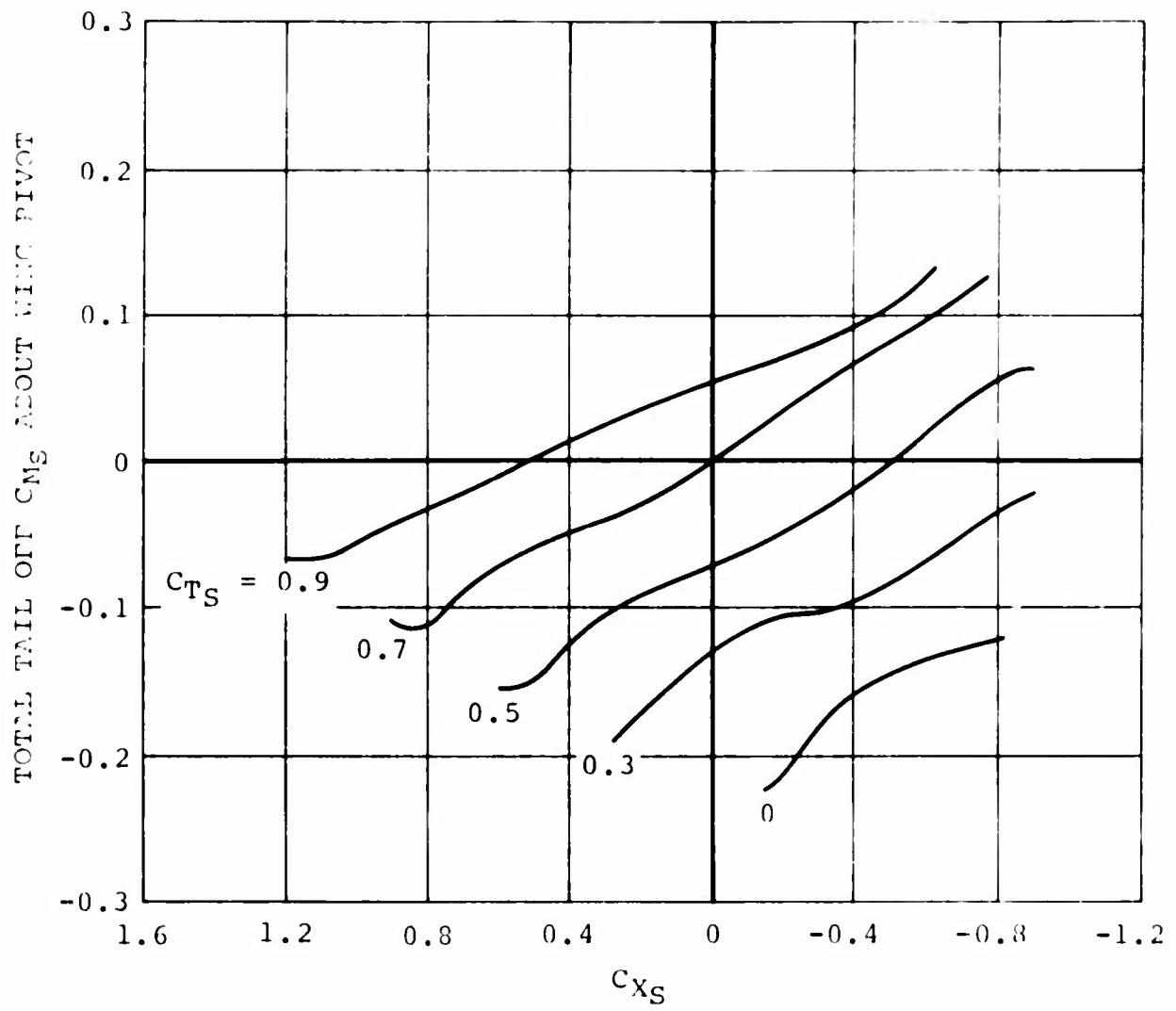


Figure 7. Total Aircraft Moments About Pivot - Tail Off,
 $\alpha_f = 0^\circ$. (2 of 3)

c) $\alpha_f = 40^\circ$

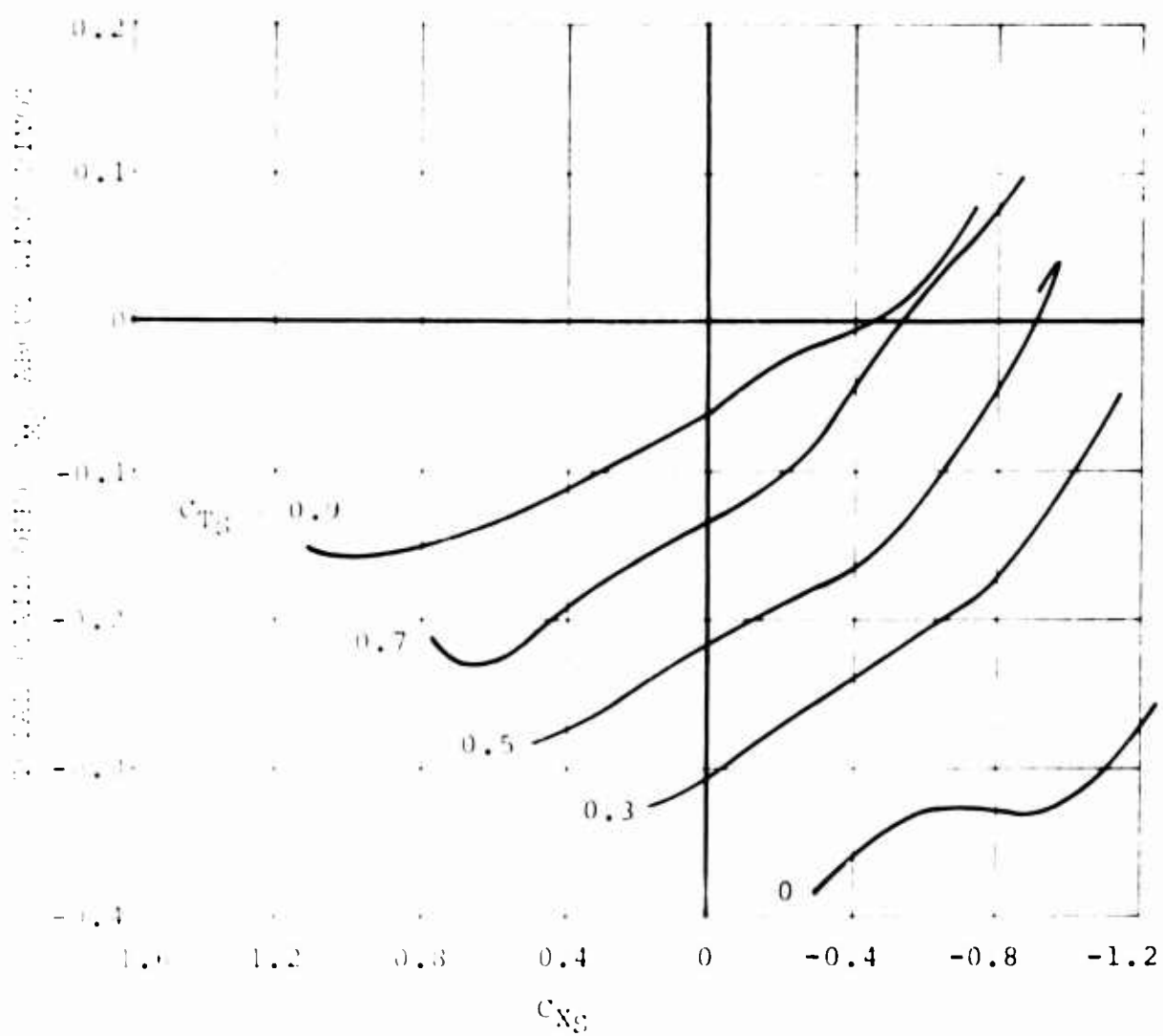


Figure 1. Total Aircraft Moments About Pivot - Tail Off,
 $\alpha_f = 0^\circ$. (3 of 3)

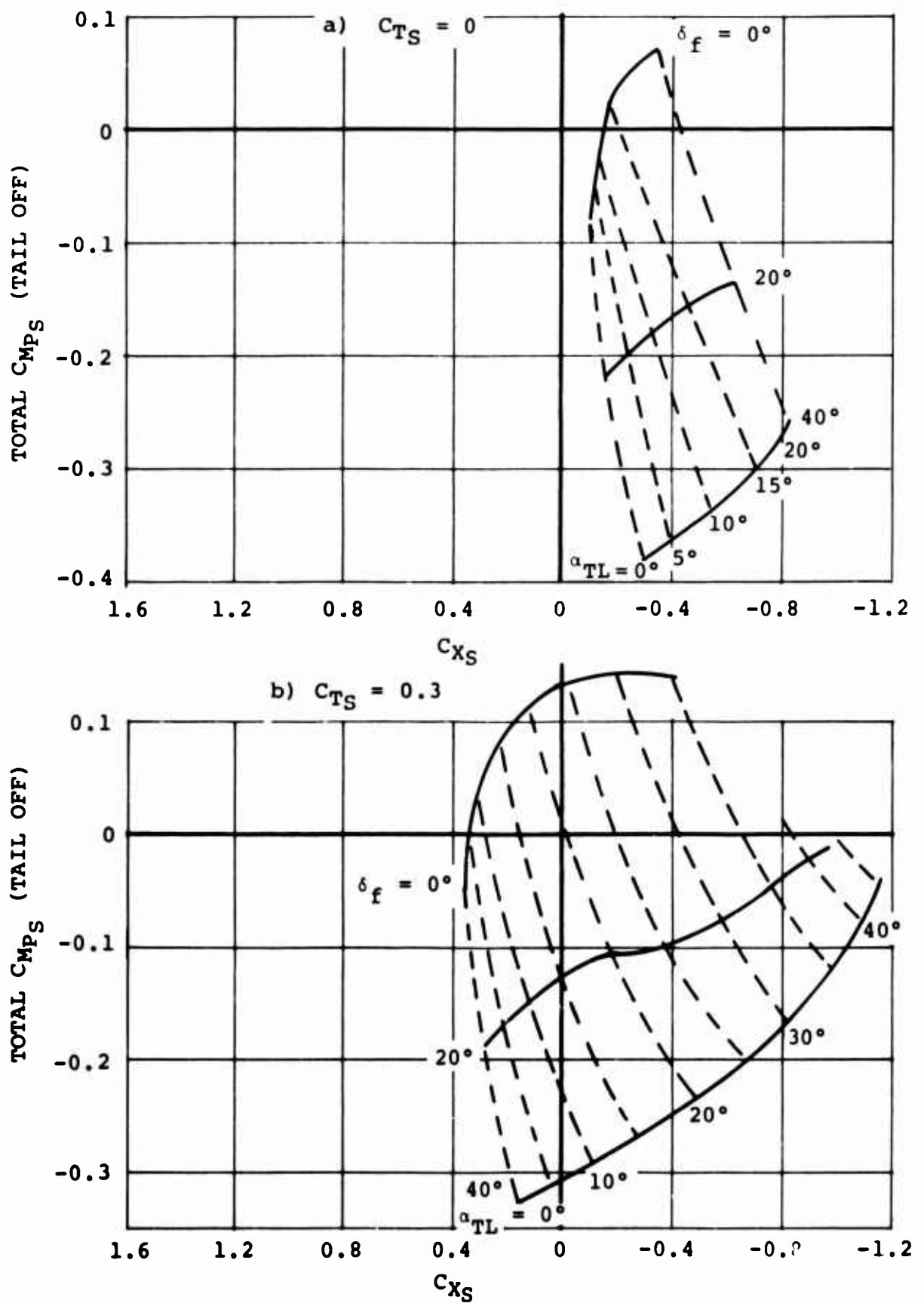


Figure 8. Variation of Total Moment at Constant C_{TS} . (1 of 3)

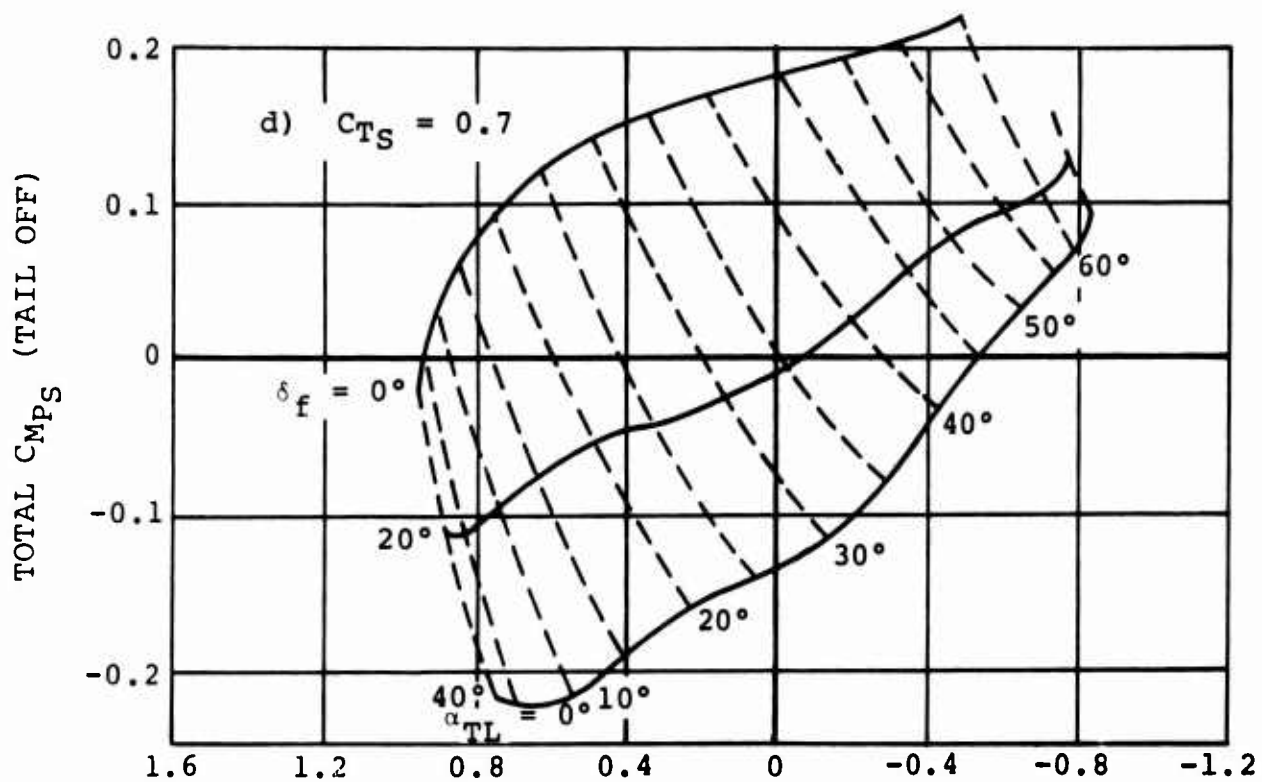
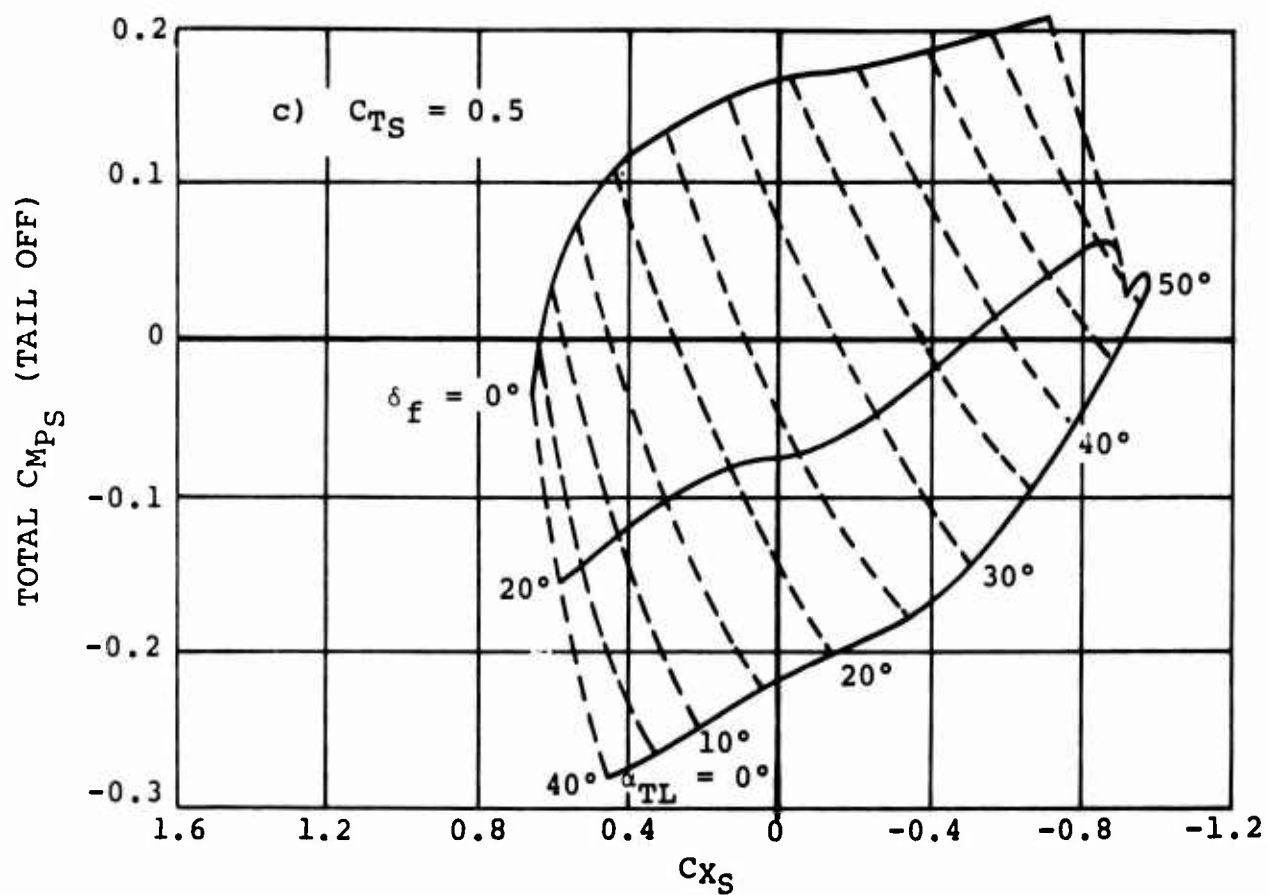


Figure 8. Variation of Total Moment at Constant C_{TS} . (2 of 3)

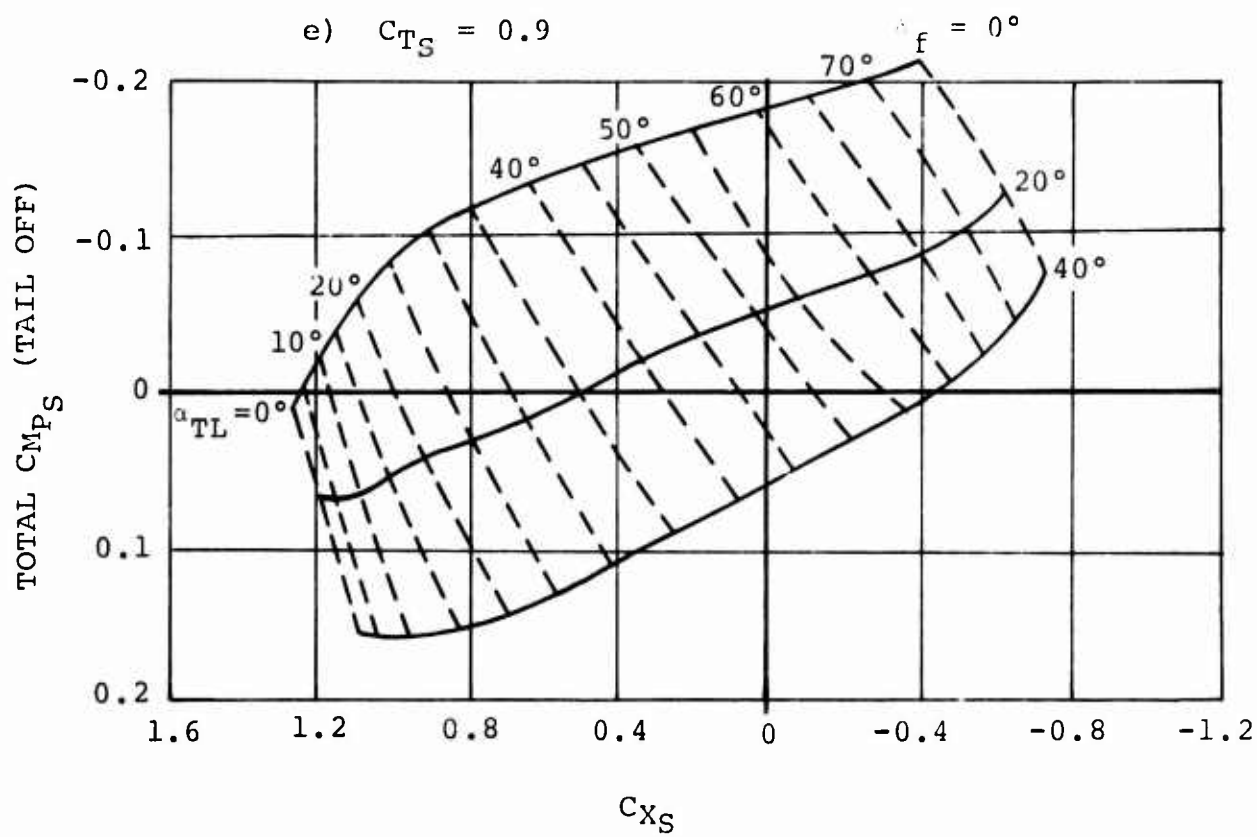


Figure 8. Variation of Total Moment at Constant C_{TS} , (3 of 3)

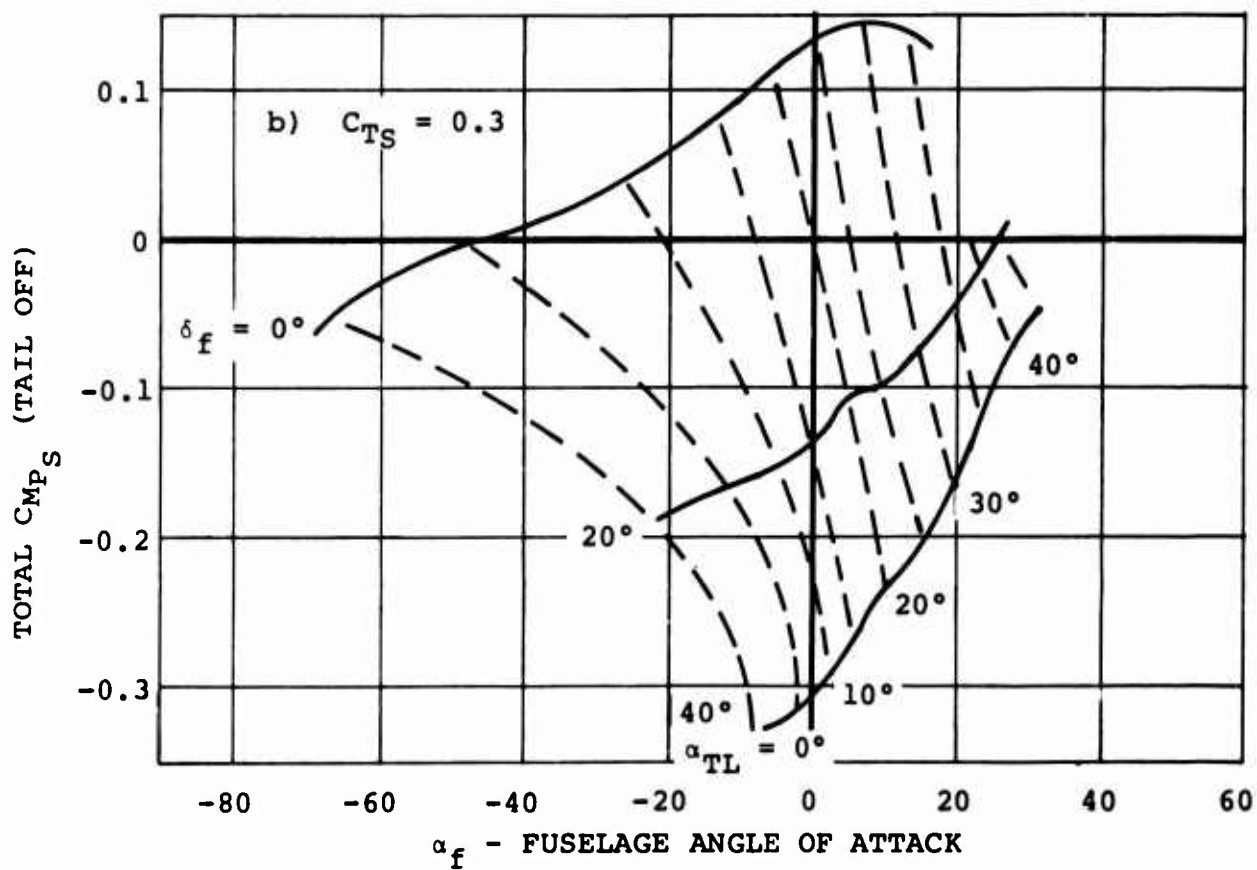
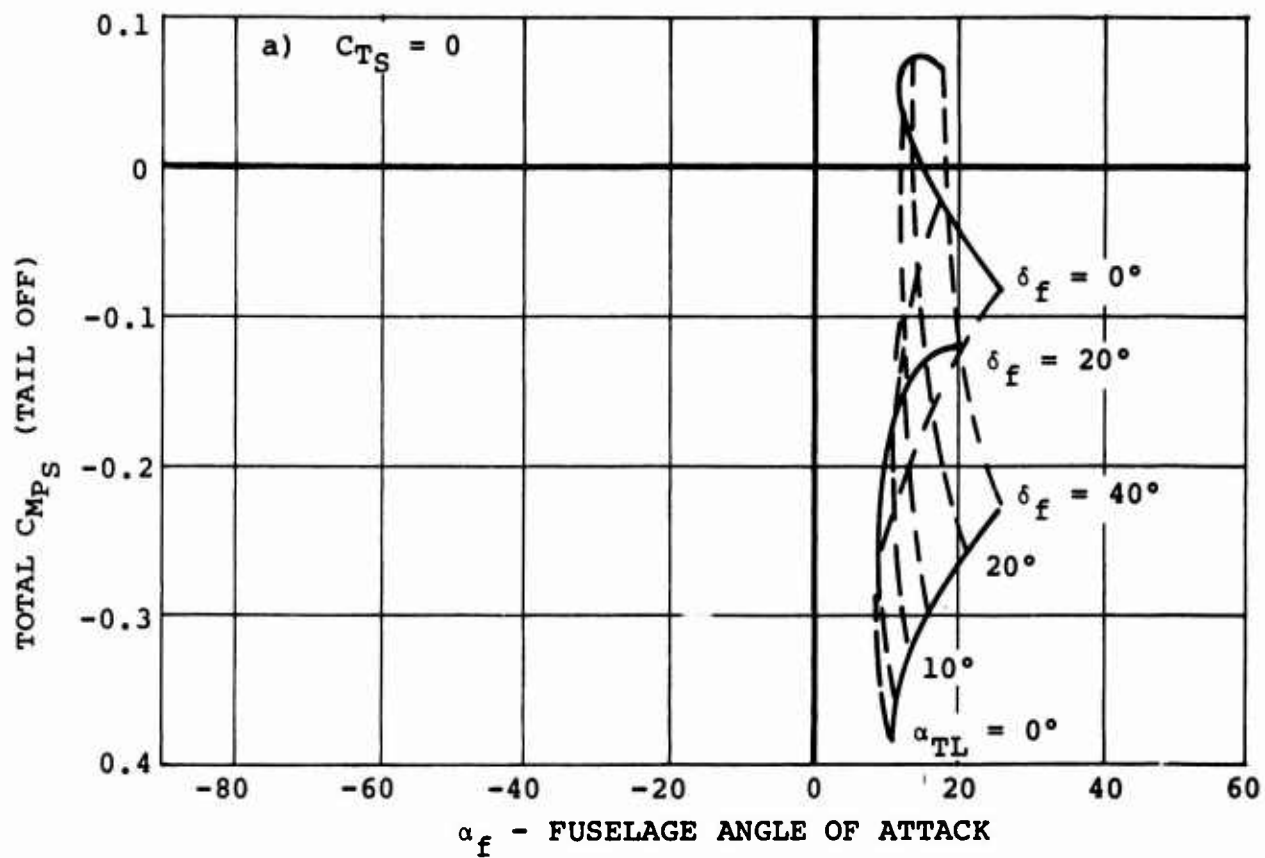


Figure 9. Variation of Total Moment with Fuselage Angle of Attack. (1 of 3)

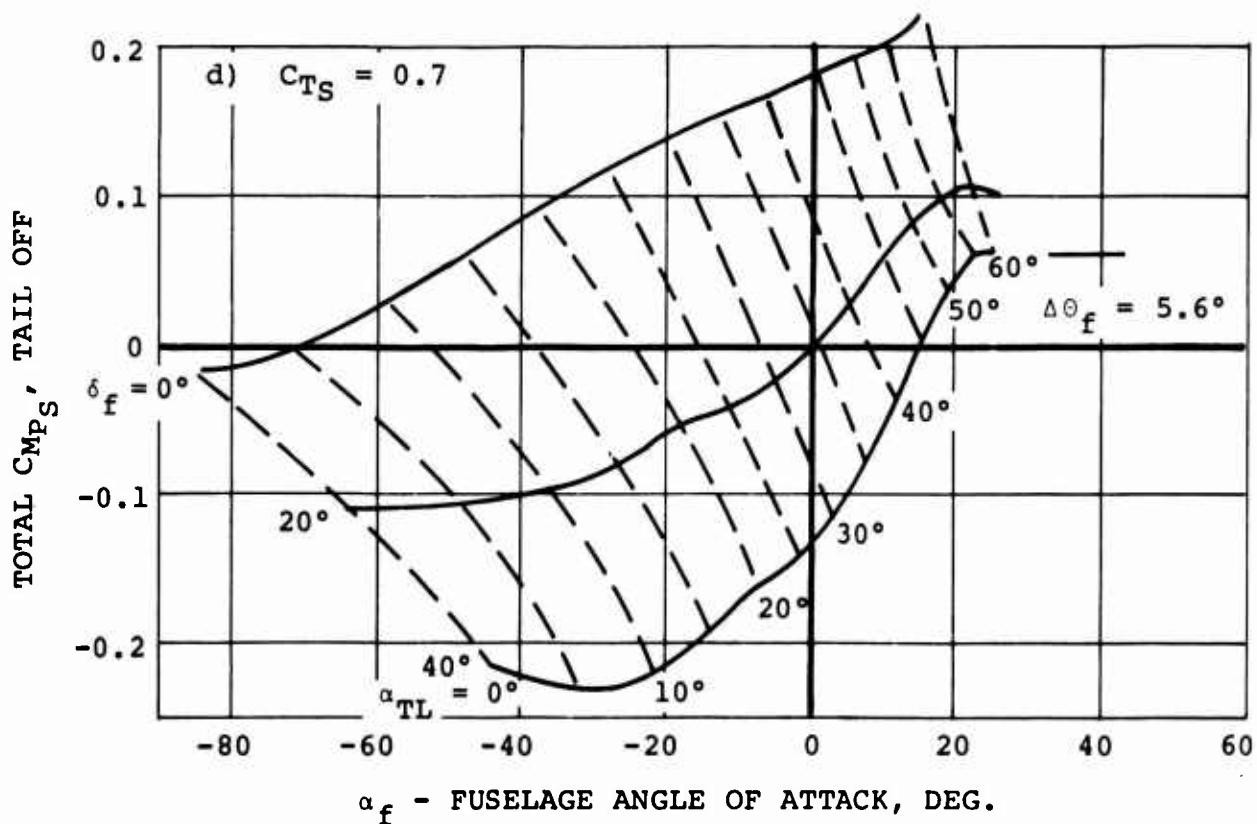
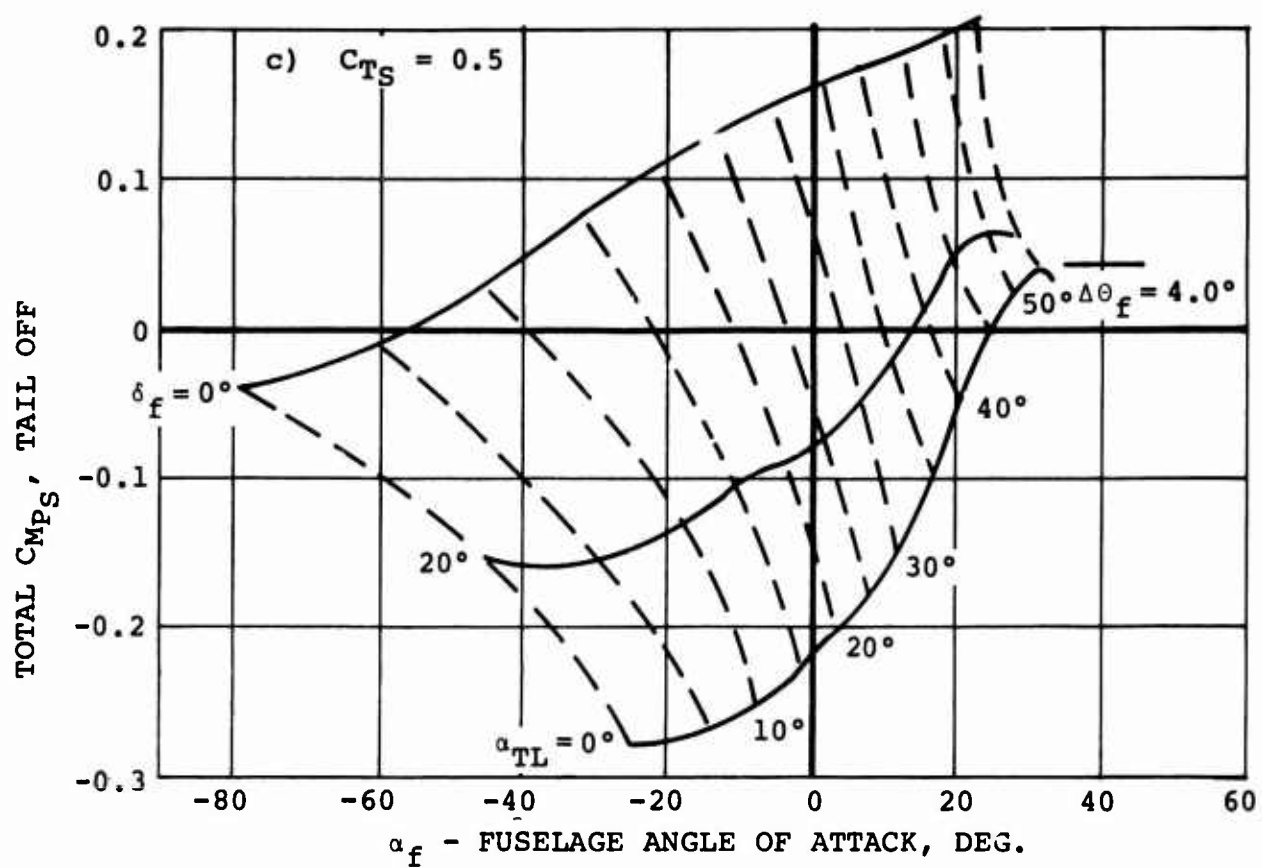


Figure 9. Variation of Total Moment with Fuselage Angle of Attack. (2 of 3)

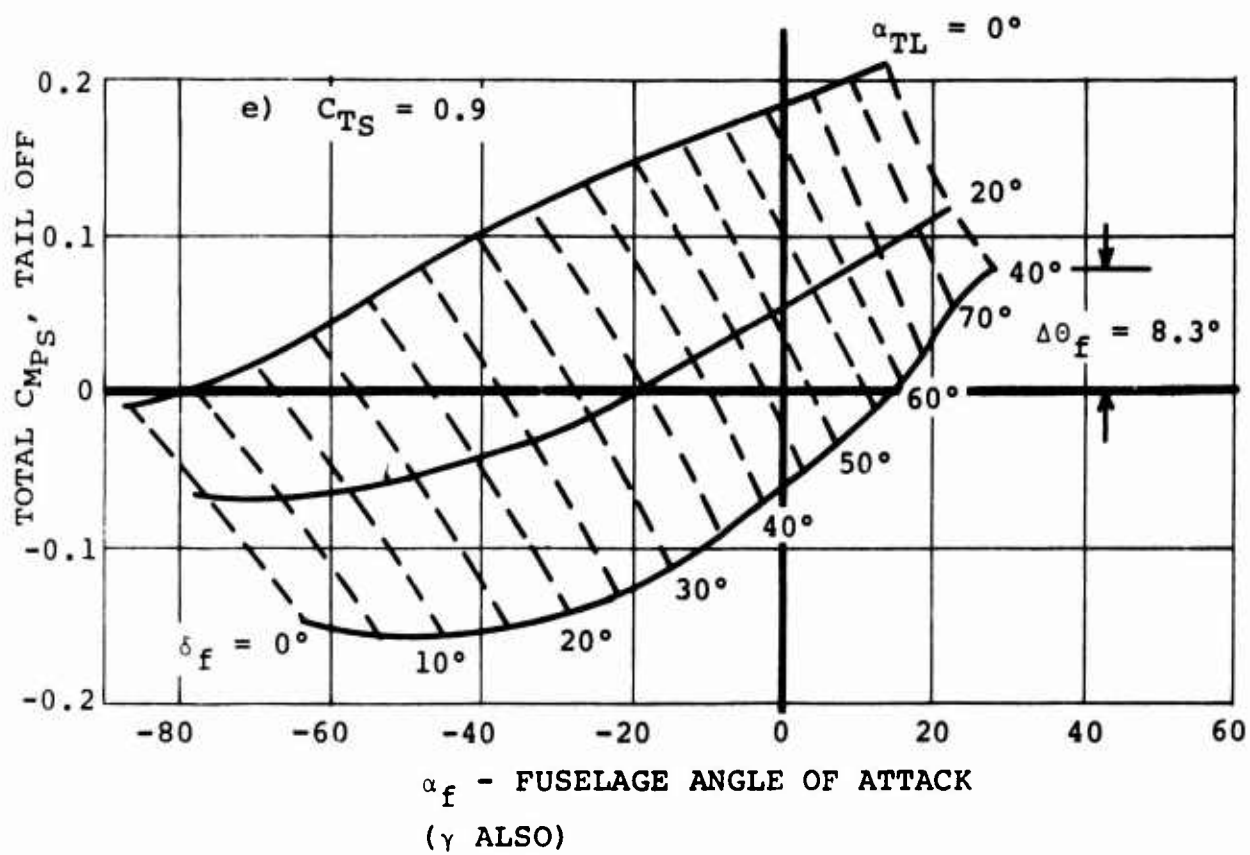


Figure 9. Variation of Total Moment with Fuselage Angle of Attack. (3 of 3)

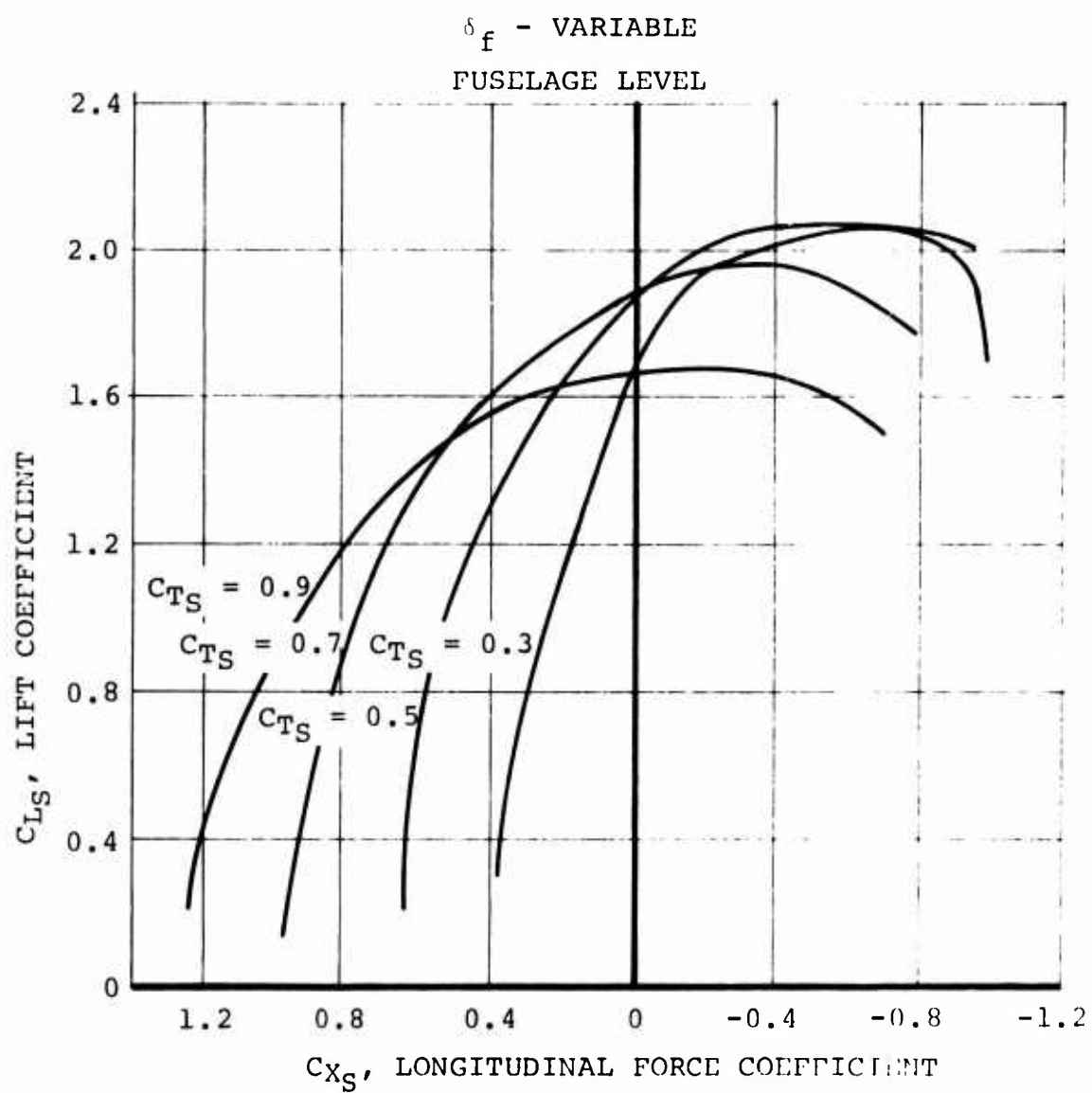


Figure 10. Geared Flap Control Trimmed Polars.

LEVEL FUSILAGE - $\alpha_f = 0^\circ$ (TAIL OFF)

CONFIGURATION

MODEL 147 WITH AGTW FLAP

$W/S = 56.7 \text{ LB/FT}^2$, $DL = 40 \text{ LB/FT}^2$

MAX POWER

(1.15 T/W
AT HOVER)

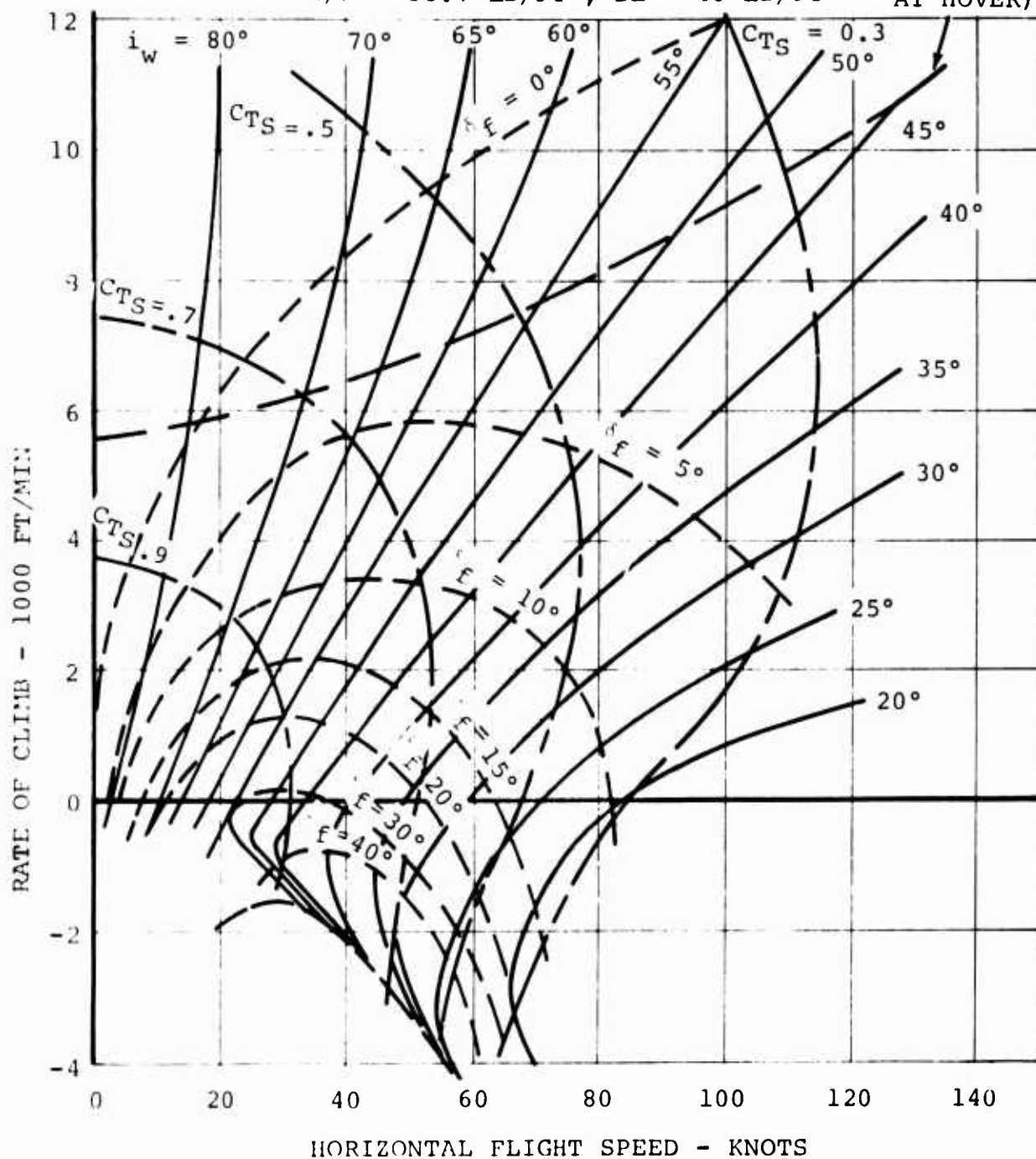


Figure 11. Geared Flap Transition Corridor.

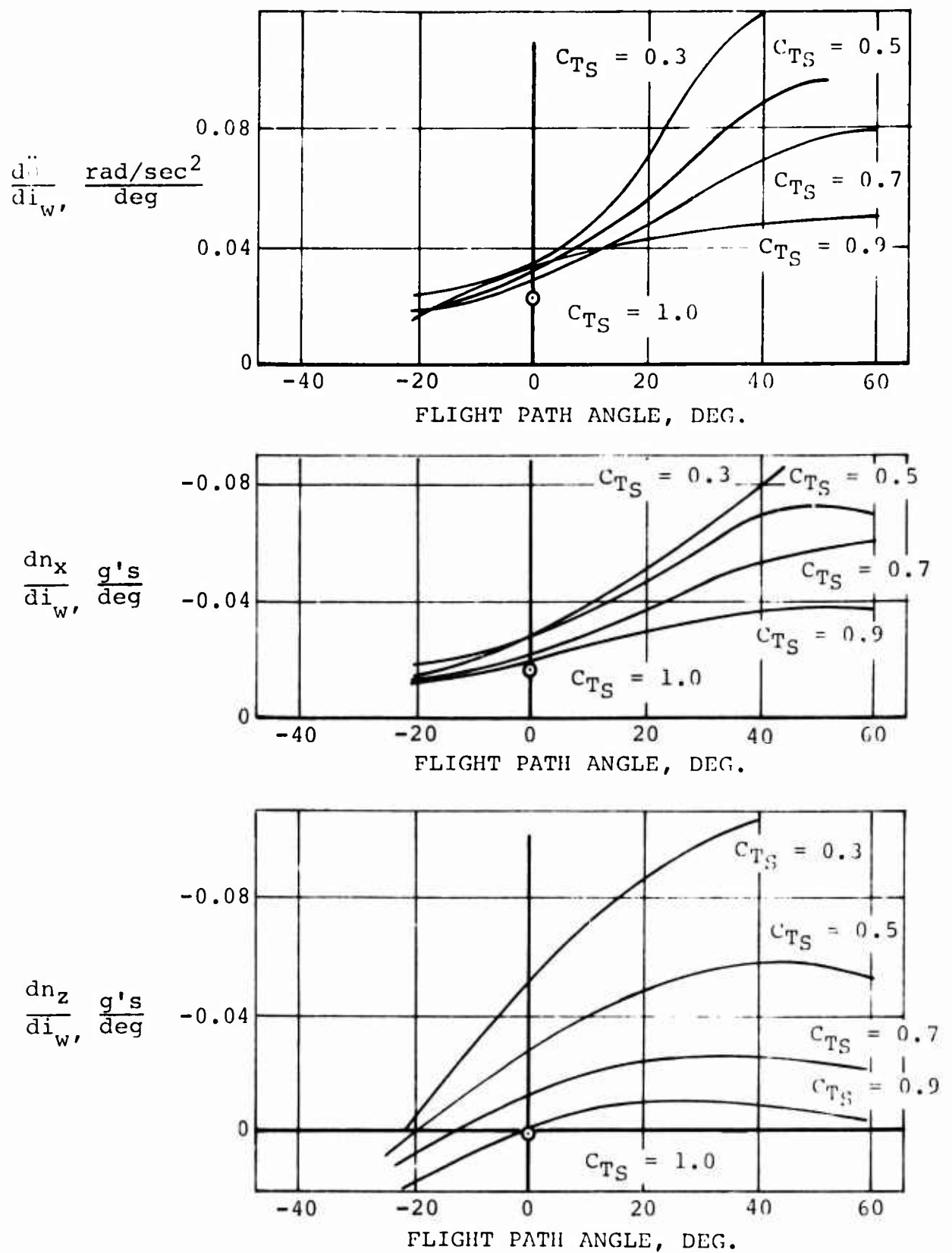


Figure 12. Fuselage Response to Wing Incidence Change.

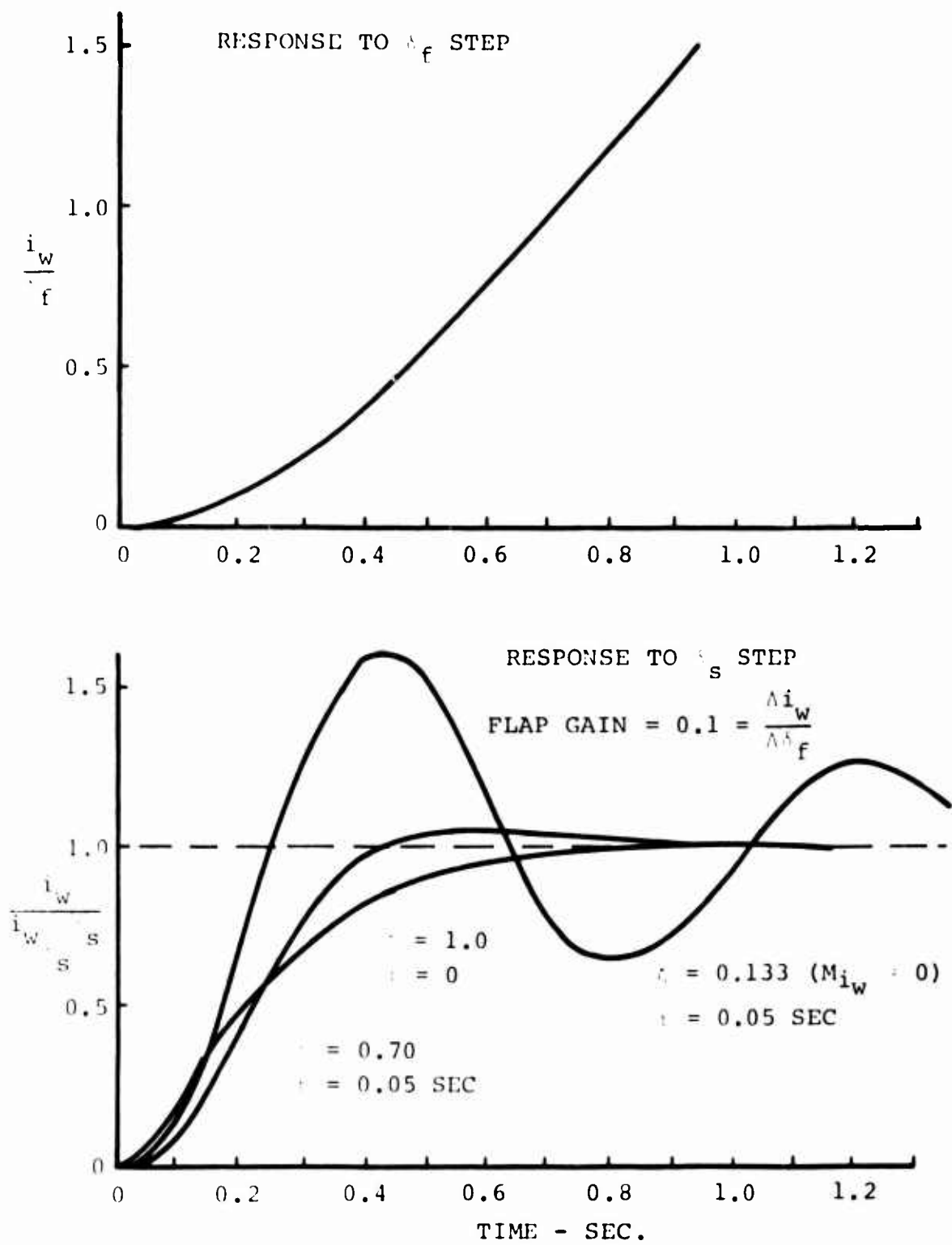


Figure 13. Geared Flap Hovering Control Response.

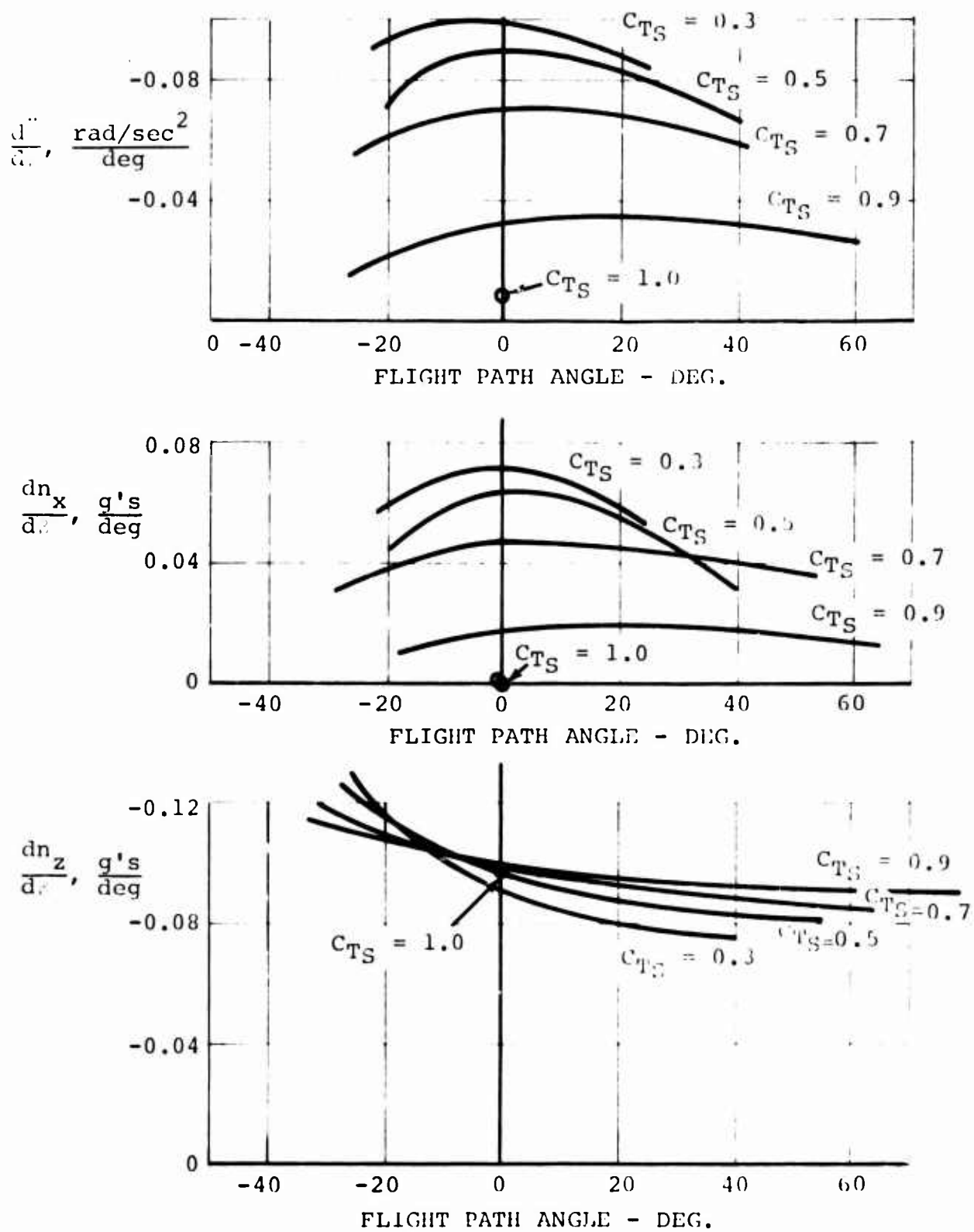


Figure 14. Fuselage Response to Propeller Blade Pitch Changes.

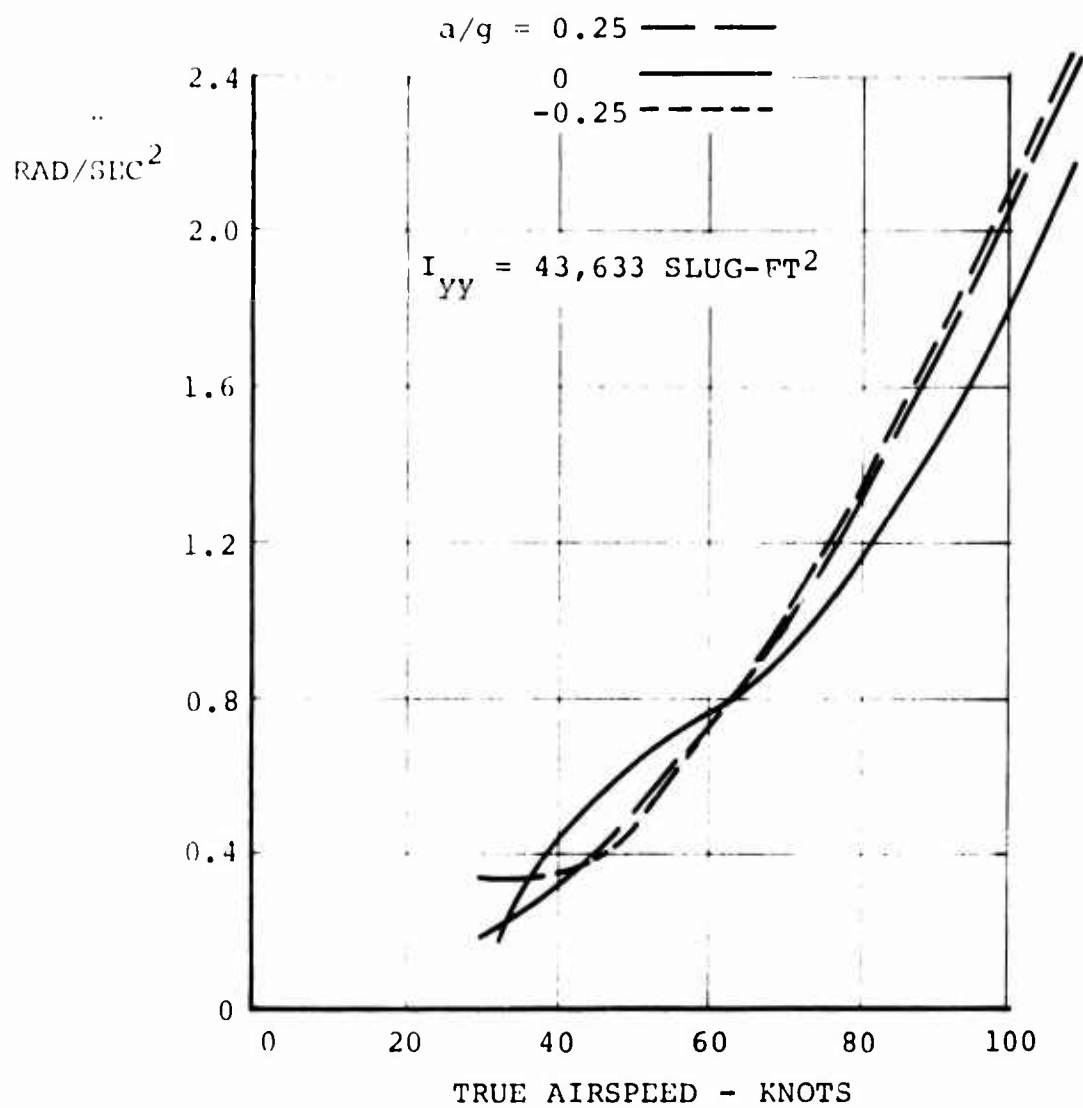


Figure 15. Geared Flap Transition Horizontal Tail
Effectiveness Low Horizontal Tail @ $C_{LT} = 1.0$.

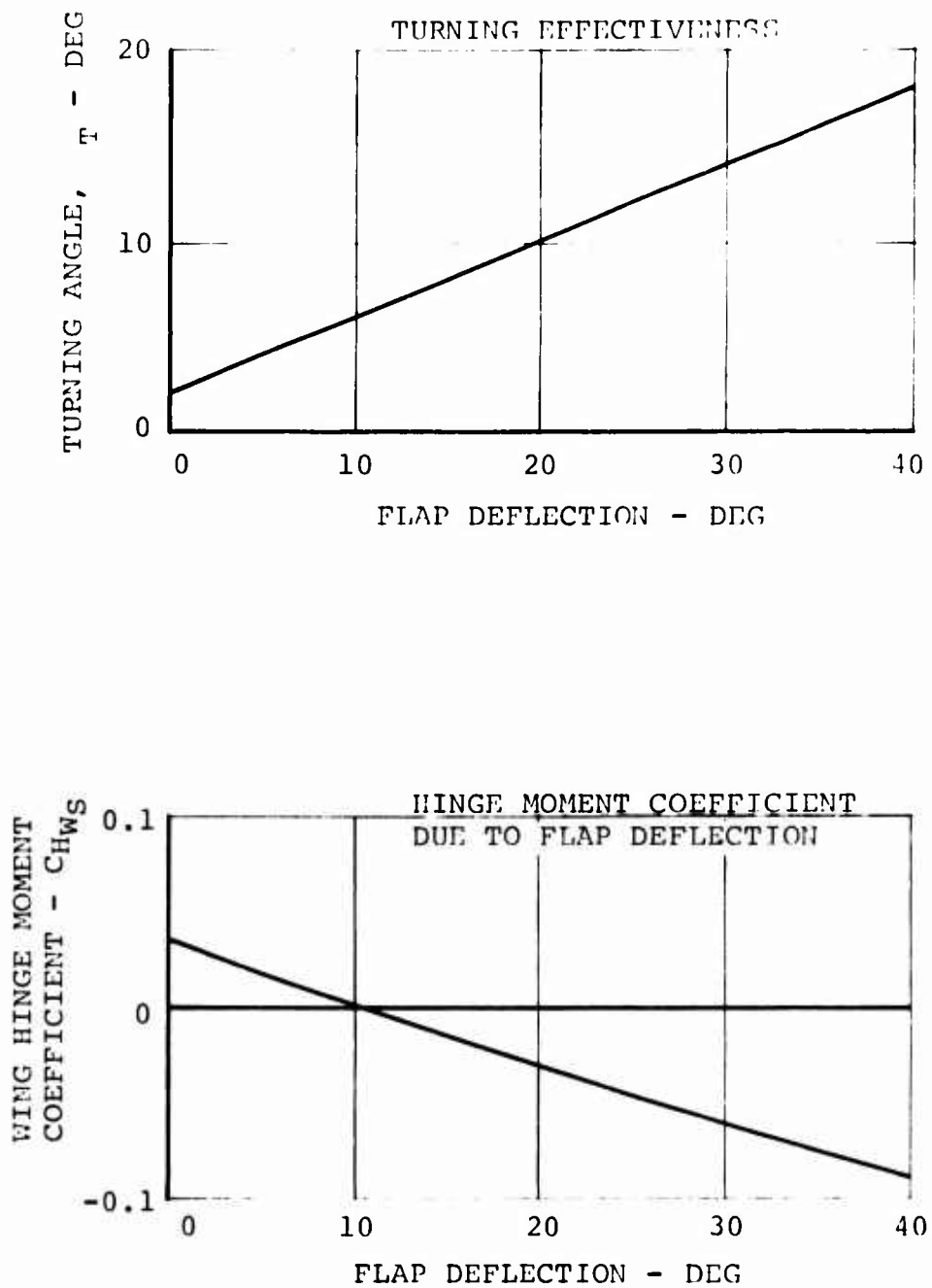


Figure 16. Aerodynamic Characteristics in Hover, $C_{TS} = 1.0$.

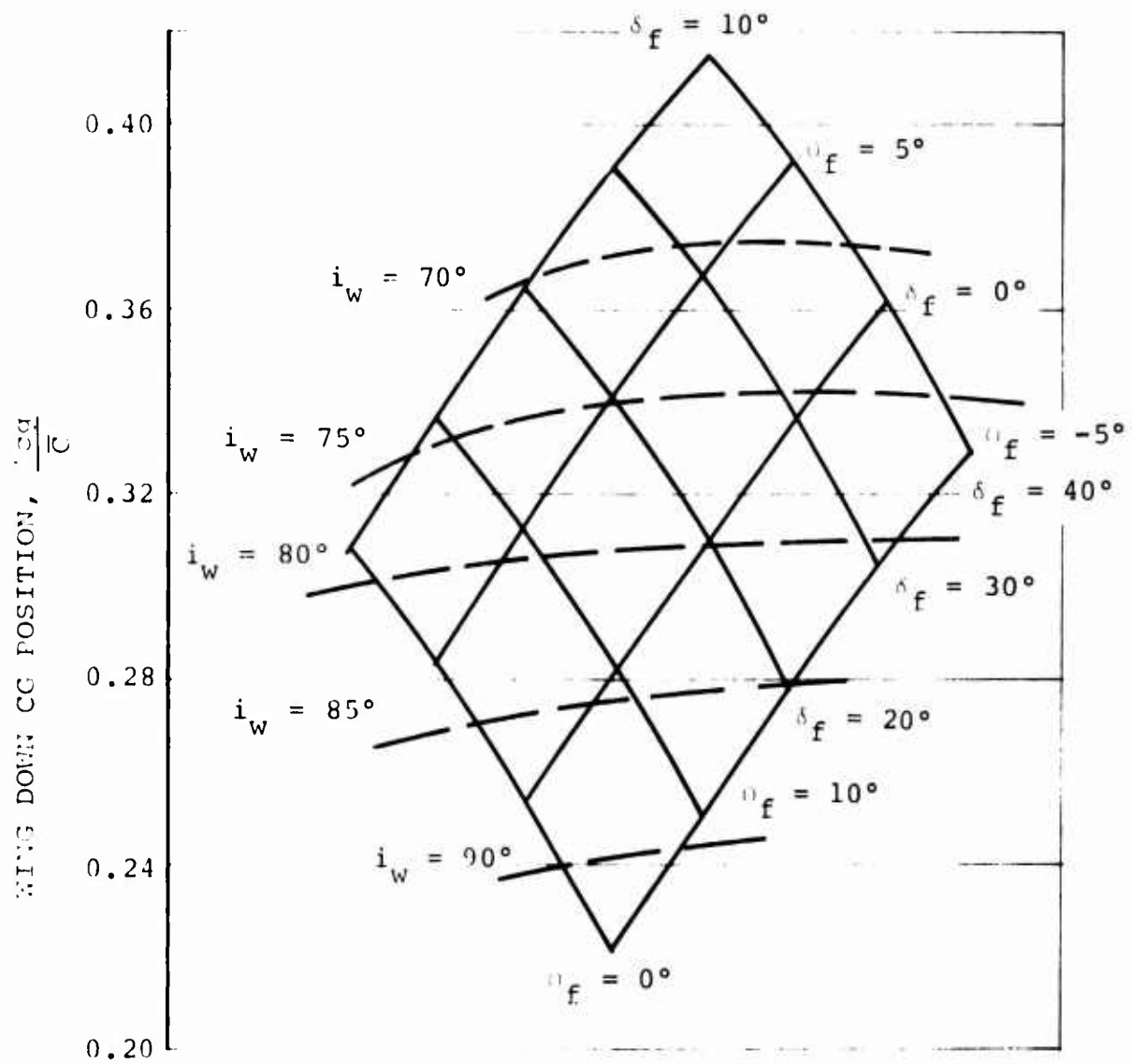


Figure 17. Flap Trim with Geared Flap.

APPENDIX A

BASIC DATA REQUIRED FOR ANALYSIS OF GEARED FLAP TRANSITION

The basic source of performance data used in this report is the powered Advanced Geometry Tilt-Wing Model Test which has conducted at the LTV wind tunnel facilities in November of 1966. A three-view of the test configuration is shown in Figure A-1. The general arrangement of the model balance and pivot point positions are shown in Figure A-2. The wing of the subject model incorporates a 15% chord leading edge slat and a 40% chord extending trailing edge flap as shown in Figures A-3 and A-4 respectively. The basic data, C_{L_S} , C_{X_S} , X/L and C_{WHS} vs C_{T_S} , are presented in Figures A-5 through A-16. These data were not included in Reference (6), and for that reason are presented here. The ϵ and η_t data for a low horizontal tail location were presented in Reference (6), but for completeness are included in Figures A-17 to A-29.

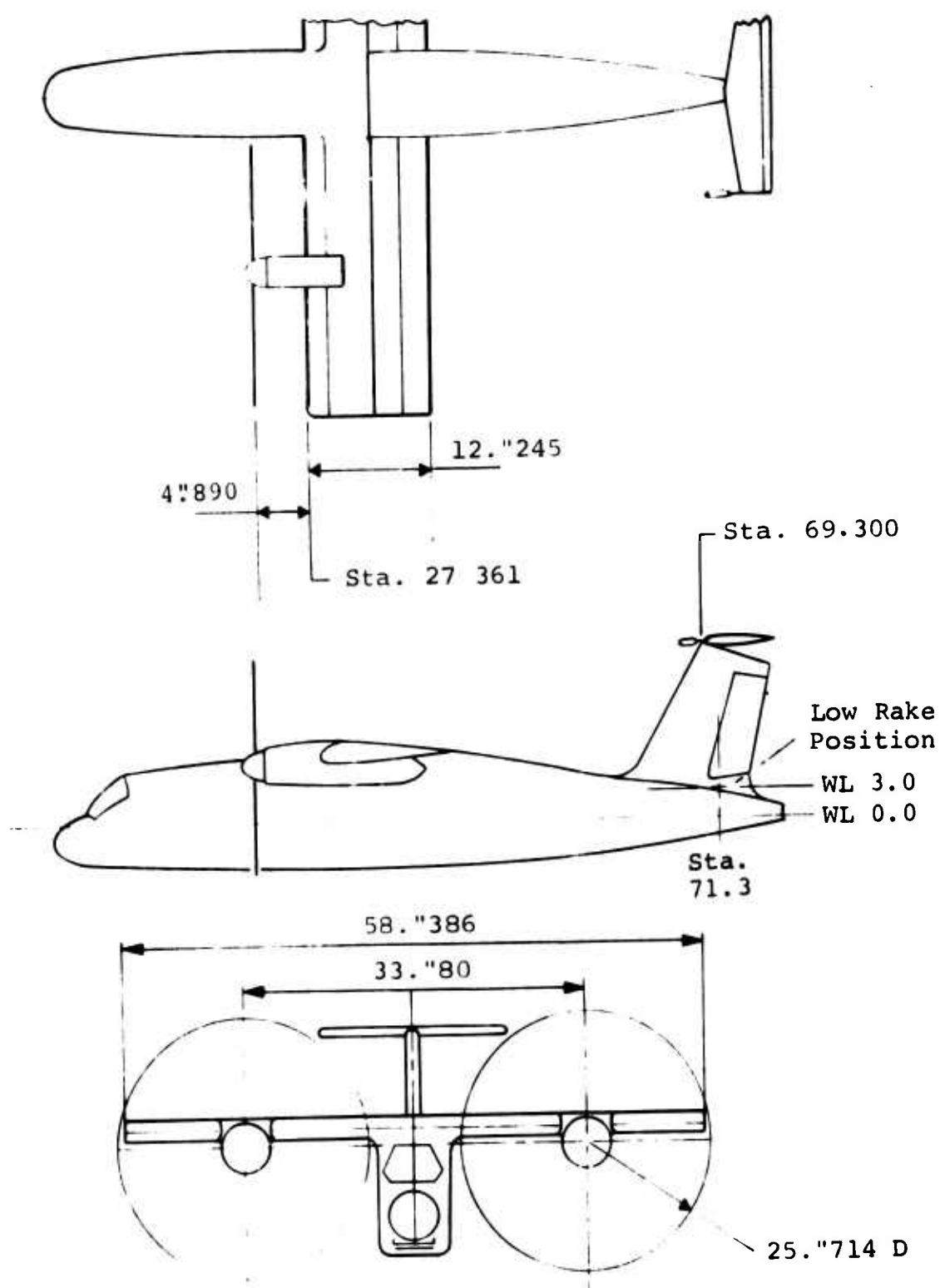


Figure A-1. Three View and Principal Model Dimensions.

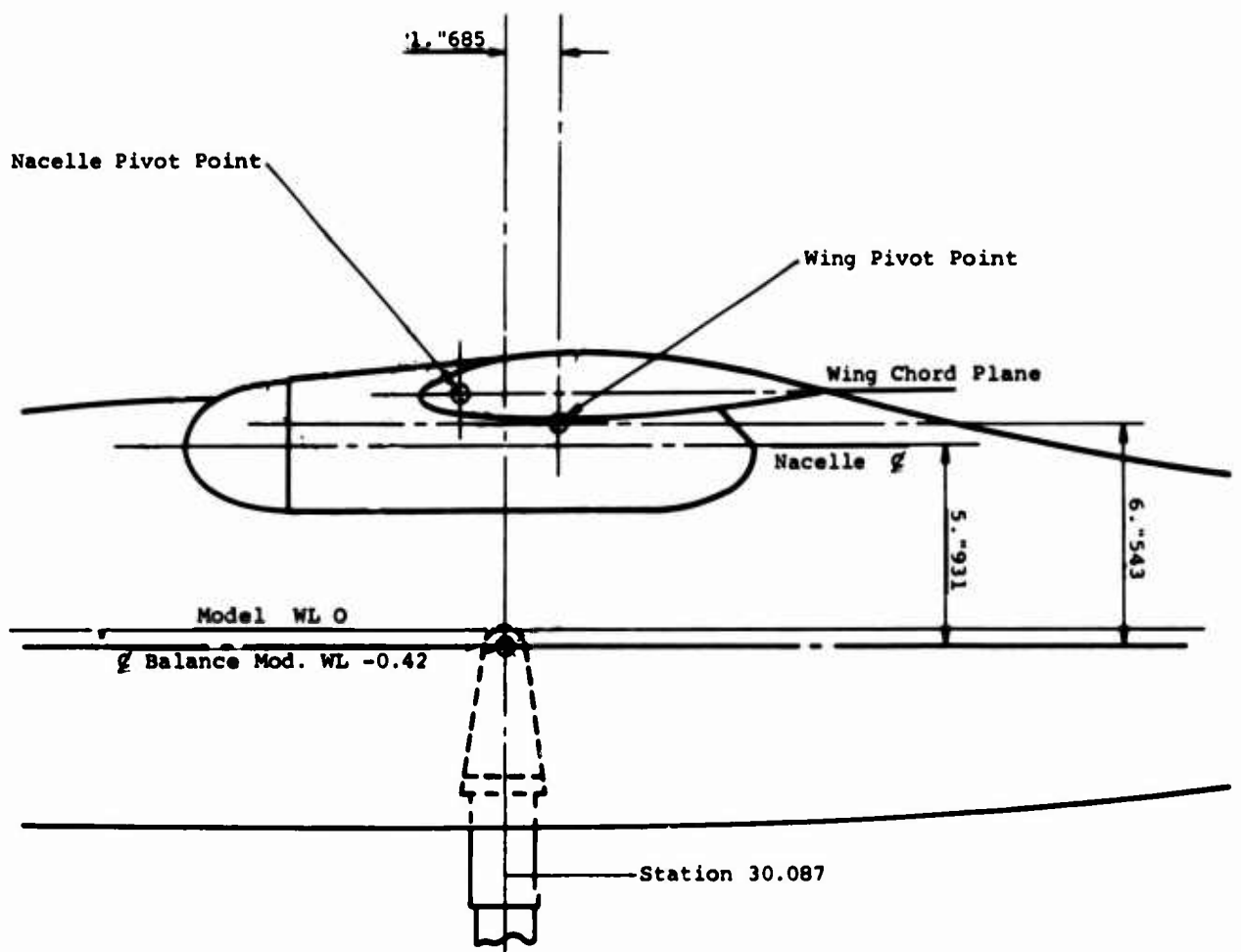


Figure A-2. Pivot Point Positions.

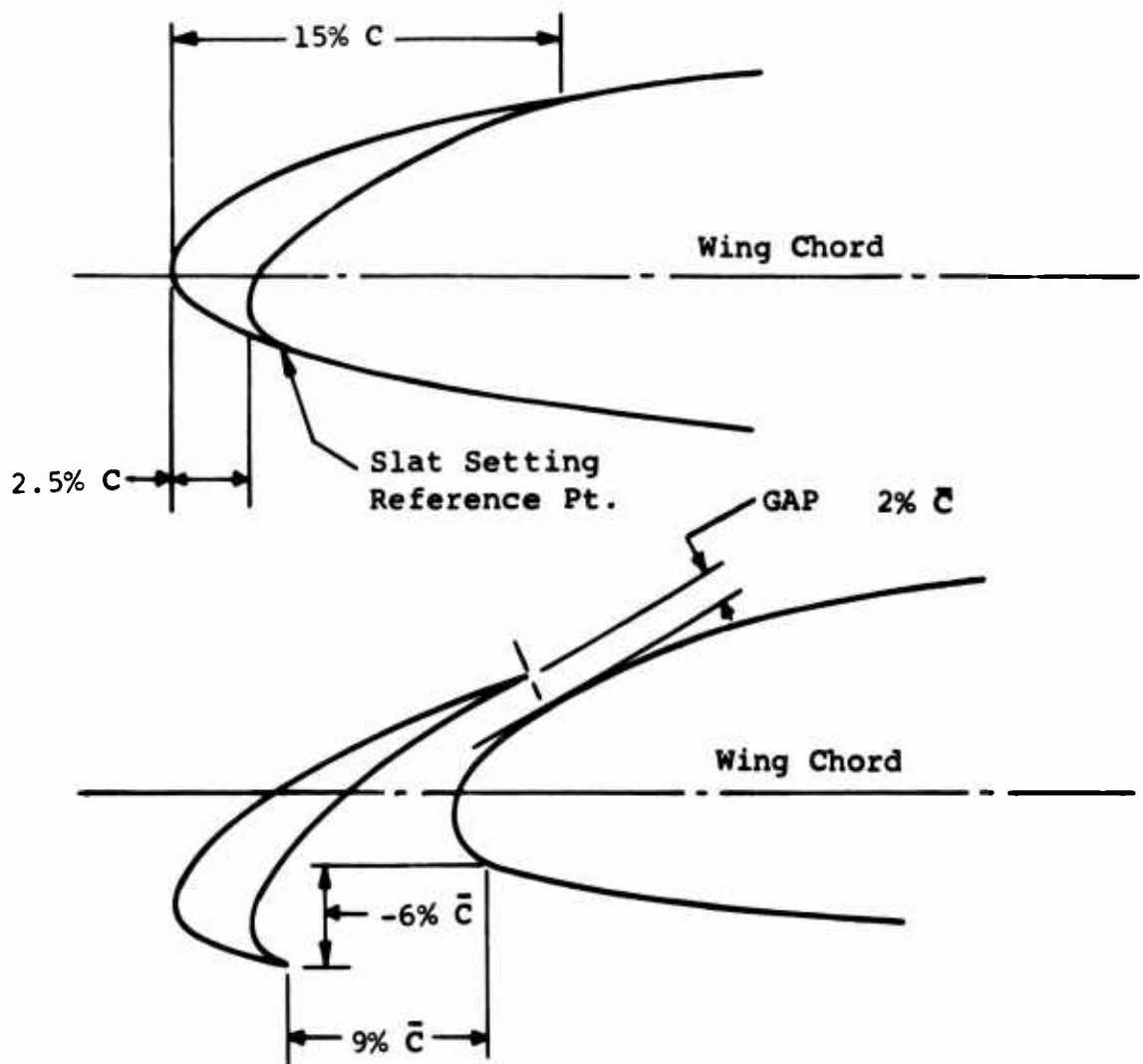


Figure A-3. Slat Arrangement.

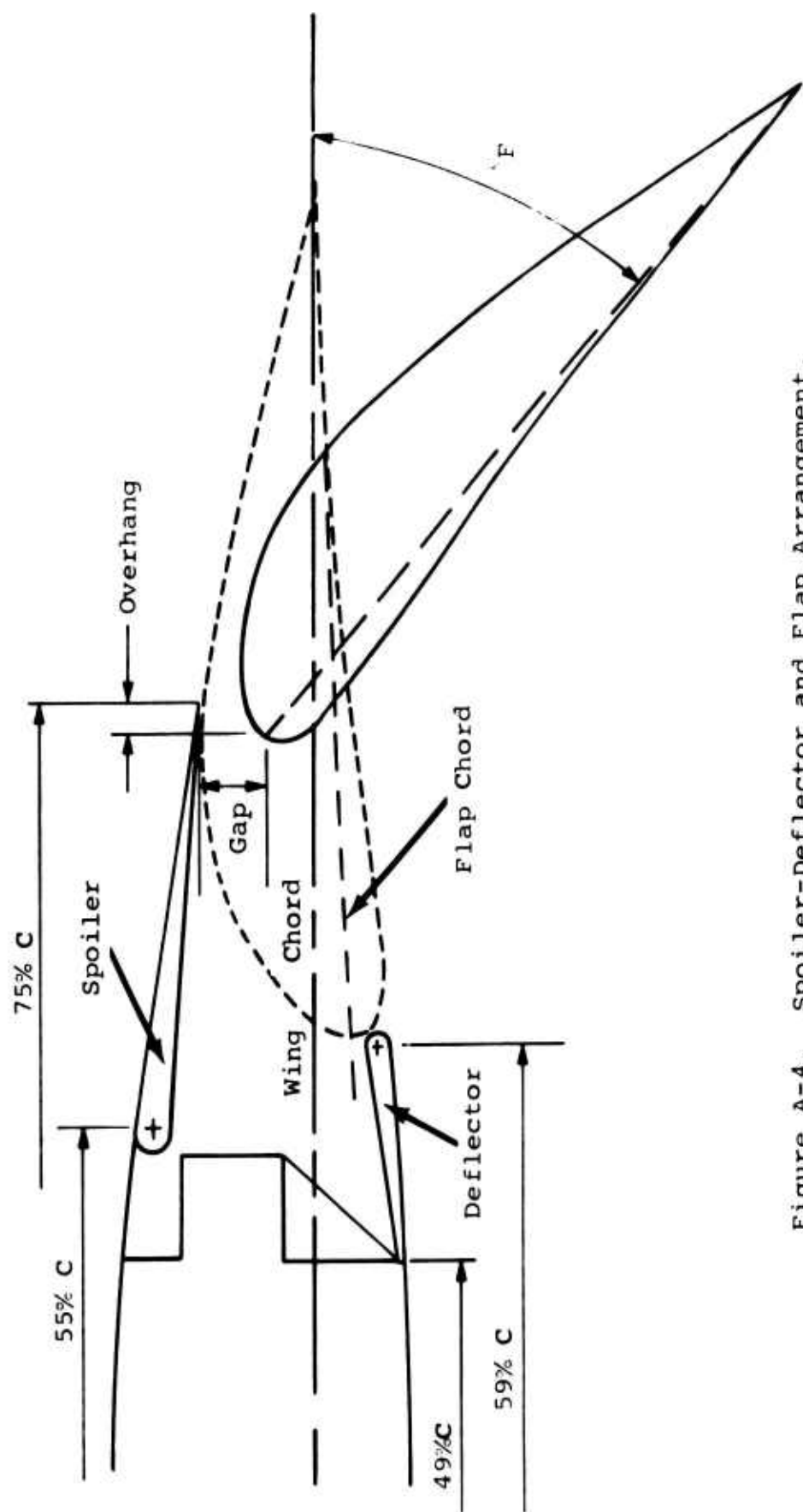


Figure A-4. Spoiler-Deflector and Flap Arrangement.

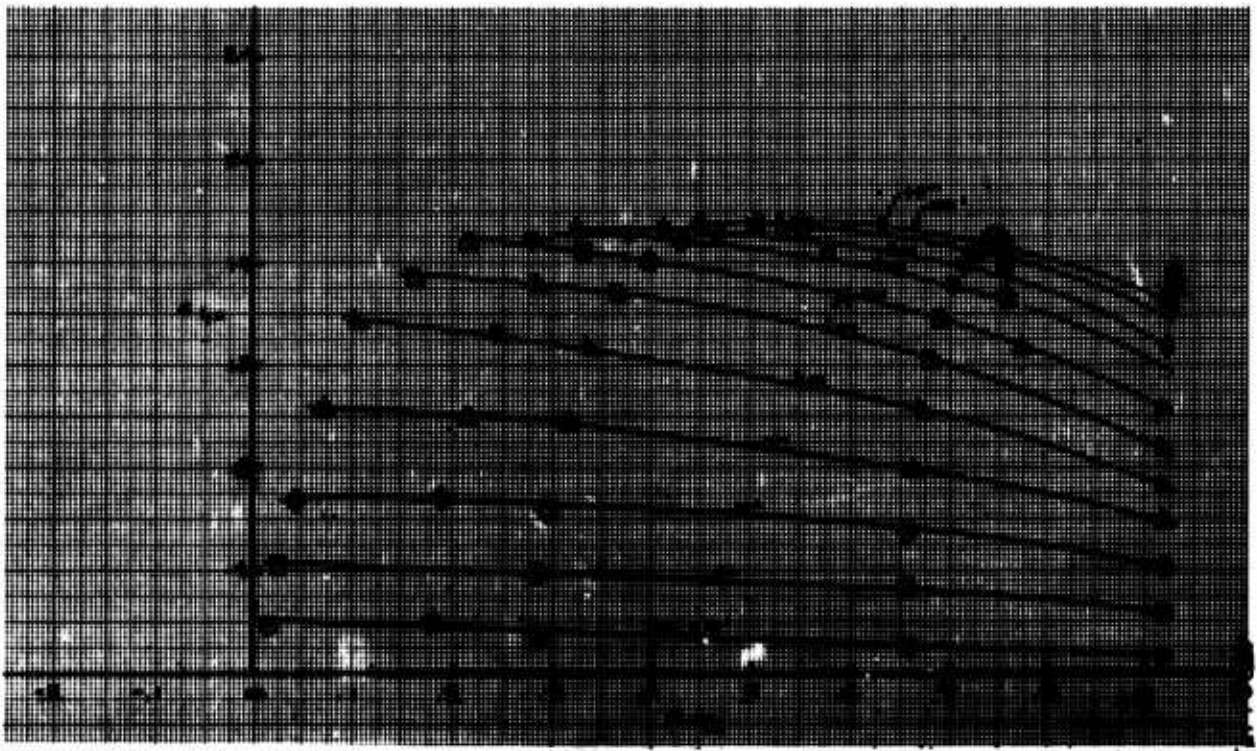


Figure A-5. Lift Coefficient vs. Thrust Coefficient
 $\delta_f = 0^\circ$ $\alpha_f = 0^\circ$ $\beta = 12^\circ$

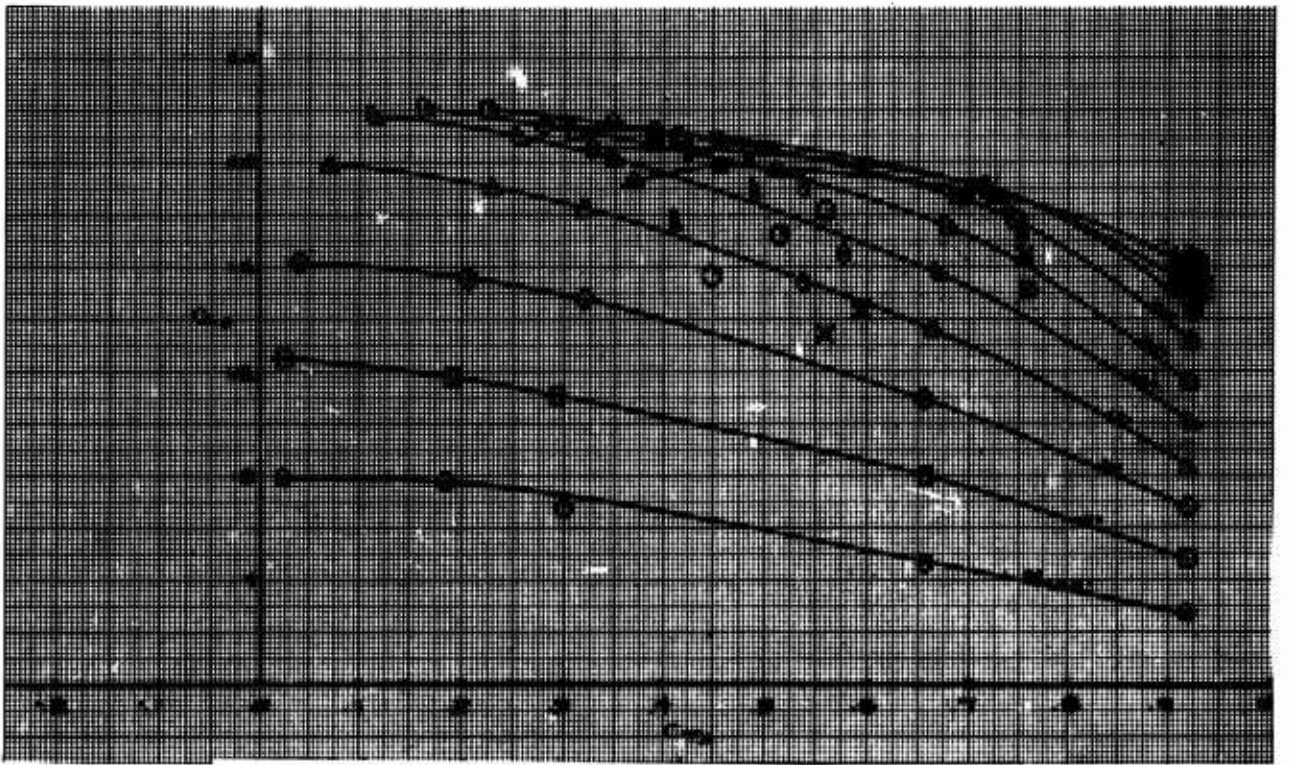


Figure A-6. Lift Coefficient vs. Thrust Coefficient
 $\delta_f = 20^\circ$ $\alpha_f = 0^\circ$ $\beta = 12^\circ$

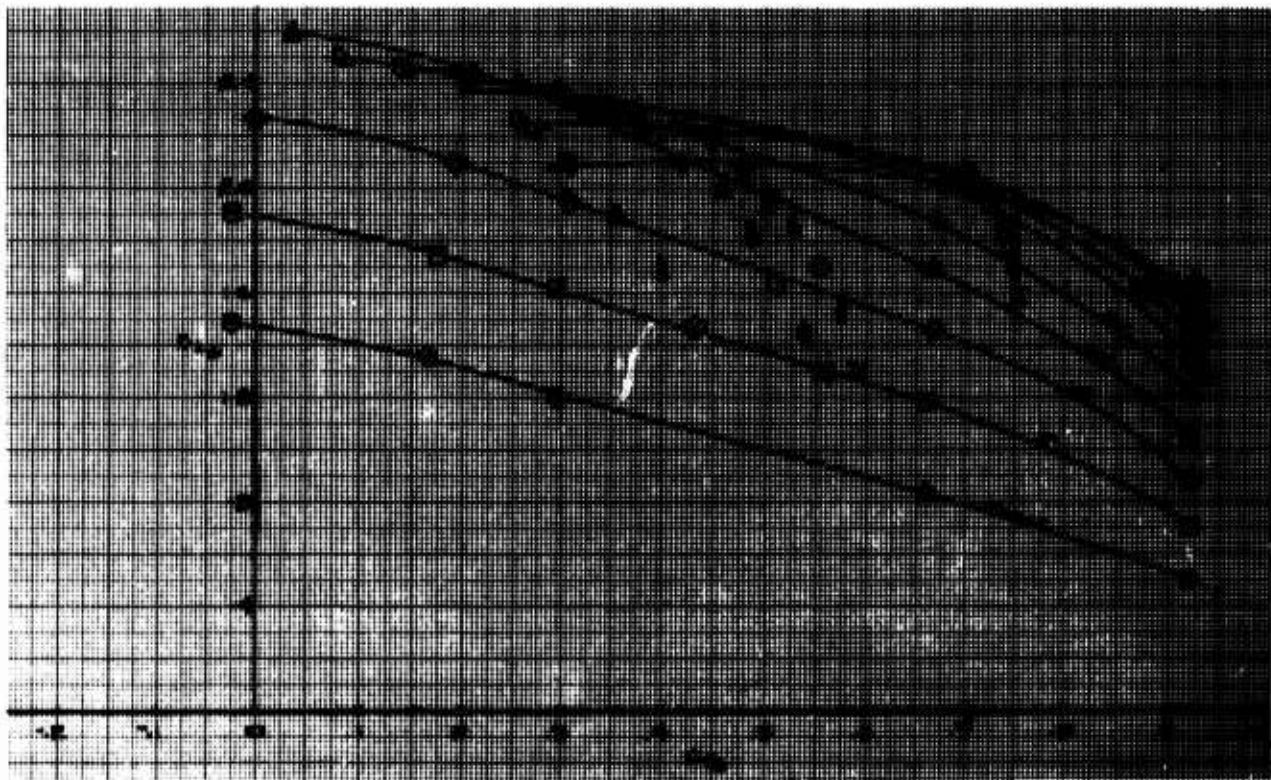


Figure A-7. Lift Coefficient vs. Thrust Coefficient
 $\delta_f = 40^\circ$ $\alpha_f = 0^\circ$ $\beta = 12^\circ$

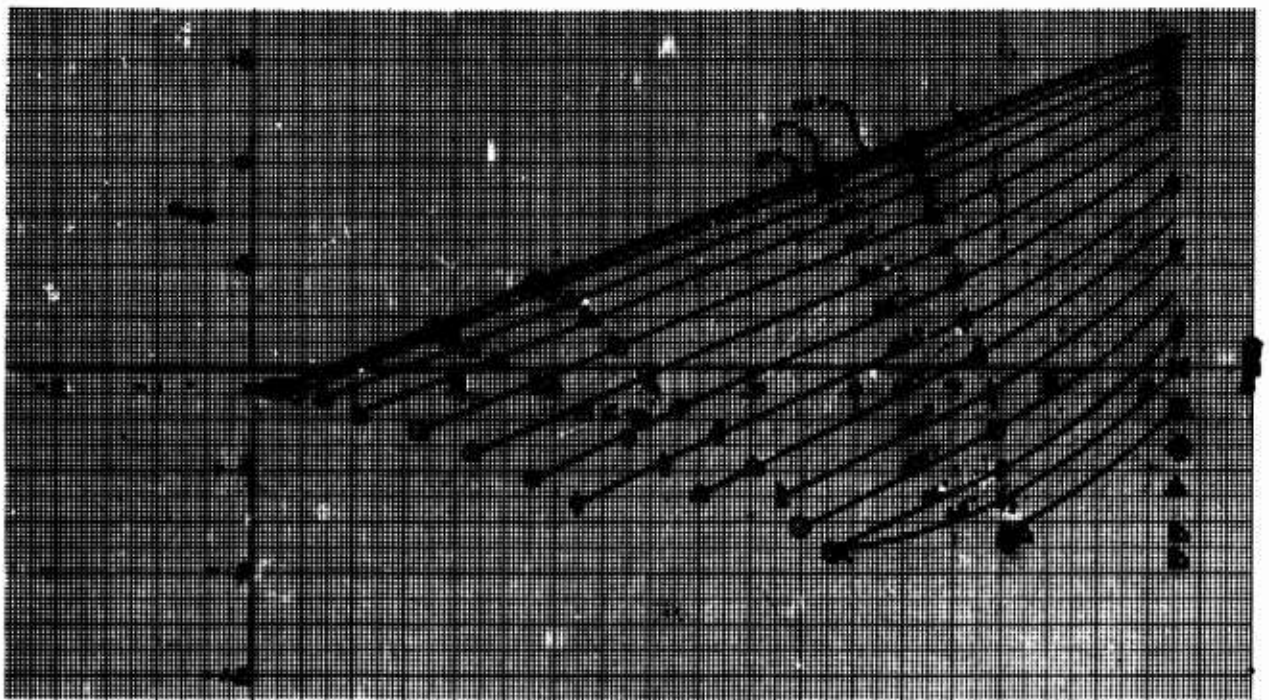


Figure A-8. Longitudinal Force Coefficient vs. Thrust Coefficient $\delta_f = 0^\circ$ $\alpha_f = 0^\circ$ $\beta = 12^\circ$

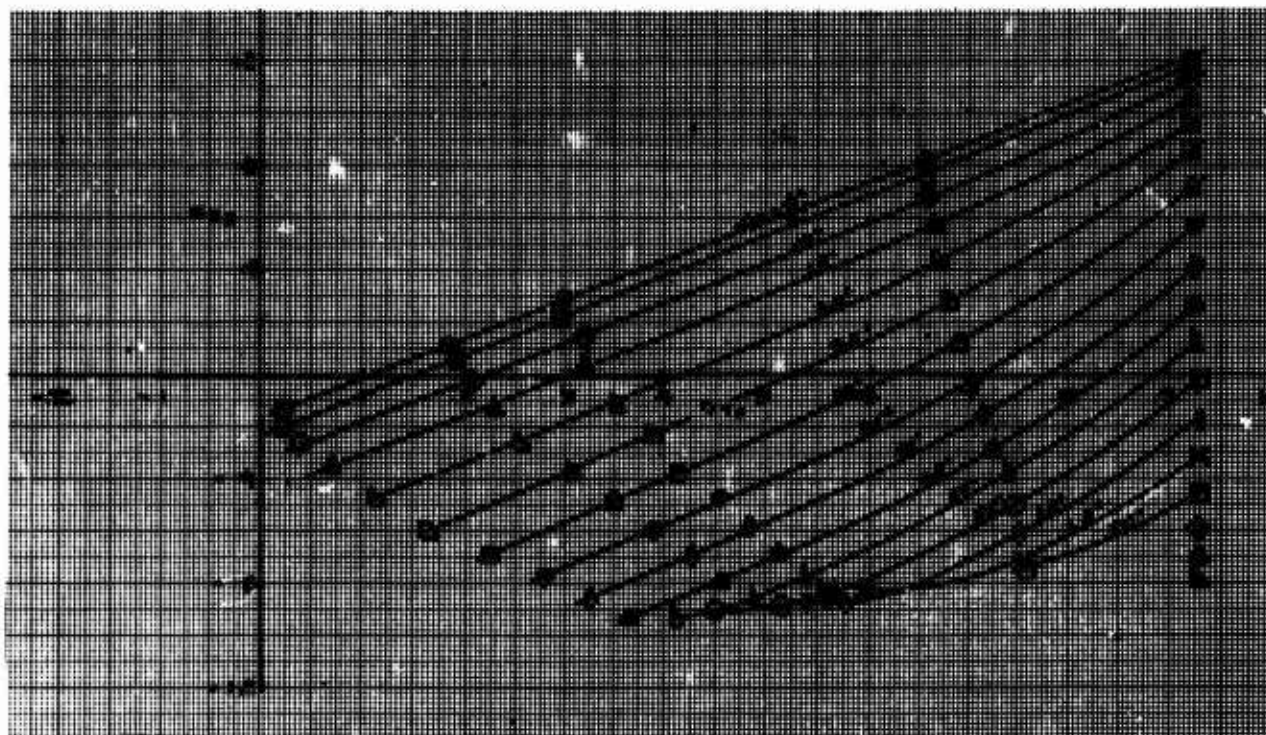


Figure A-9. Longitudinal Force Coefficient vs. Thrust Coefficient $\delta_f = 20^\circ$ $\alpha_f = 0^\circ$ $\beta = 12^\circ$

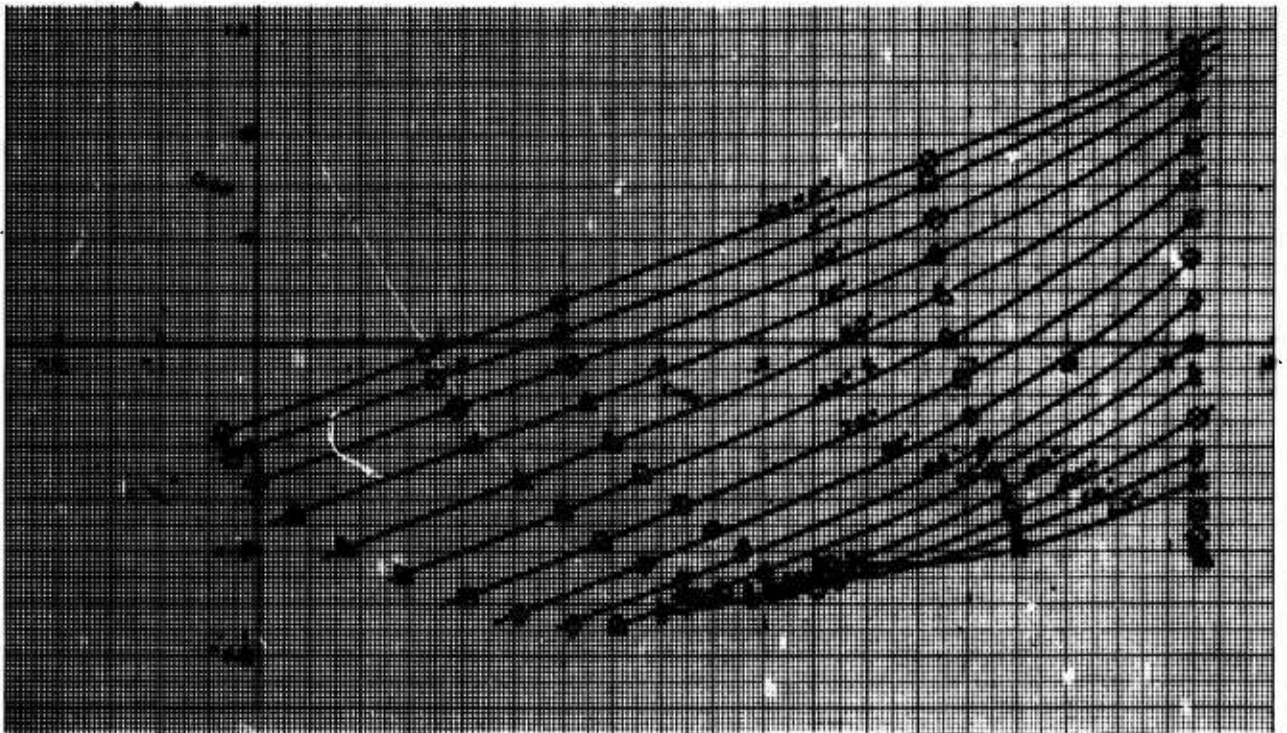


Figure A-10. Longitudinal Force Coefficient vs. Thrust Coefficient $\delta_f = 40^\circ$ $\alpha_f = 0^\circ$ $\beta = 12^\circ$

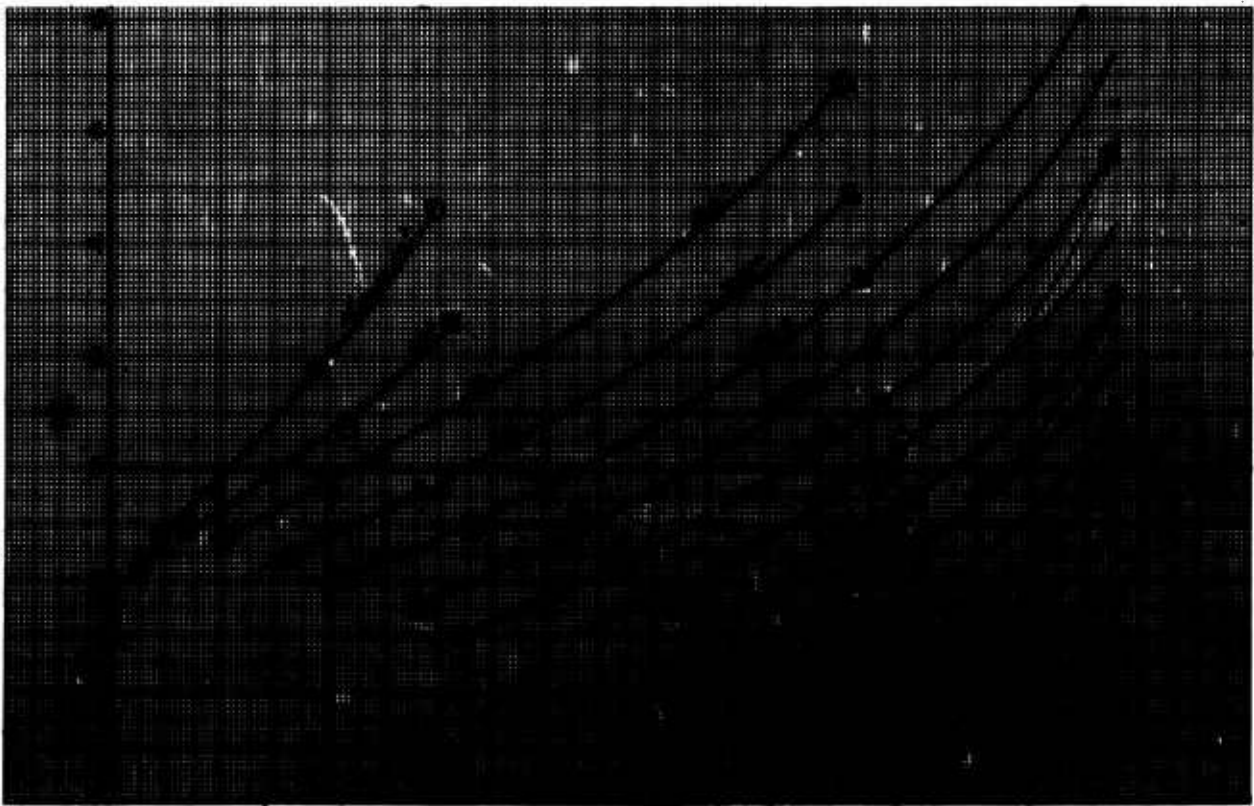


Figure A-11. Level Flight Acceleration Capability
 $\delta_f = 0^\circ$ $\alpha_f = 0^\circ$ $\beta = 12^\circ$

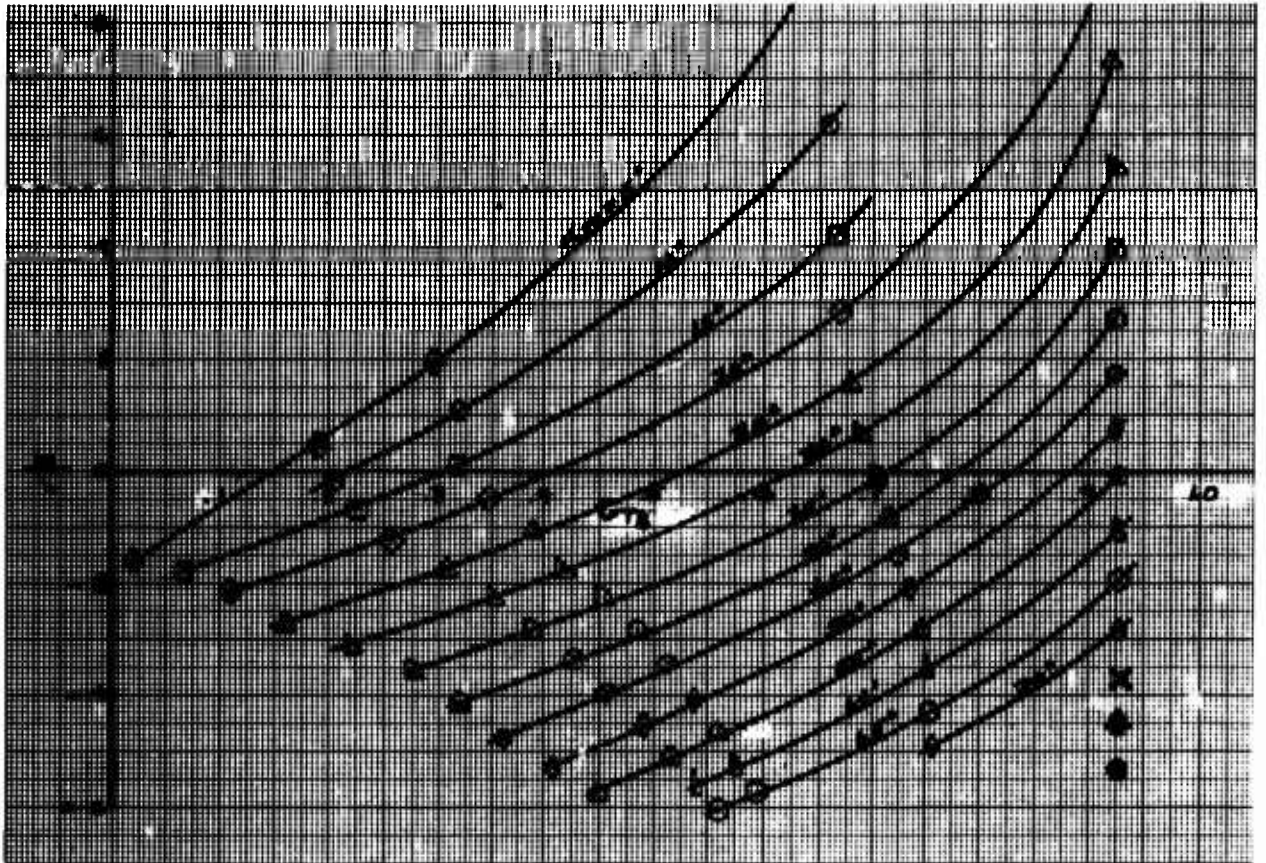


Figure A-12. Level Flight Acceleration Capability
 $\delta_f = 20^\circ$ $\alpha_f = 0^\circ$ $\beta = 12^\circ$

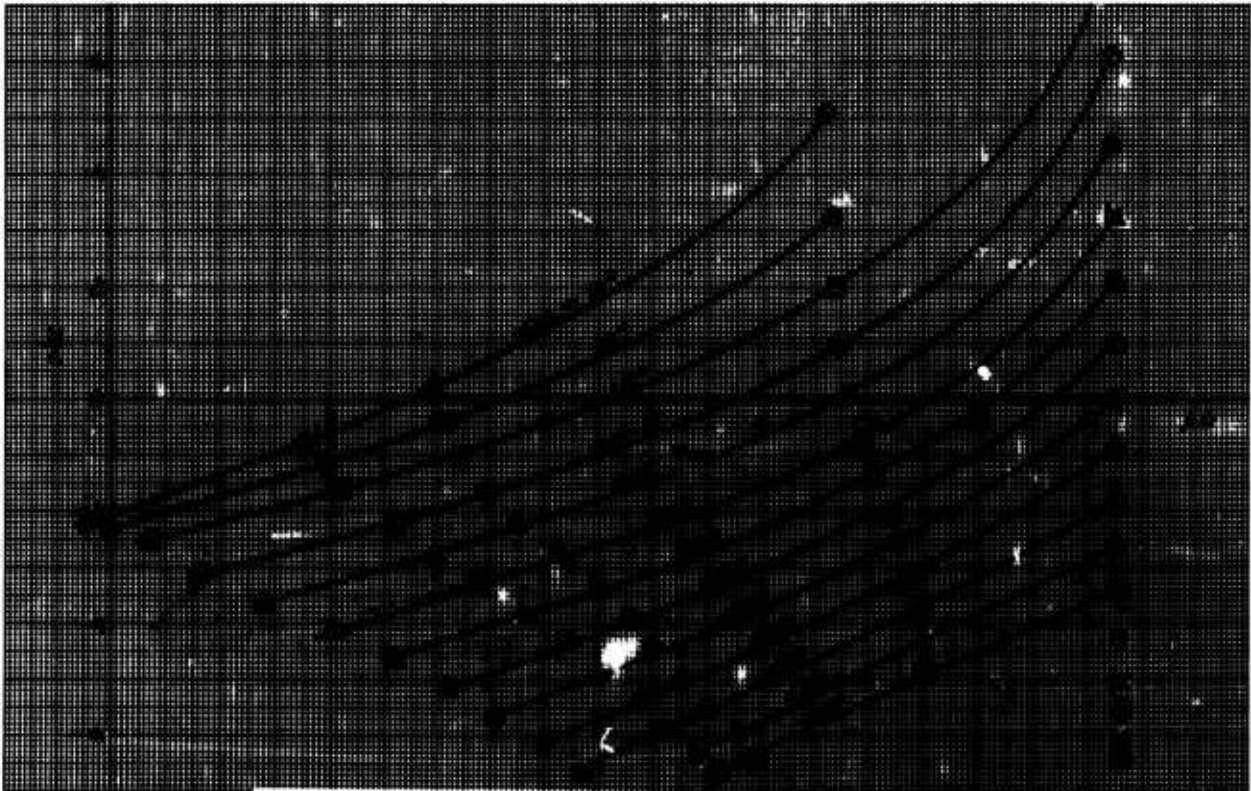


Figure A-13. Level Flight Acceleration Capability
 $\delta_f = 40^\circ$ $\alpha_f = 0^\circ$ $\beta = 12^\circ$

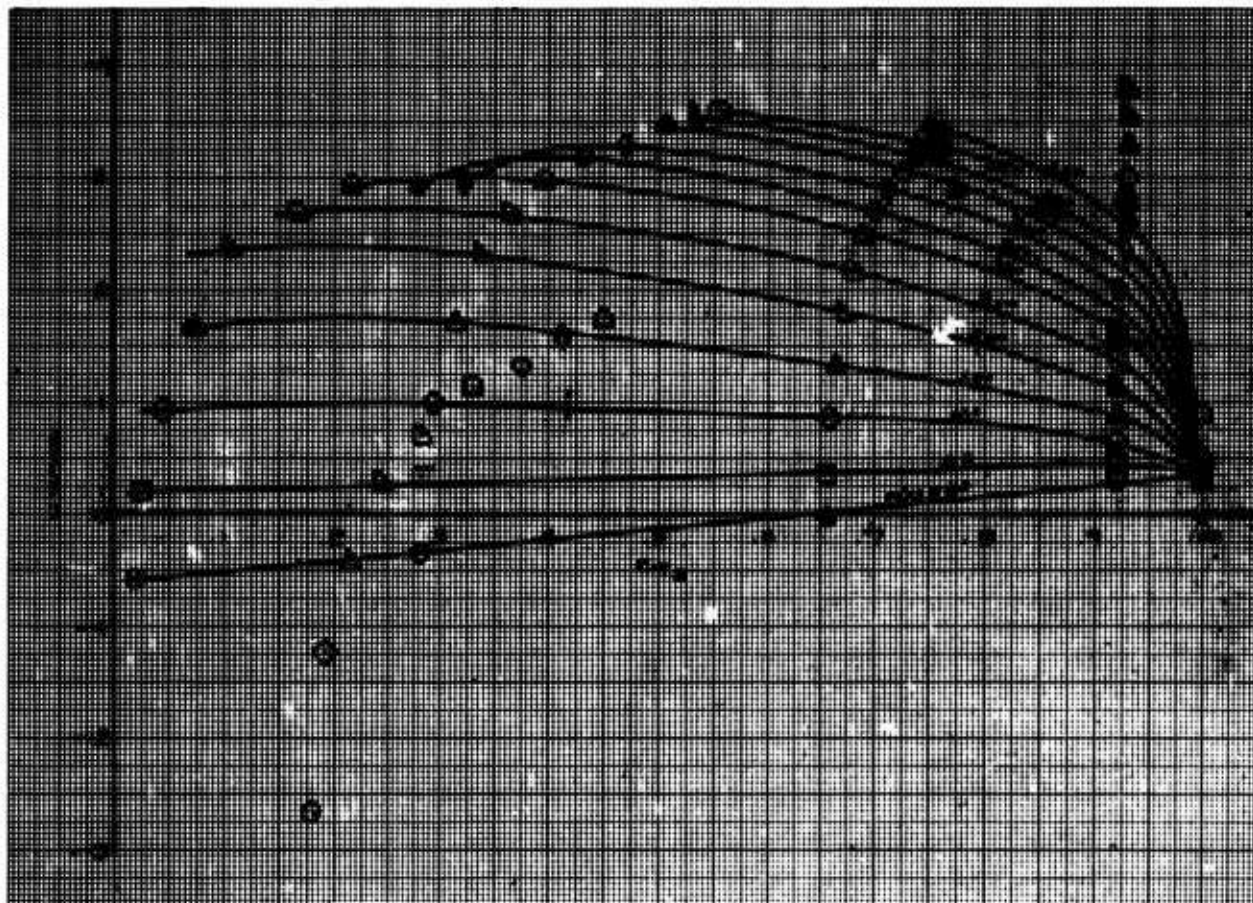


Figure A-14. Wing Hinge Moment
 $\delta_f = 0^\circ \quad \alpha_f = 0^\circ \quad \beta = 12^\circ$

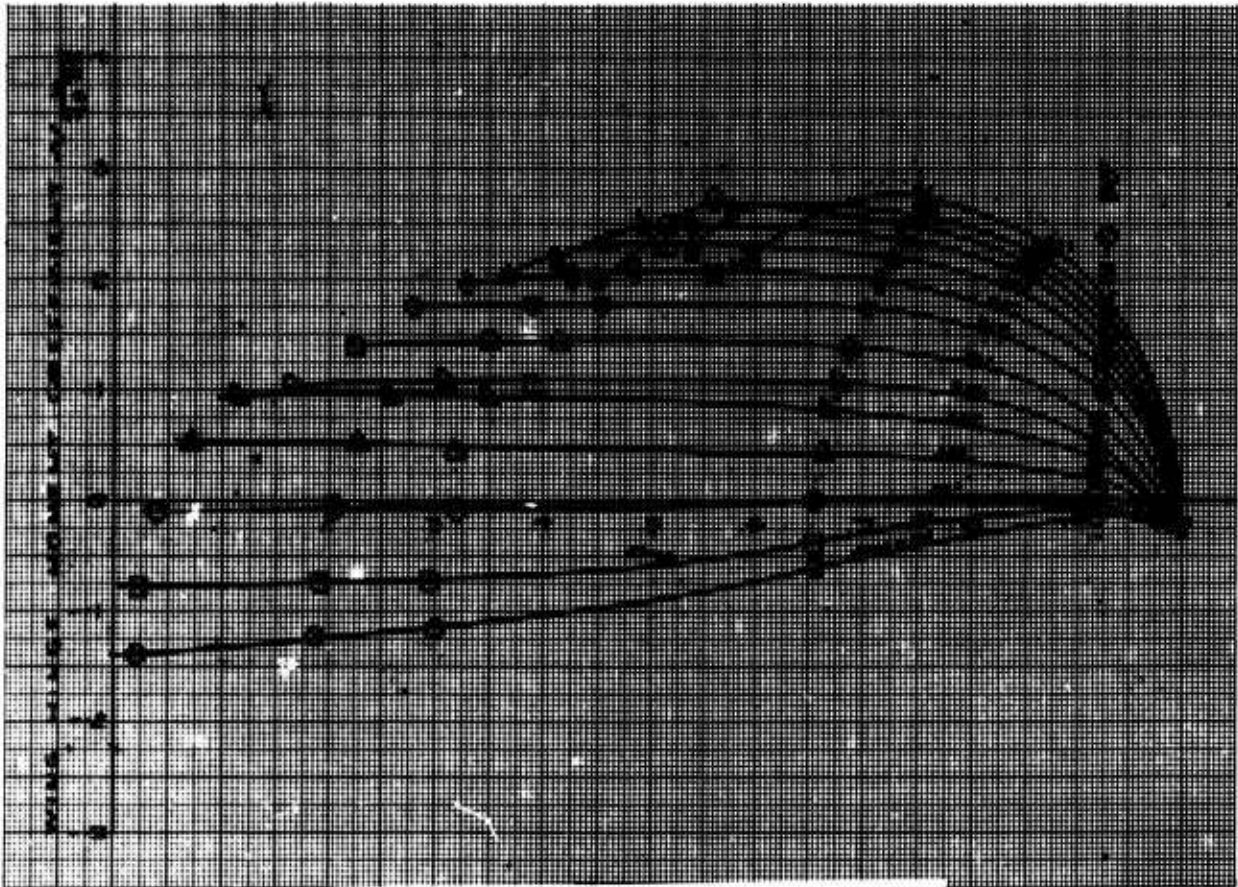


Figure A-15. Wing Hinge Moment
 $\delta_f = 20^\circ$ $\alpha_f = 0^\circ$ $\beta = 12^\circ$

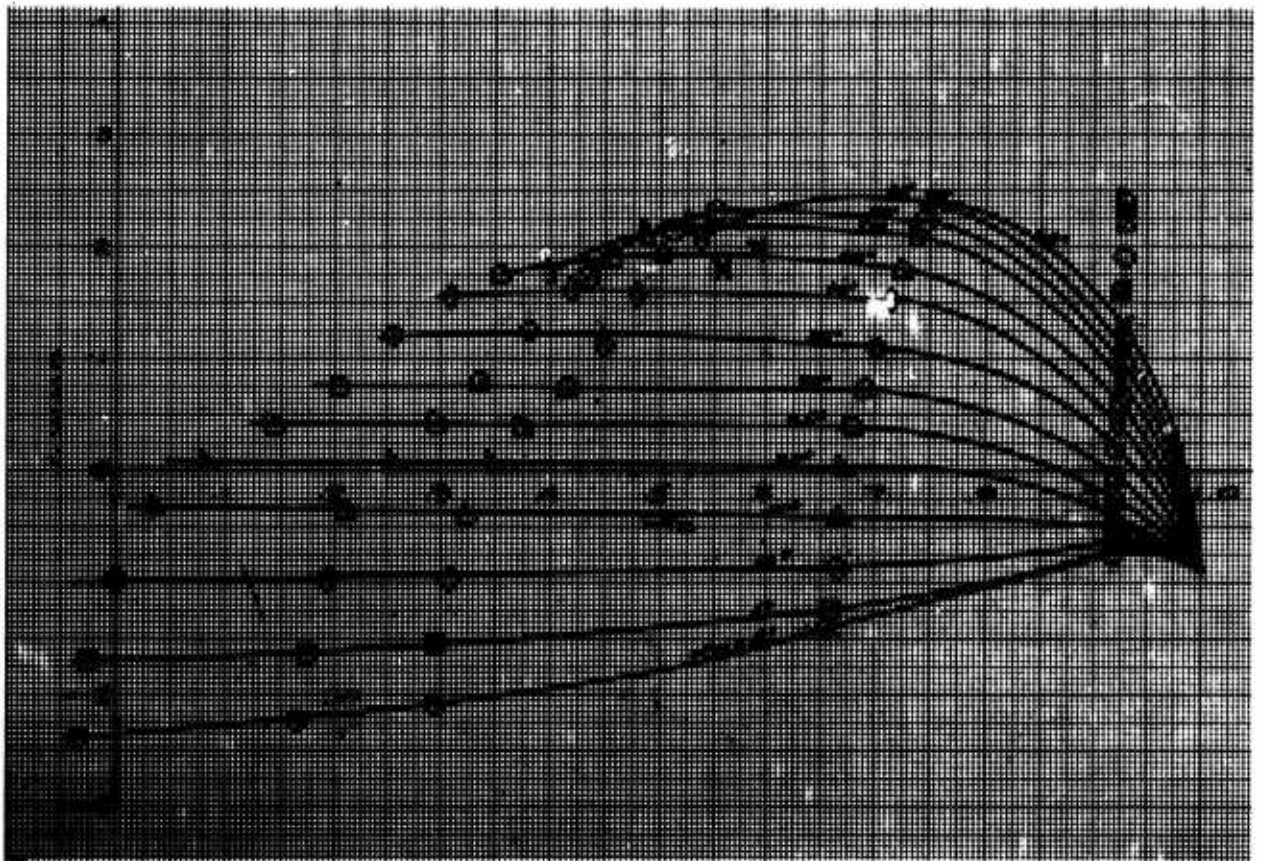


Figure A-16. Wing Hinge Moment
 $\delta_f = 40^\circ$ $\alpha_f = 0^\circ$ $\beta = 12^\circ$.

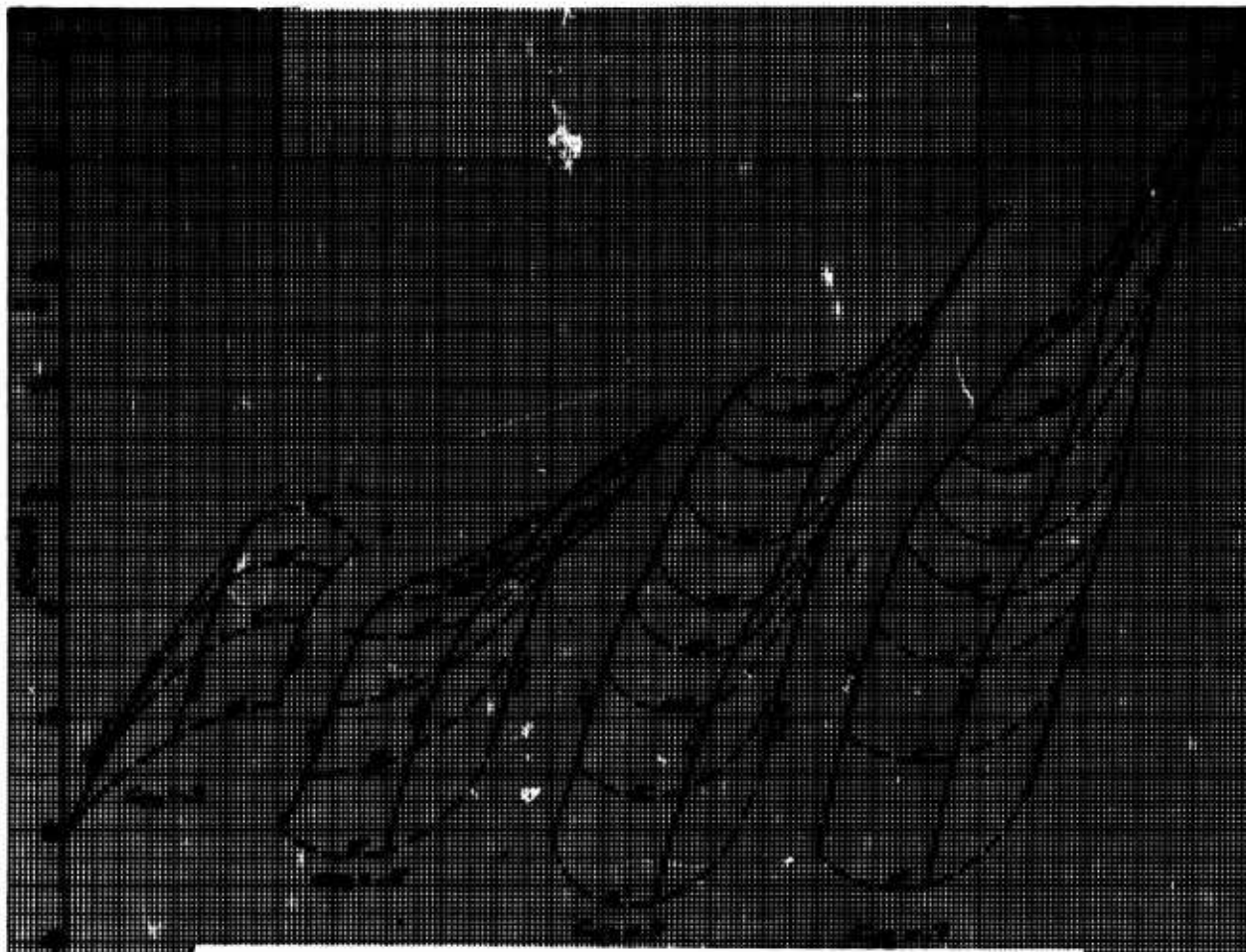


Figure A-17. Effect of Flap on Downwash at Low Tail Position
 $\alpha_f = 0^\circ$ $\beta = 12^\circ$.

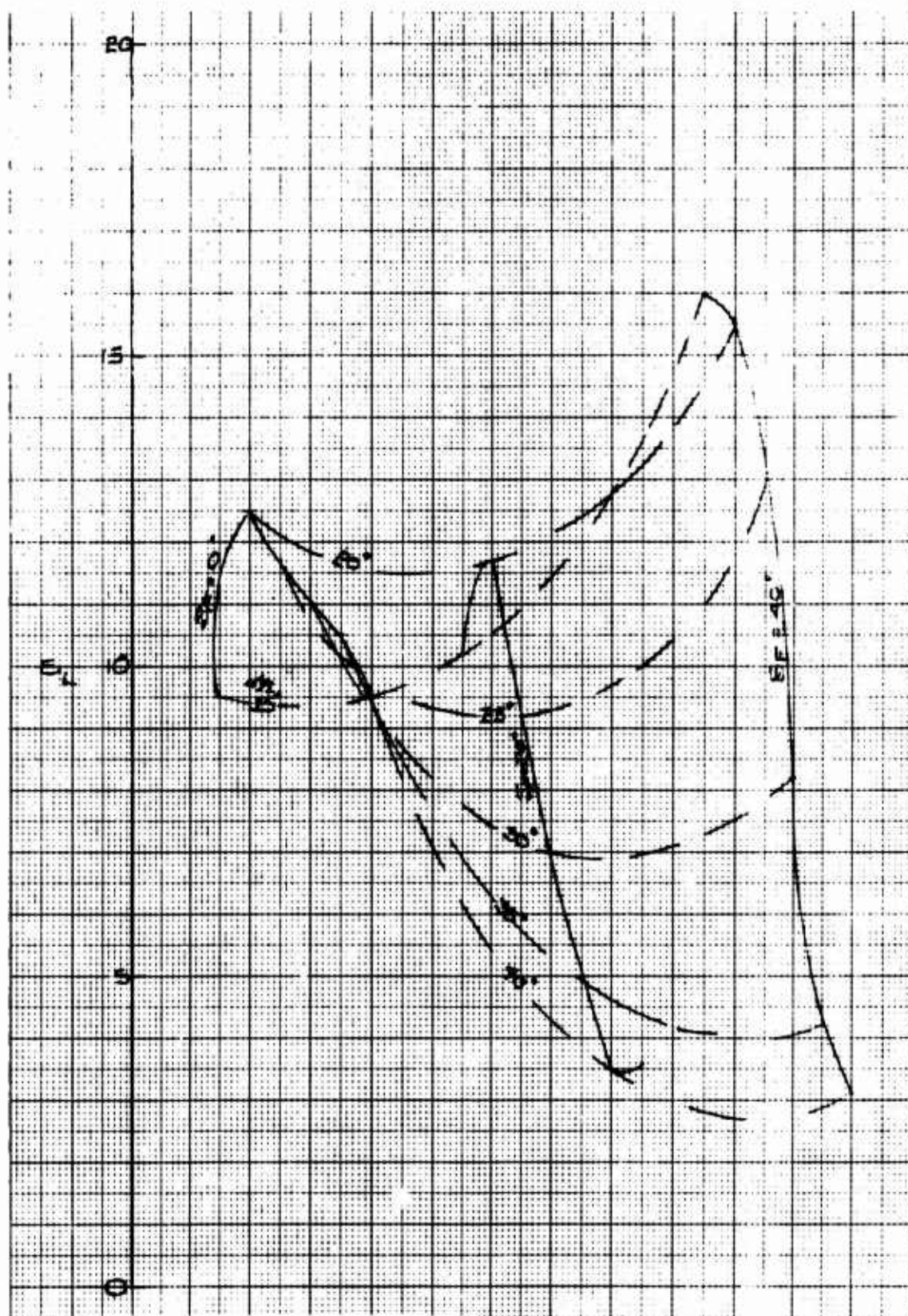


Figure A-18. Effect of Flap on Downwash
 $i_w = 20^\circ$ $\beta = 12^\circ$ $C_{TS} = 0.3$.

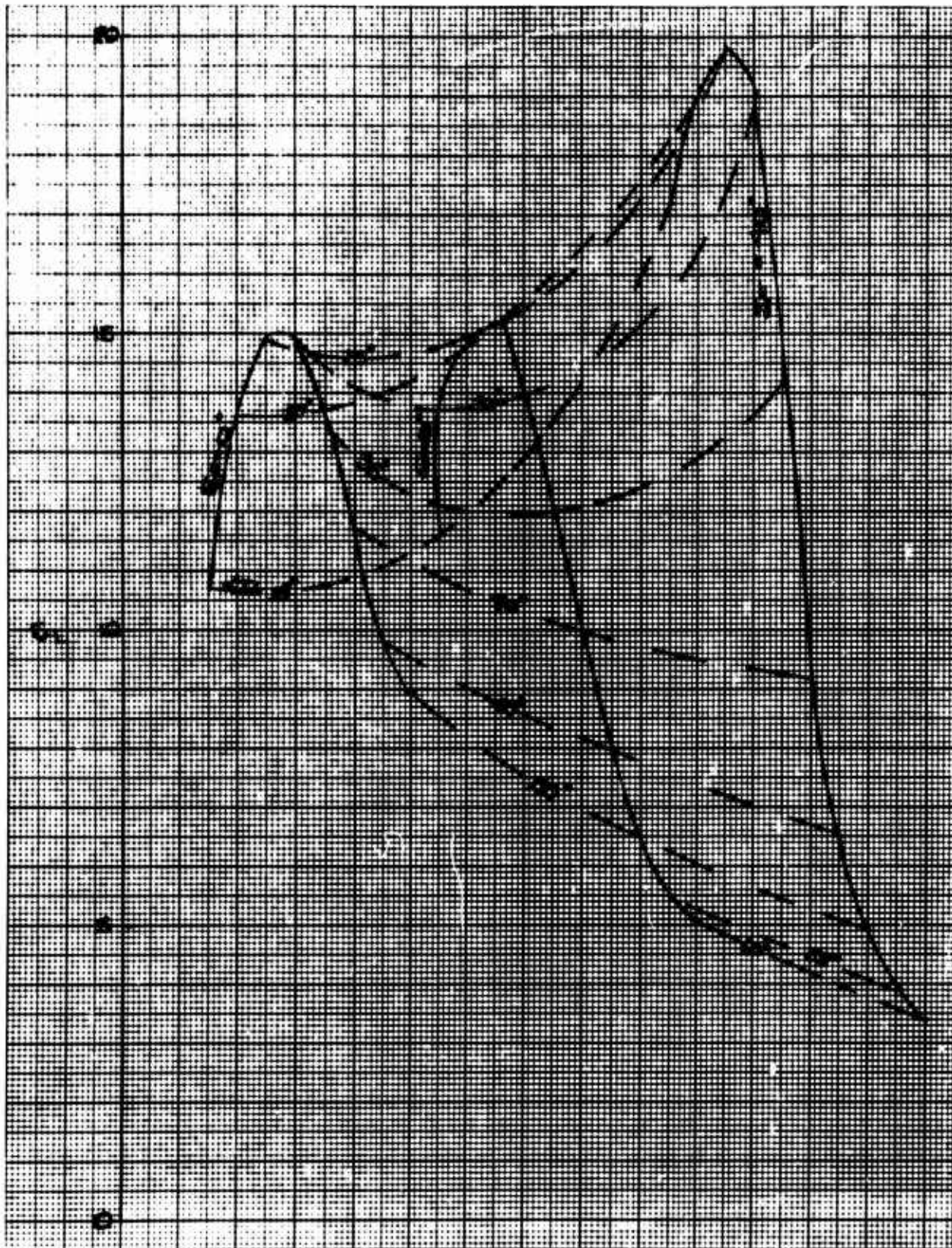


Figure A-19. Effect of Flap on Downwash
 $i_w = 20^\circ$ $\beta = 12^\circ$ $C_{TS} = 0.5$.

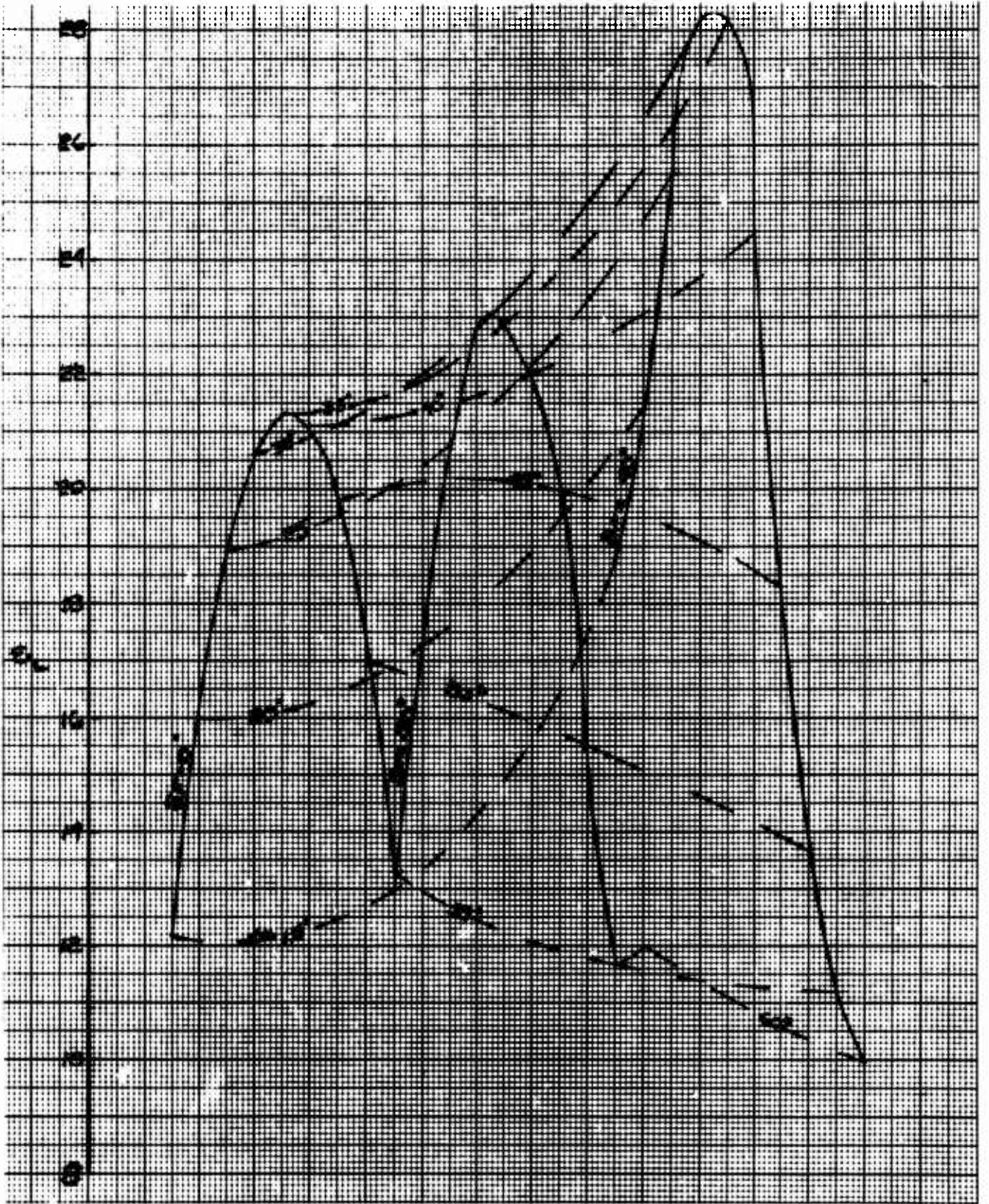


Figure A-20. Effect of Flap on Downwash
 $i_w = 20^\circ$ $\beta = 12^\circ$ $C_{TS} = 0.7$.

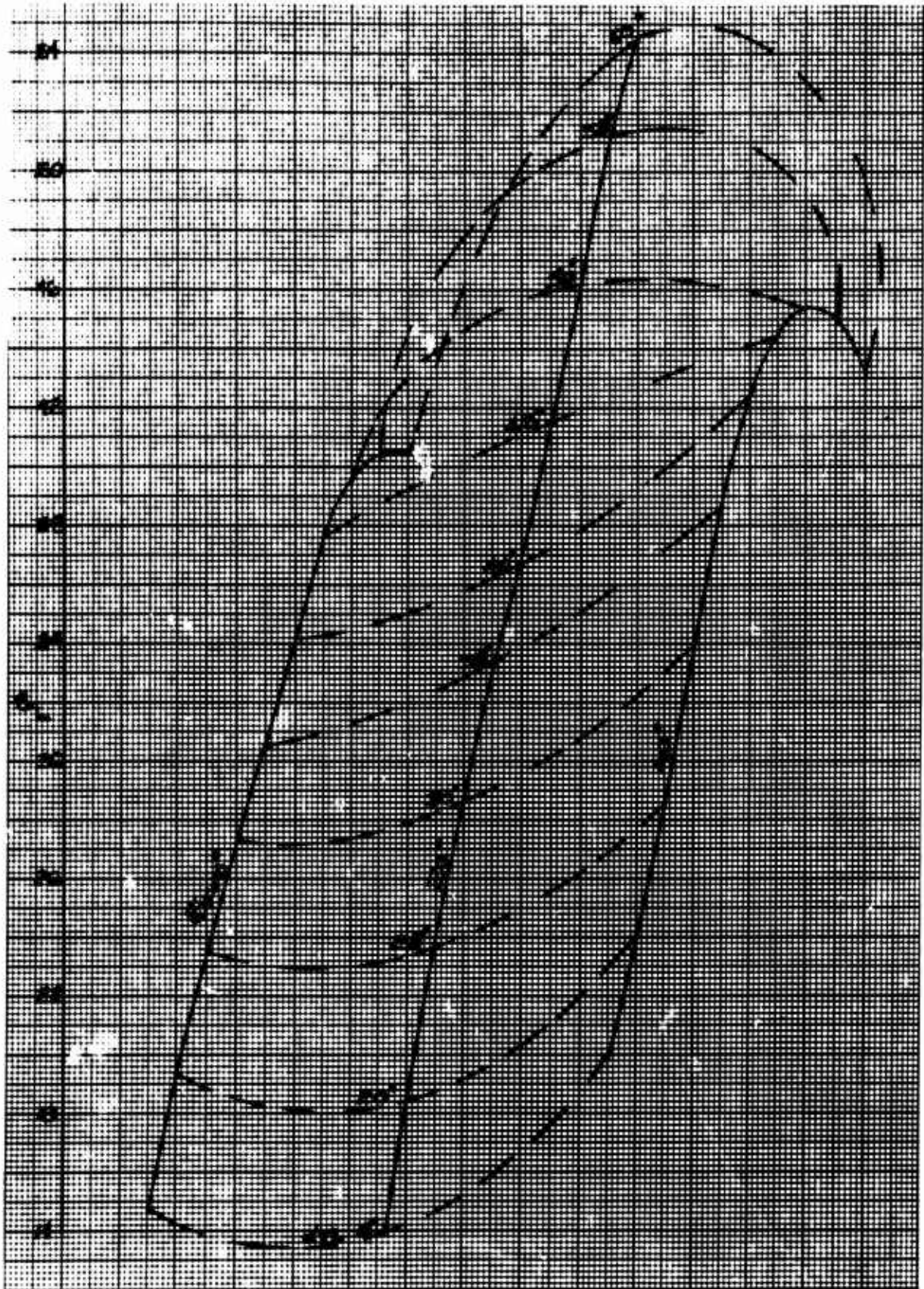


Figure A-21. Effect of Flap on Downwash
 $i_w = 20^\circ$ $\beta = 12^\circ$ $C_{TS} = 0.9$.

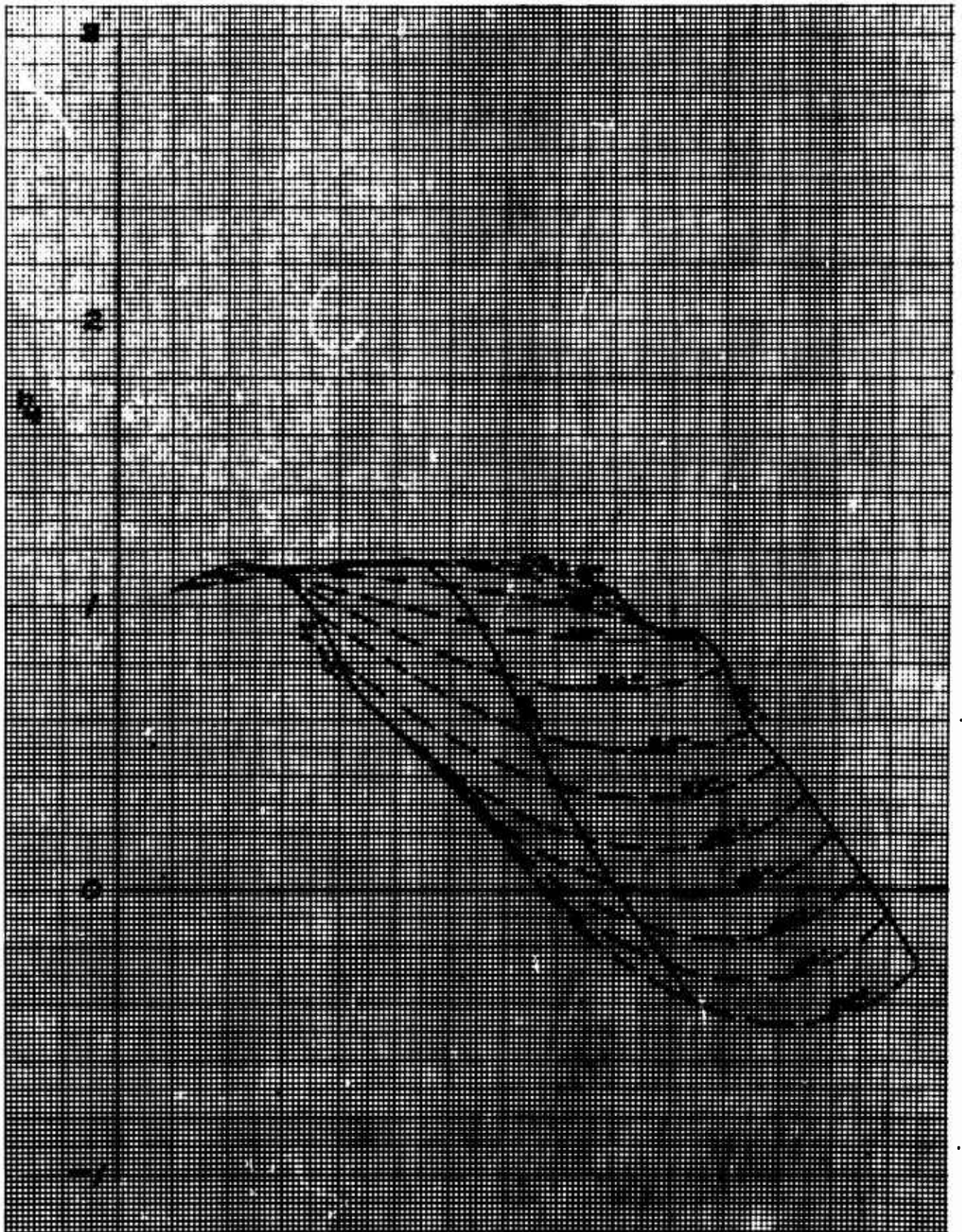


Figure A-22. Effect of Flap on Tail Efficiency of Low Tail
 $\alpha_f = 0^\circ$ $\beta = 12^\circ$ $C_{TS} = 0.3$.

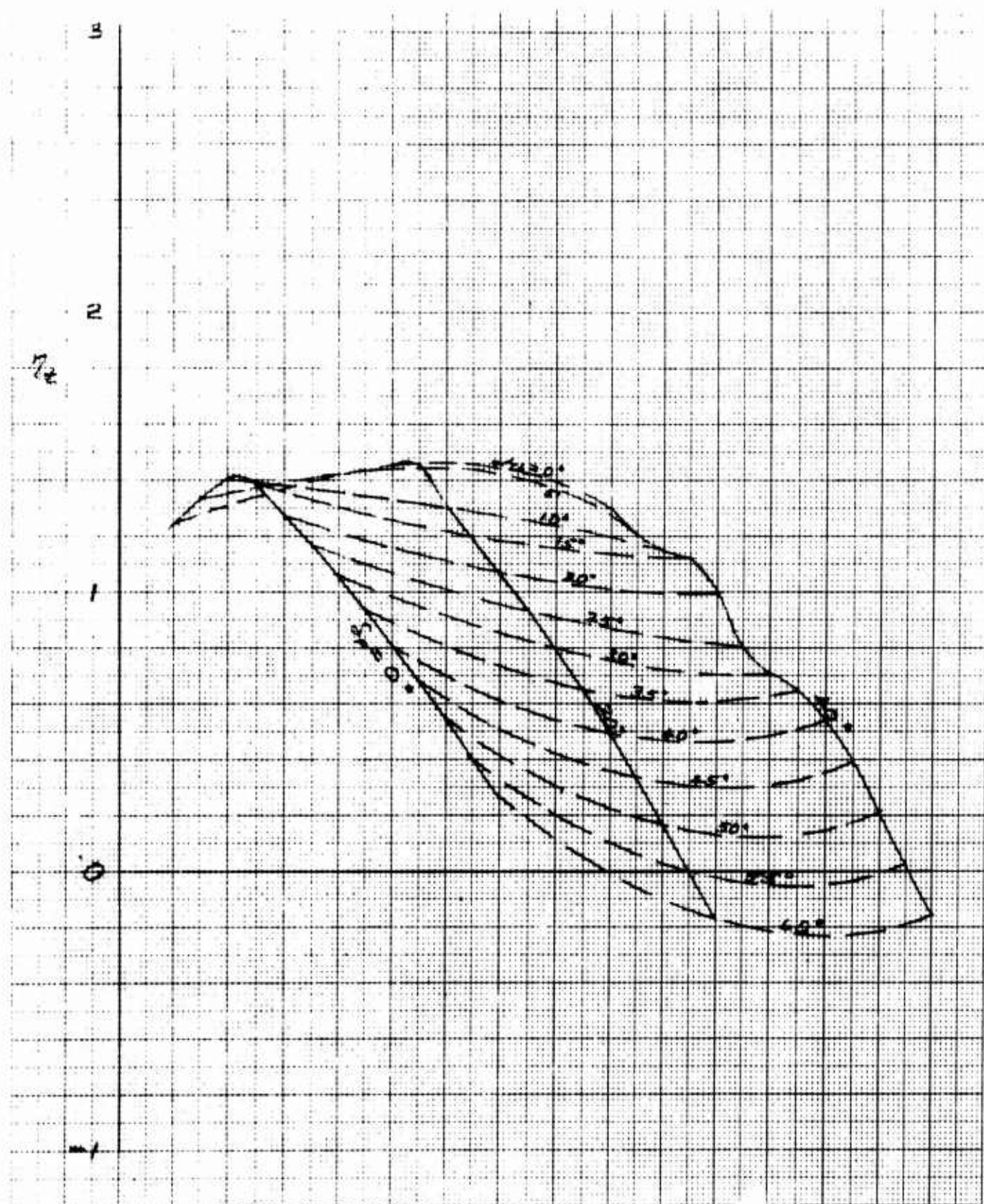


Figure A-23. Effect of Flap on Tail Efficiency of Low Tail
 $\delta_f = 0^\circ$ $\beta = 12^\circ$ $C_{TS} = 0.5$.

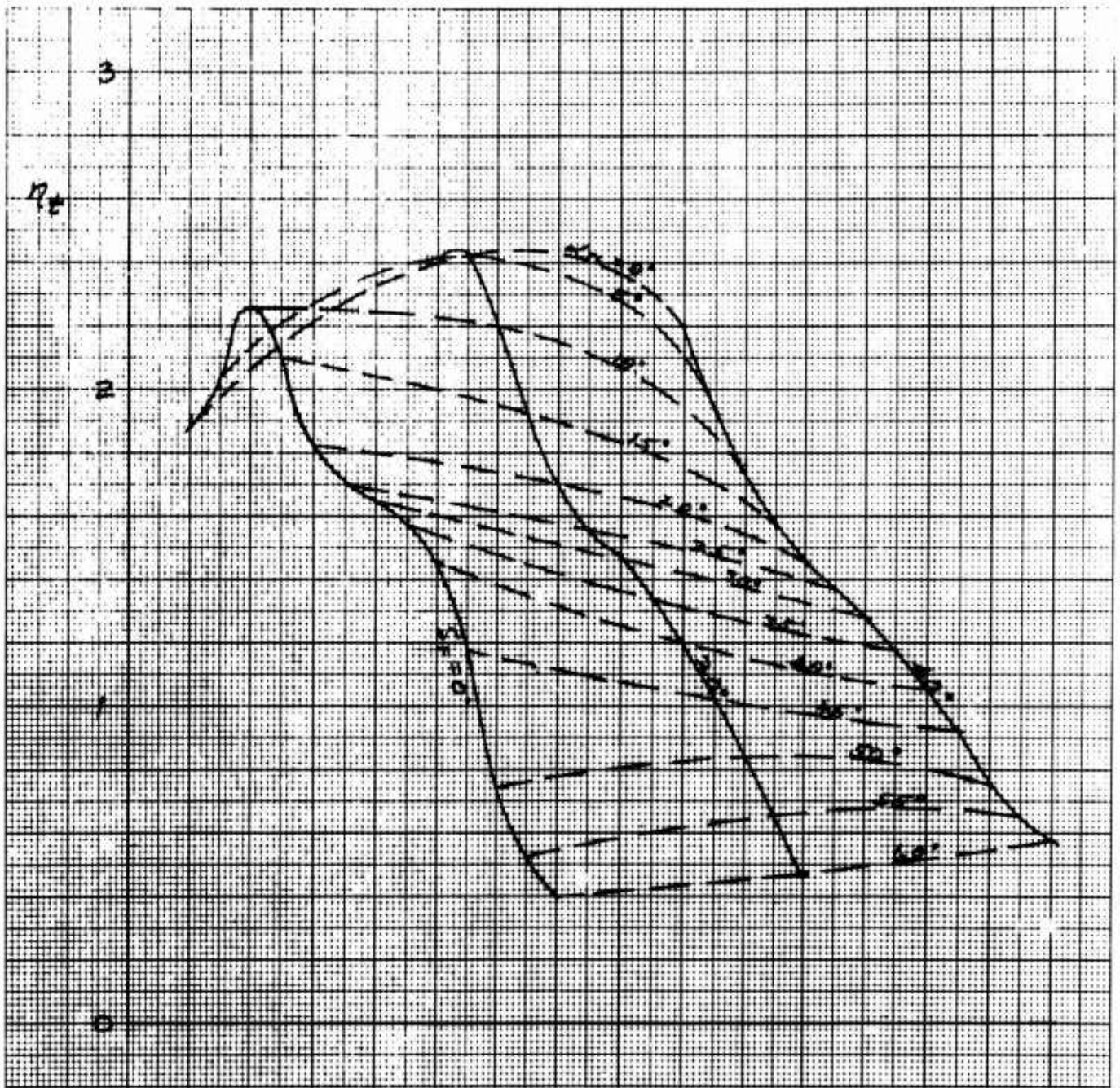


Figure A-24. Effect of Flap on Tail Efficiency of Low Tail
 $\alpha_f = 0^\circ$ $\beta = 12^\circ$ $C_{TS} = 0.7$.

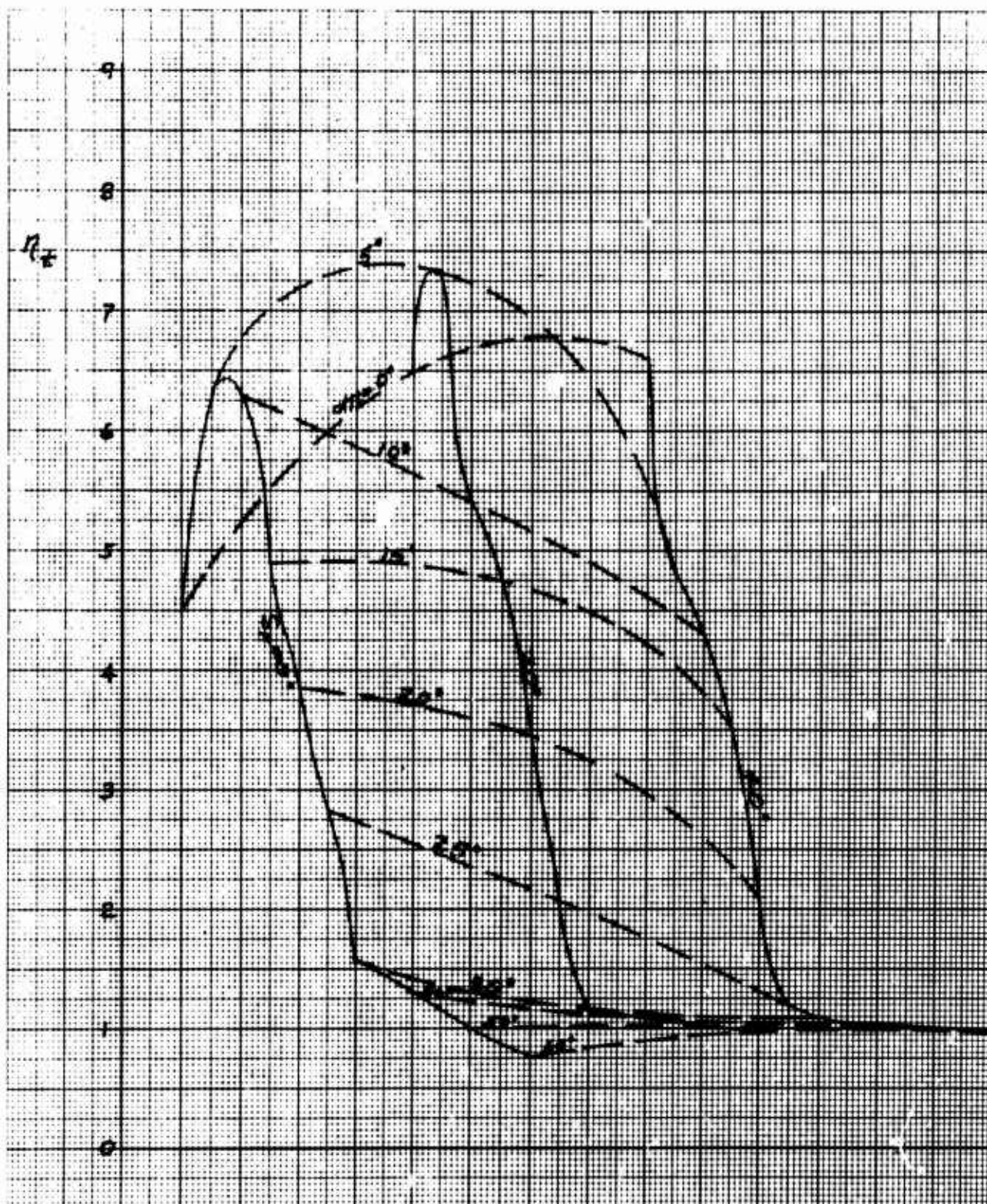


Figure A-25. Effect of Flap on Tail Efficiency of Low Tail
 $\alpha_f = 0^\circ$ $\beta = 12^\circ$ $C_{TS} = 0.9$.

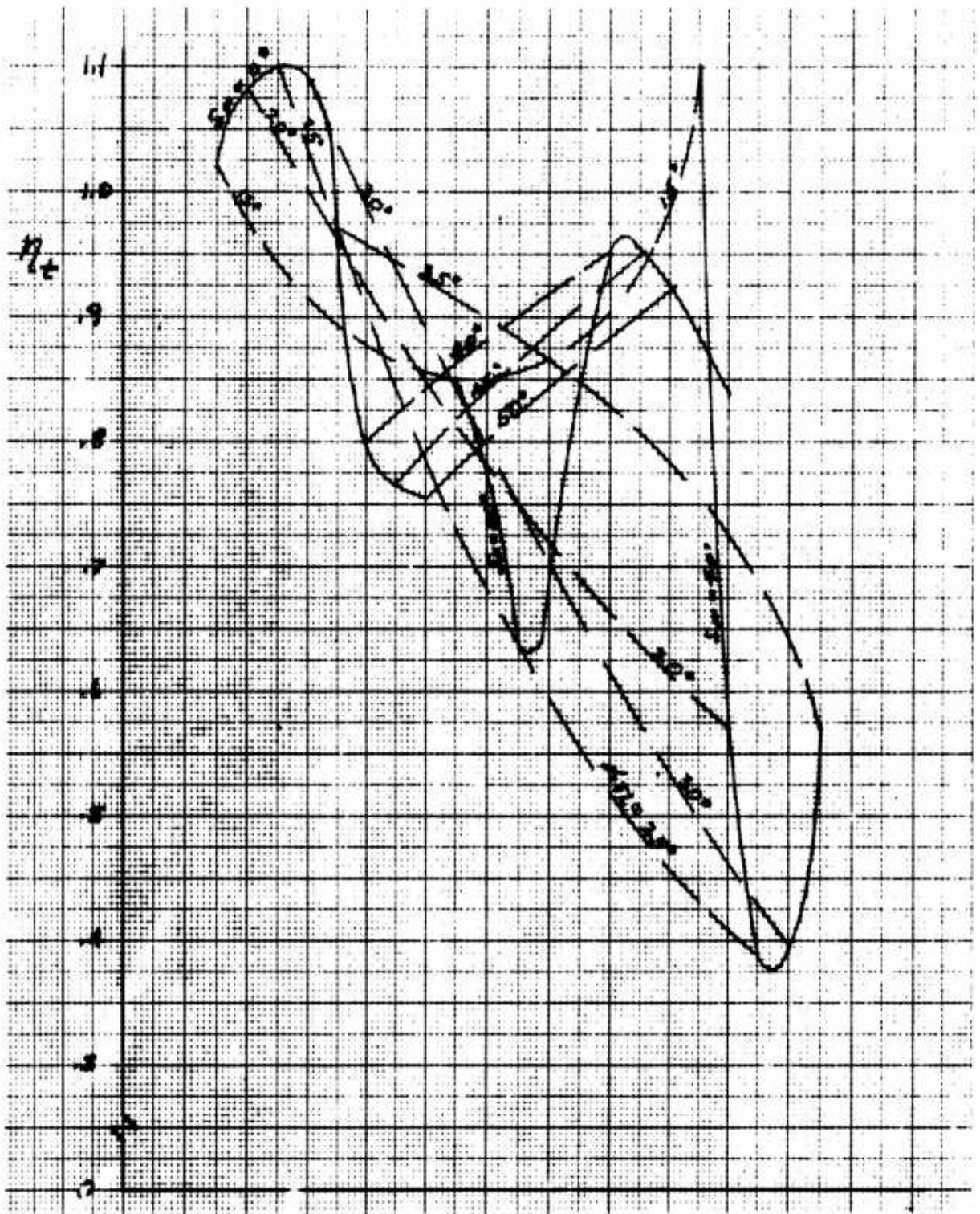


Figure A-26. Effect of Flap on Tail Efficiency of Low Tail
 $i_w = 20^\circ$ $\beta = 12^\circ$ $C_{TS} = 0.3$.

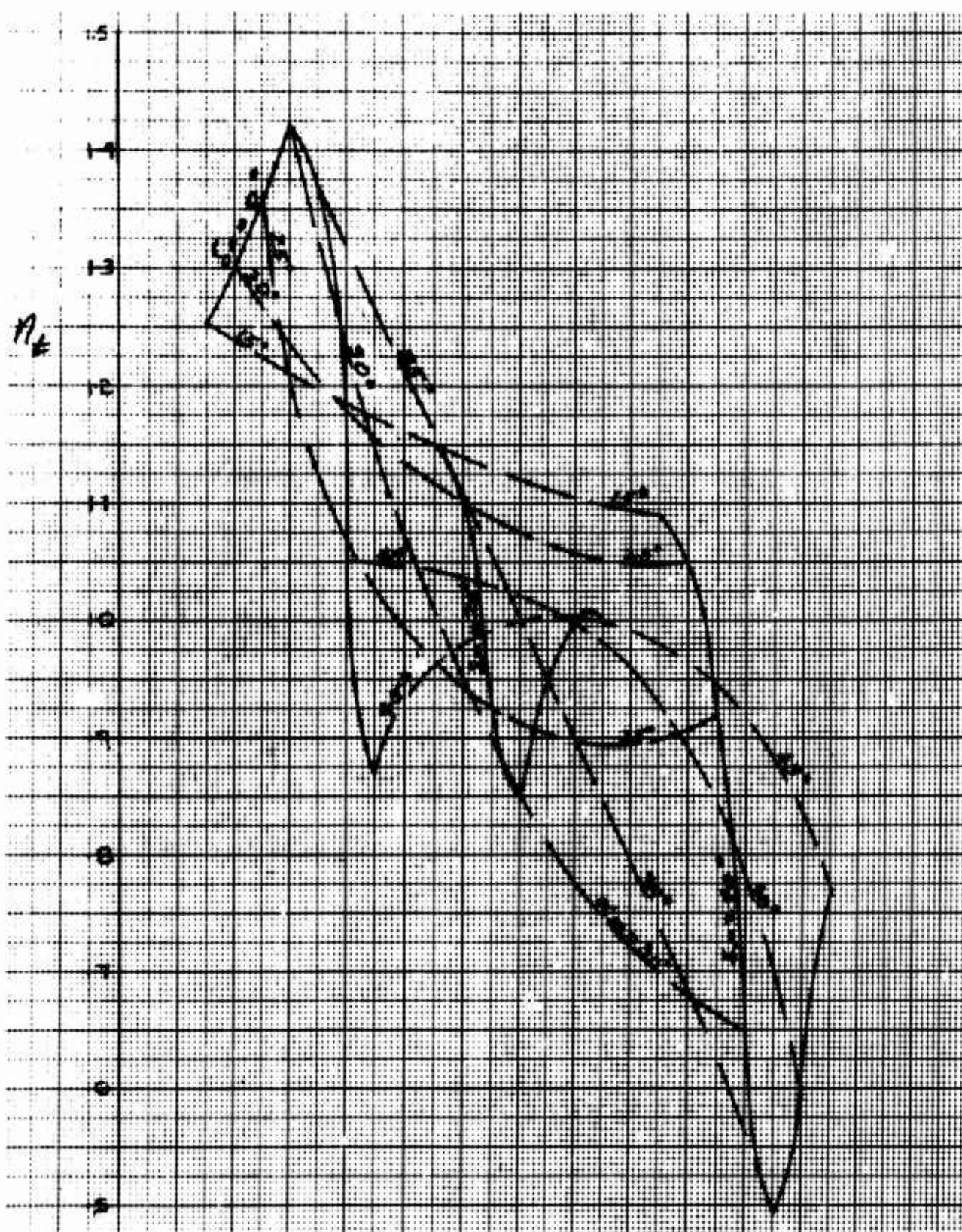


Figure A-27. Effect of Flap on Tail Efficiency of Low Tail
 $i_w = 20^\circ$ $\beta = 12^\circ$ $C_{TS} = 0.5$.

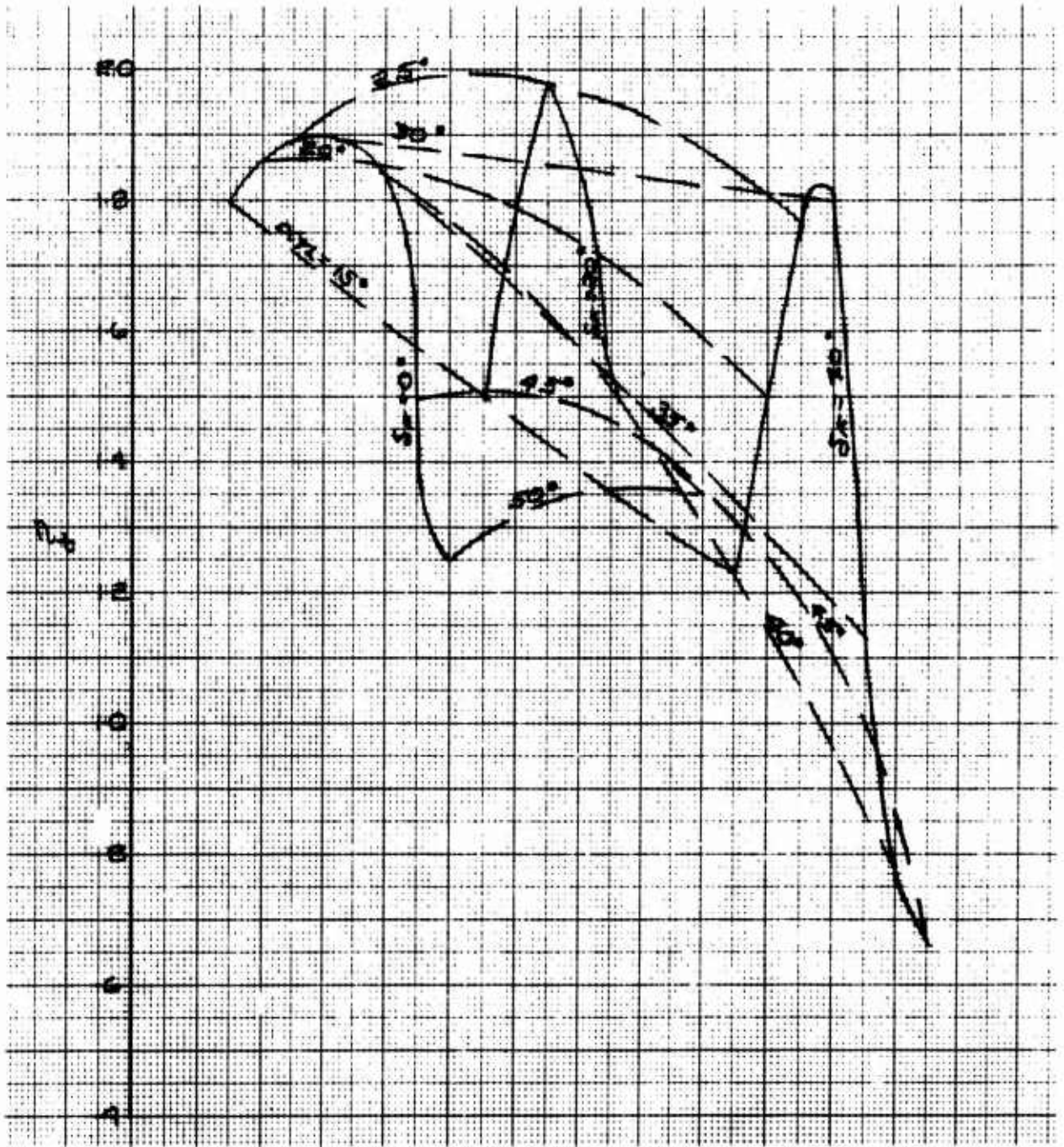


Figure A-28. Effect of Flap on Tail Efficiency of Low Tail
 $i_w = 20^\circ$ $\beta = 12^\circ$ $C_{TS} = 0.7$.

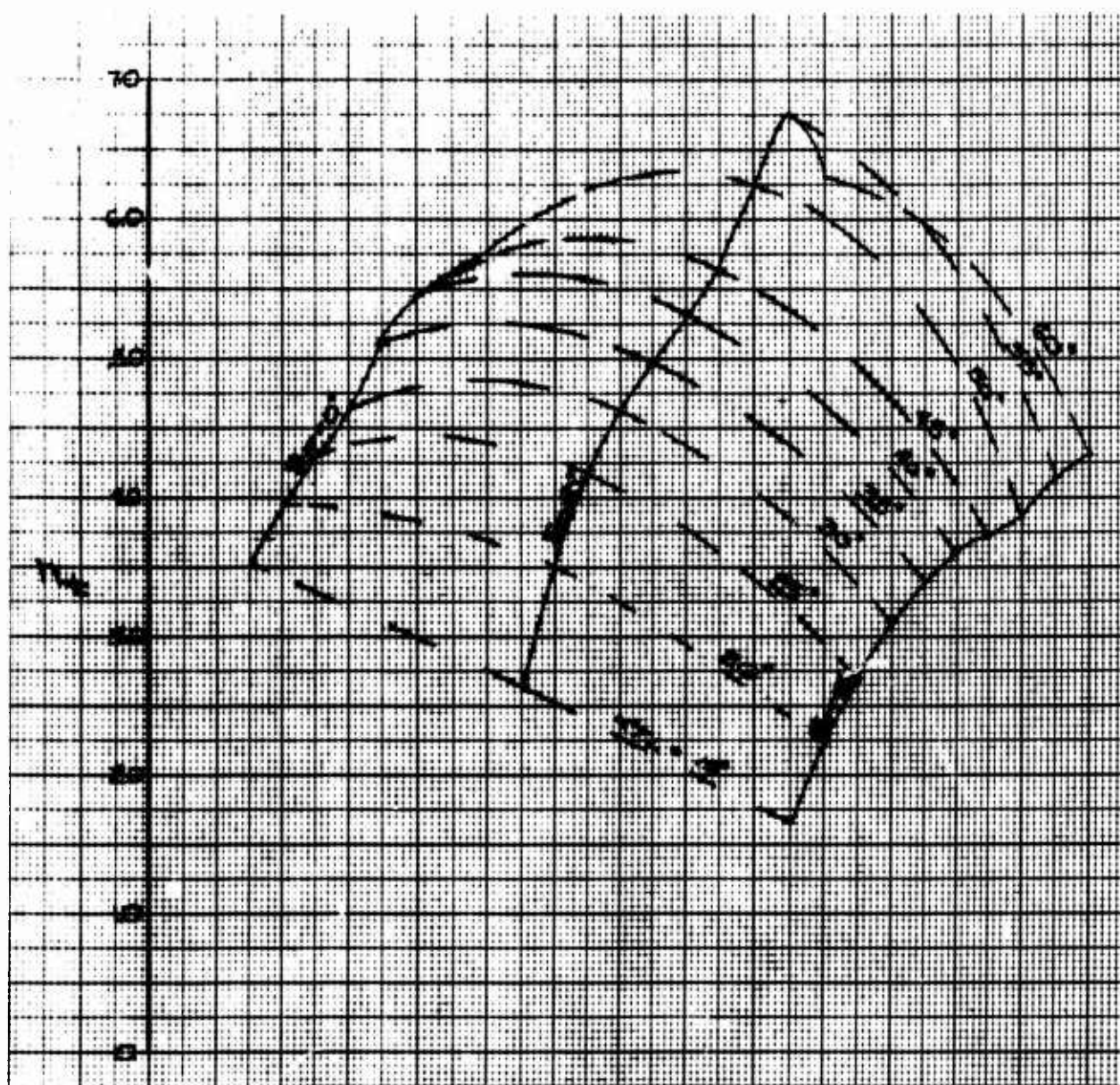


Figure A-29. Effect of Flap on Tail Efficiency of Low Tail
 $i_w = 20^\circ$ $\beta = 12^\circ$ $C_{TS} = 0.9$.

APPENDIX B

LONGITUDINAL EQUATIONS OF MOTION FOR TILT-WING AIRCRAFT

INTRODUCTION

The equations of motion required for perturbation analysis of a conventional tilt-wing V/STOL aircraft are conventional three degree of freedom equations (u, w, θ). Analysis of the "Geared Flap" control system requires an additional degree of freedom (i_w). Since these equations are not readily available in literature, the equations and derivations are presented herein in their entirety.

LONGITUDINAL EQUATIONS OF MOTION

Tilt wing equations of motion are complicated by the fact that not only does the CG of the aircraft vary with wing incidence, but the effects of wing accelerations relative to the fuselage cause fuselage accelerations. The following derivation is as complete as required for complete longitudinal analysis, and higher order terms are dropped as they occur. Figures 1B and 2B contain the definitions of terms used in the derivation.

The derivation is performed for an axis system with its origin at the total aircraft center of gravity, and the x and z axes parallel to the fuselage body axis, respectively.

The total aircraft center of gravity location relative to the pivot is defined by:

$$x_{CG} = \frac{m_f}{m} l + \frac{m_w}{m} L_w \cos \lambda \quad (1)$$

$$z_{CG} = \frac{m_f}{m} h - \frac{m_w}{m} L_w \sin \lambda \quad (2)$$

The velocity of the center of gravity relative to the pivot is:

$$\dot{x}_{CG} = -\dot{i}_w \frac{m_w}{m} L_w \sin \lambda \quad (3)$$

$$\dot{z}_{CG} = -\dot{i}_w \frac{m_w}{m} L_w \cos \lambda \quad (4)$$

and the accelerations are:

$$\ddot{x}_{CG} = -\ddot{i}_w \frac{m_w}{m} L_w \sin \lambda - \dot{i}_w^2 \frac{m_w}{m} L_w \cos \lambda \quad (5)$$

$$\ddot{z}_{CG} = -\ddot{i}_w \frac{m_w}{m} L_w \cos \lambda + \dot{i}_w^2 \frac{m_w}{m} L_w \sin \lambda \quad (6)$$

Treating the wing contributions first, the velocity of the wing center of gravity is:

$$\begin{aligned} V_{CG_w)_x} &= U - \dot{x}_{CG} - \dot{i}_w L_w \sin \lambda - \dot{\theta} (z_{CG} + L_w \sin \lambda) \\ &= U - \dot{\theta} \frac{m_f}{m} (h + L_w \sin \lambda) - \dot{i}_w \frac{m_f}{m} L_w \sin \lambda \end{aligned} \quad (7)$$

$$\begin{aligned} V_{CG_w)_z} &= W - \dot{z}_{CG} - \dot{i}_w L_w \cos \lambda + \dot{\theta} (x_{CG} - L_w \cos \lambda) \\ &= W + \dot{\theta} \frac{m_f}{m} (l - L_w \cos \lambda) - \dot{i}_w L_w \frac{m_f}{m} \cos \lambda \end{aligned} \quad (8)$$

The acceleration of the wing center of gravity for an axis fixed in space is obtained by differentiation and is, neglecting higher order terms:

$$\dot{V}_{CG_w)_x} = \dot{U} - \ddot{\theta} \frac{m_f}{m} (h + L_w \sin \lambda) - \ddot{i}_w \frac{m_f}{m} L_w \sin \lambda \quad (9)$$

$$\dot{V}_{CG_w)_z} = \dot{W} + \ddot{\theta} \frac{m_f}{m} (l - L_w \cos \lambda) - \ddot{i}_w \frac{m_f}{m} L_w \cos \lambda \quad (10)$$

The additional acceleration due to the rotating of the axis system with the aircraft gives total wing accelerations of:

$$a_{x_w} = \dot{V}_{CG_w)_x} + \dot{\theta} W \quad (11)$$

$$a_{z_w} = \dot{V}_{CG_w)_z} - \dot{\theta} U \quad (12)$$

REV

The summation of wing forces and moments may now be written (designating reaction forces and moments at the pivot with subscript p):

$$F_{x_w} + F_{x_p} = m_w [\ddot{u} + g \sin \theta + \dot{\theta} \omega - \ddot{\theta} \frac{m_f}{m} (h + L_w \sin \lambda) - \ddot{i}_w \frac{m_f}{m} L_w \sin \lambda] \quad (13)$$

$$F_{z_w} + F_{z_p} = m_w [\ddot{w} - g \cos \theta - \dot{\theta} u + \ddot{\theta} \frac{m_f}{m} (\ell - L_w \cos \lambda) - \ddot{i}_w \frac{m_f}{m} L_w \cos \lambda] \quad (14)$$

$$M_w + M_p + (F_{x_w} + F_{x_p}) L_w \sin \lambda + (F_{z_w} + F_{z_p}) L_w \cos \lambda = I_w (\ddot{\theta} + \ddot{i}_w) \quad (15)$$

The derivation of the fuselage contributions is performed in the same manner as for wing contributions:

The velocities of the fuselage CG are:

$$\begin{aligned} V_{CG_f}_x &= u - \dot{x}_{CG} + \dot{\theta} (h - z_{CG}) \\ &= u + \dot{\theta} \frac{m_w}{m} [h + L_w \sin \lambda] + \dot{i}_w \frac{m_w}{m} L_w \sin \lambda \end{aligned} \quad (16)$$

$$\begin{aligned} V_{CG_f}_z &= w - \dot{z}_{CG} - \dot{\theta} (\ell - x_{CG}) \\ &= w - \dot{\theta} \frac{m_w}{m} [\ell - L_w \cos \lambda] + \dot{i}_w \frac{m_w}{m} L_w \cos \lambda \end{aligned} \quad (17)$$

The accelerations are (neglecting higher order terms):

$$\dot{V}_{CG_f}_x = \ddot{u} + \ddot{\theta} \frac{m_w}{m} (h + L_w \sin \lambda) + \ddot{i}_w \frac{m_w}{m} L_w \sin \lambda \quad (18)$$

$$\dot{V}_{CG_f}_z = \ddot{w} - \ddot{\theta} \frac{m_w}{m} (\ell - L_w \cos \lambda) + \ddot{i}_w \frac{m_w}{m} L_w \cos \lambda \quad (19)$$

REV.

A rotating axis system provides total accelerations of:

$$a_{x_f} = \dot{V}_{CG_f})_x + \dot{\theta} \omega \quad (20)$$

$$a_{z_f} = \dot{V}_{CG_f})_z - \dot{\theta} u \quad (21)$$

Summation of the fuselage forces and moments then gives:

$$X_{ft} - F_{xp} = m_f [\ddot{u} + g \sin \theta + \dot{\theta} \omega + \ddot{\theta} \frac{m_w}{m} (h + L_w \sin \lambda) + \ddot{\omega} \frac{m_w}{m} L_w \sin \lambda] \quad (22)$$

$$Z_{ft} - F_{zp} = m_f [\ddot{w} - g \cos \theta - \dot{\theta} u - \ddot{\theta} \frac{m_w}{m} (\ell - L_w \cos \lambda) + \ddot{\omega} \frac{m_w}{m} L_w \cos \lambda] \quad (23)$$

$$M_f - M_p - (X_{ft} - F_{xp})h + (Z_{ft} - F_{zp})\ell = I_f \ddot{\theta} \quad (24)$$

Before obtaining the total aircraft equations, the reaction forces at the pivots, F_{xp} and F_{zp} may be eliminated from the moment equations by substitution of equations (13) and (14) into (15) and (22) and (23) into (24) respectively, giving:

$$\ddot{\theta} [I_w + m_w \frac{m_f}{m} L_w (h \sin \lambda - \ell \cos \lambda + L_w)] = \quad (25)$$

$$M_w + M_p + \frac{m_w}{m} L_w (X_{tot} \sin \lambda + Z_{tot} \cos \lambda) - \ddot{\omega} (I_w + m_w \frac{m_f}{m} L_w^2)$$

$$\ddot{\theta} [I_f + m_f \frac{m_w}{m} (h^2 + \ell^2 + h L_w \sin \lambda - \ell L_w \cos \lambda)] = \quad (26)$$

$$M_{ft} - M_p - \frac{m_f}{m} (X_{tot} h - Z_{tot} \ell) - \ddot{\omega} m_f \frac{m_w}{m} L_w (h \sin \lambda - \ell \cos \lambda)$$

REV

The total aircraft equations may now be obtained by the respective sums of equations (13) and (22), (14) and (23), and (25) and (26), giving:

$$\dot{U} = -g \sin \theta - \dot{\theta} \omega + X_{tot} / m \quad (27)$$

$$\dot{\omega} = g \cos \theta + \dot{\theta} U + Z_{tot} / m \quad (28)$$

$$\begin{aligned} \ddot{\theta} \{ I_{y_f} + I_{y_w} + m_w \frac{m}{m} [L_w^2 + h^2 + \ell^2 + 2L_w(h \sin \lambda - \ell \cos \lambda)] \} = \\ M_{ft} + M_w + \frac{m_f}{m} (Z_{tot} \ell - X_{tot} h) + L_w \frac{m_w}{m} (X_{tot} \sin \lambda + Z_{tot} \cos \lambda) \\ - \ddot{i}_w \{ I_{y_w} + m_w \frac{m}{m} [L_w^2 + L_w(h \sin \lambda - \ell \cos \lambda)] \} \end{aligned} \quad (29)$$

The effects of the moment about the wing pivot, M_p , (used to generate \ddot{i}_w) are obtained from the difference between equations (25) and (26).

$$\begin{aligned} \ddot{i}_w \{ I_{y_w} + m_w \frac{m}{m} [L_w^2 + L_w(h \sin \lambda - \ell \cos \lambda)] \} = 2M_p + M_w - M_{ft} \\ - \frac{m_f}{m} (Z_{tot} \ell - X_{tot} h) + \frac{m_w}{m} L_w (X_{tot} \sin \lambda + Z_{tot} \cos \lambda) \\ + \ddot{\theta} [I_{y_f} - I_{y_w} + m_w \frac{m}{m} (h^2 + \ell^2 - L_w^2)] \end{aligned} \quad (30)$$

REV.

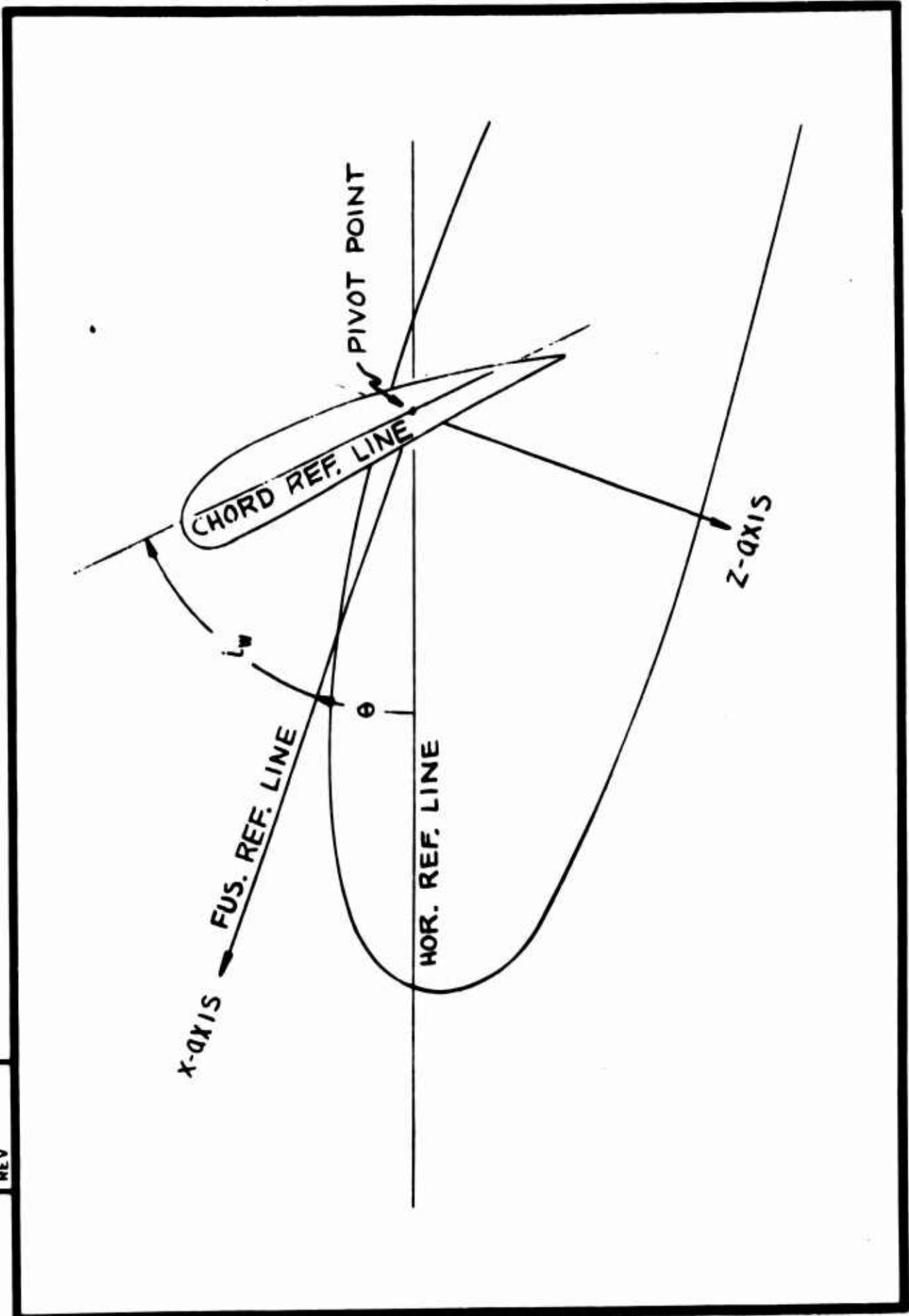


Figure B1. Axis System.

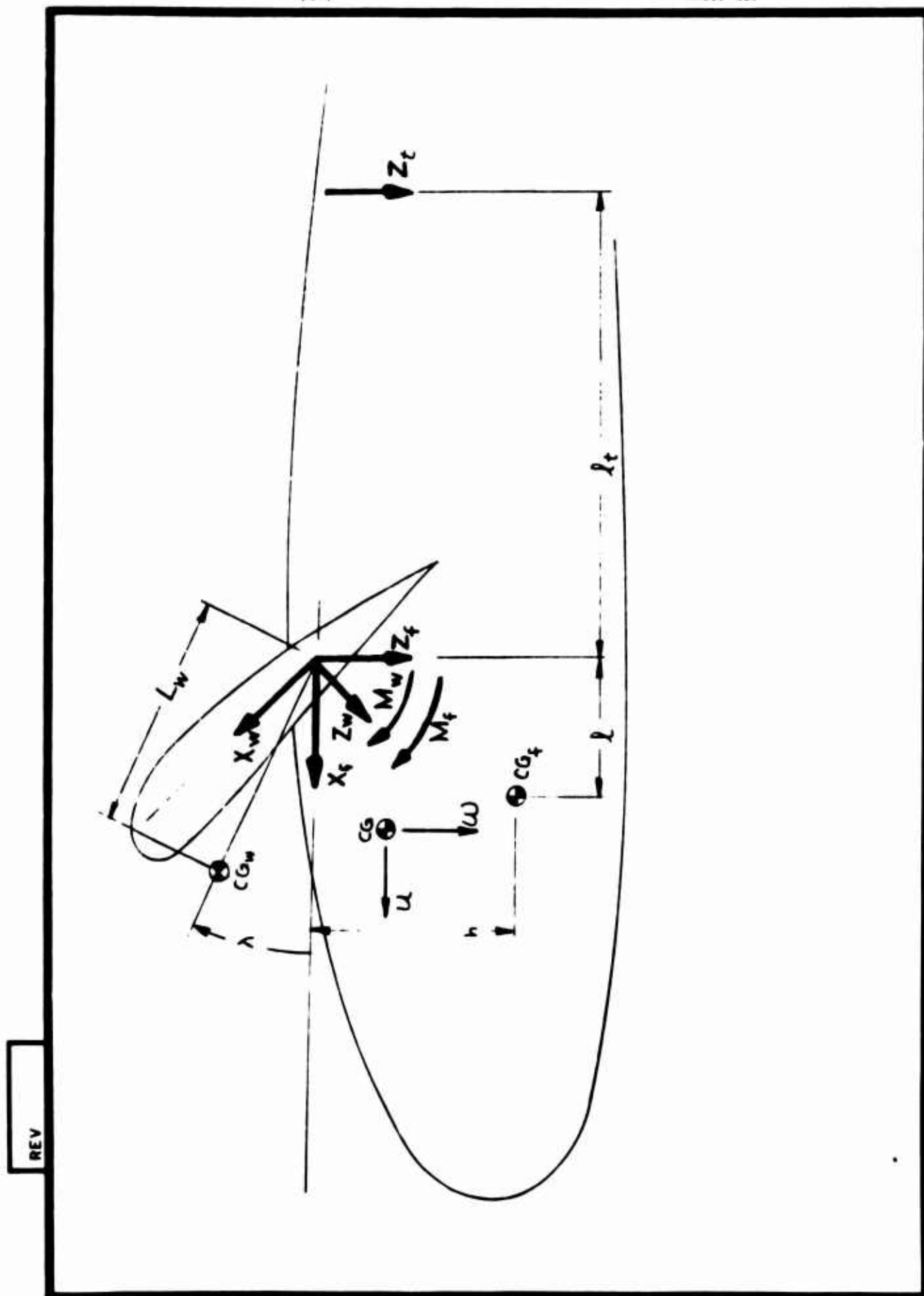


Figure B2. Schematic Definition of Parameters.

References

1. deDecker, R.W., Investigation of an Isolated Monocyclic V/STOL Propeller Performance and Oscillatory Stress, Report Number R-423; (Contract DA44-177-AMC-319(T)), Vertol Division of The Boeing Company, Philadelphia, Pennsylvania.
2. Wind Tunnel Test of the Boeing-Vertol 147 Tilt-Wing Powered Model with Monocyclic Rotors, Report Number D8- -3, Vertol Division of The Boeing Company, Philadelphia, Pennsylvania.
3. Mort, K.W. and Yoggy, P.F., Aerodynamic Characteristics of a Full Scale Propeller Tested with both Rigid and Flapping Blades and with Cyclic Pitch Control, NASA TN D-1774, April 1963.
4. U.S. Patent 3,029,043, Free Floating Wing Structure and Control System for Convertible Aircraft, Issued to G.B. Churchill, April 10, 1962.
5. Churchill, G.B., Improved Transition Flight Control System for Tilt-Wing VTOL Aircraft, Available from the Author, 673 Mount Alverno Road, Media, Pennsylvania, dated January 20, 1964.
6. Carpenter, B., A Low Speed Wind Tunnel Test of the Powered Boeing-Vertol Advanced Geometry Tilt-Wing Aircraft Model - [LTV Test 228], Report Number D8-0957, Vertol Division of The Boeing Company, Philadelphia, Pennsylvania.
7. Wickens, R.H., Aerodynamic Force and Moment Characteristics of a Four-Bladed Propeller Yawed through 120 Degrees, National Research Council of Canada Aeronautical Report LR-454, National Aeronautical Establishment, Ottawa, Canada.
8. Beppu, G., and Curtiss, H.C., Jr., An Analytical Study of Various Factors Influencing the Longitudinal Stability Derivatives of a Typical Tilt-Wing VTOL Aircraft, Department of Aerospace and Mechanical Science, Report Number 756, Princeton University, Princeton, New Jersey.